




# Loss of adipose TET proteins enhances $\beta$ -adrenergic responses and protects against obesity by epigenetic regulation of $\beta$ 3-AR expression

Seongjun Byun<sup>a,1</sup>, Chan Hyeong Lee<sup>b,1</sup>, Hyeongmin Jeong<sup>a,1</sup>, Hyejin Kim<sup>a</sup>, Hyug Moo Kwon<sup>a</sup>, Sungho Park<sup>a</sup>, Kyungjae Myung<sup>c,d</sup> , Jungeun An<sup>b,2</sup>, and Myunggon Ko<sup>a,d,2</sup>

Edited by C. Ronald Kahn, Harvard Medical School, Boston, MA; received April 6, 2022; accepted April 25, 2022

$\beta$ -adrenergic receptor ( $\beta$ -AR) signaling plays predominant roles in modulating energy expenditure by triggering lipolysis and thermogenesis in adipose tissue, thereby conferring obesity resistance. Obesity is associated with diminished  $\beta$ 3-adrenergic receptor ( $\beta$ 3-AR) expression and decreased  $\beta$ -adrenergic responses, but the molecular mechanism coupling nutrient overload to catecholamine resistance remains poorly defined. Ten-eleven translocation (TET) proteins are dioxygenases that alter the methylation status of DNA by oxidizing 5-methylcytosine to 5-hydroxymethylcytosine and further oxidized derivatives. Here, we show that TET proteins are pivotal epigenetic suppressors of  $\beta$ 3-AR expression in adipocytes, thereby attenuating the responsiveness to  $\beta$ -adrenergic stimulation. Deletion of all three *Tet* genes in adipocytes led to increased  $\beta$ 3-AR expression and thereby enhanced the downstream  $\beta$ -adrenergic responses, including lipolysis, thermogenic gene induction, oxidative metabolism, and fat browning in vitro and in vivo. In mouse adipose tissues, *Tet* expression was elevated after mice ate a high-fat diet. Mice with adipose-specific ablation of all TET proteins maintained higher levels of  $\beta$ 3-AR in both white and brown adipose tissues and remained sensitive to  $\beta$ -AR stimuli under high-fat diet challenge, leading to augmented energy expenditure and decreased fat accumulation. Consequently, they exhibited improved cold tolerance and were substantially protected from diet-induced obesity, inflammation, and metabolic complications, including insulin resistance and hyperlipidemia. Mechanistically, TET proteins directly repressed  $\beta$ 3-AR transcription, mainly in an enzymatic activity-independent manner, and involved the recruitment of histone deacetylases to increase deacetylation of its promoter. Thus, the TET–histone deacetylase– $\beta$ 3-AR axis could be targeted to treat obesity and related metabolic diseases.

TET proteins |  $\beta$ 3-AR | catecholamine resistance | obesity | HDACs

Beta-adrenergic signaling is a crucial modulator of energy expenditure that triggers lipolysis and heat dissipation in brown and beige adipocytes (1, 2). Upon cold exposure, sympathetic nerve terminals release the catecholamines norepinephrine and epinephrine, which bind to  $\beta$ -adrenergic receptors ( $\beta$ -ARs) and activate the intracellular signaling cascade involving adenylyl cyclase/cyclic adenosine monophosphate (cAMP)/protein kinase A (PKA) (3, 4). This event ultimately triggers hydrolysis of stored triglycerides (TGs) by activating key lipases, including hormone-sensitive lipase (HSL). Fatty acids derived from lipolysis are transported to the mitochondria and consumed as fuels to produce thermal energy (1, 2). Furthermore, free fatty acids are proposed to be allosteric activators of uncoupling protein 1 (UCP1) (5). During adaptive thermogenesis,  $\beta$ -AR signals also activate key thermogenic genes, including *Ppargc1a* (encoding PPAR $\gamma$  coactivator-1 $\alpha$  [Pgc-1 $\alpha$ ]), *Ucp1*, and various components of the electron transport chain, thus promoting mitochondrial biogenesis, fatty acid oxidation, and thermogenesis (2–4). Additionally,  $\beta$ -ARs are important regulators of fat browning. There are three  $\beta$ -AR subtypes:  $\beta$ 1-,  $\beta$ 2-, and  $\beta$ 3-AR. In mice,  $\beta$ 3-AR plays important roles in inducing beige adipocytes from pre-existing white adipocytes in response to  $\beta$ -adrenergic agonists, whereas  $\beta$ 1-AR mainly mediates beige adipocyte generation following cold exposure (6).  $\beta$ 3-AR is also important for browning, lipolysis, and thermogenesis in human adipocytes (7, 8).

In addition to cold-induced thermogenesis,  $\beta$ -ARs also play essential roles in diet-induced thermogenesis. A Trp64Arg mutation in the  *$\beta$ 3-AR* gene is associated with abdominal obesity and increased susceptibility to weight gain and insulin resistance (9, 10). Mice lacking all three  $\beta$ -ARs subtypes (known as “ $\beta$ -less” mice) are prone to diet-induced obesity, due to a significantly lower metabolic rate (11). Strikingly, the brown adipose tissue (BAT) from  $\beta$ -less mice display white adipose tissue (WAT)-like features, mainly populated by markedly enlarged adipocytes with unilocular lipid

## Significance

The  $\beta$ 3-adrenergic receptor ( $\beta$ 3-AR) is a major regulator of energy expenditure that triggers lipolysis and thermogenesis in adipose tissue, thereby significantly attenuating the risk of obesity. Obesity is associated with diminished  $\beta$ 3-AR expression and decreased  $\beta$ -adrenergic responses, but the underlying molecular mechanisms remain elusive. Here, we show that ten-eleven translocation (TET) proteins, the crucial modifiers of DNA methylation, act as epigenetic suppressors of  $\beta$ 3-AR in adipocytes by recruiting histone deacetylases to its promoter, thereby reducing the sensitivity to  $\beta$ -adrenergic stimulation. Adipose-specific ablation of all TET proteins in mice prevents body weight gain and metabolic disorders under high-fat diet challenge via enhanced fat browning, lipolysis, and thermogenesis. Modulation of adipocyte TET proteins may provide a new therapeutic avenue to treat obesity.

Author contributions: S.B., C.H.L., H.J., H.K., J.A., and M.K. designed research; S.B., C.H.L., H.J., and J.A. performed research; H.M.K. and K.M. contributed new reagents/analytic tools; S.B., C.H.L., H.K., S.P., K.M., J.A., and M.K. analyzed data; and J.A. and M.K. wrote the paper.

The authors declare no competing interest.

This article is a PNAS Direct Submission.

Copyright © 2022 the Author(s). Published by PNAS. This article is distributed under [Creative Commons Attribution-NonCommercial-NoDerivatives License 4.0 \(CC BY-NC-ND\)](https://creativecommons.org/licenses/by-nc-nd/4.0/).

<sup>1</sup>S.B., C.H.L., and H.J. contributed equally to this work.

<sup>2</sup>To whom correspondence may be addressed. Email: mgko@unist.ac.kr or jan@jbn.u.ac.kr.

This article contains supporting information online at <http://www.pnas.org/lookup/suppl/doi:10.1073/pnas.2205626119/-/DCSupplemental>.

Published June 23, 2022.

droplets that lack UCP1 expression. Consistently, the  $\beta$ -less mice are highly susceptible to cold-induced hypothermia and are unable to increase oxygen consumption in response to  $\beta$ -agonist treatment. Mice lacking  $\beta$ 3-AR alone are also susceptible to depositing more fat compared to wild-type (WT) mice (12). Notably, in both humans and rodents, obesity is associated with blunted  $\beta$ -AR-triggered responses in adipose tissue (AT), a state known as catecholamine resistance (13–15), presumably due to a significant reduction of  $\beta$ 3-AR expression and function in response to chronic nutrient overload (16–19). Furthermore,  $\beta$ -ARs, particularly  $\beta$ 1-AR and  $\beta$ 2-AR, undergo agonist-induced desensitization (20, 21). In rodents, selective  $\beta$ 3-AR agonists exert excellent antiobesity and antidiabetic effects by increasing energy expenditure, due to their abilities to induce lipolysis, mitochondrial biogenesis, fat oxidation, and the thermogenic program in AT (22–26). However, results of most clinical studies targeting  $\beta$ 3-AR have been disappointing (27), although mirabegron, a selective  $\beta$ 3-AR agonist approved for the treatment of overactive bladder syndrome (2), activated human brown and beige adipocytes and improved glucose metabolism in obese individuals when treated chronically or at high doses (7, 28–31). This might be attributed to the poor selectivity of the human  $\beta$ 3-AR agonists and different expression patterns of  $\beta$ -ARs in rodents and human ATs. Indeed,  $\beta$ 3-AR is abundantly expressed in both WAT and BAT in rodents and thus acts as the principal receptor of catecholamine signals. However, its levels are very low in human ATs. Instead,  $\beta$ -adrenergic stimulation of human adipocytes is mainly mediated by  $\beta$ 1-AR and  $\beta$ 2-AR, whose agonists often induce undesired complications, including hypertension and tachycardia (27). Together, these results strongly suggest that strategies to potentiate  $\beta$ 3-AR expression and catecholamine sensitivity with minimal side effects in AT may be promising in obesity treatments.

Ten-eleven translocation (TET) proteins are dioxygenases that reprogram or erase the methylation status of DNA by oxidizing 5-methylcytosine to 5-hydroxymethylcytosine (5hmC) and further oxidized derivatives (32). They are crucial regulators of gene expression that serve as either transcriptional activators or repressors, depending on the context (32, 33). In many cell types, including mouse embryonic stem cells, immune cells, or neuronal cells, TET proteins utilize their enzymatic activities to sequentially oxidize 5-methylcytosine to 5hmC and further oxidation products at promoters or enhancers, followed by DNA demethylation, to control gene transcription (34, 35). However, they can also control gene expression independently of their enzymatic activity, which is mainly achieved by partnering with numerous transcription factors and associated coregulators, including chromatin modifiers (36–39). For example, TET proteins can be implicated in the formation of transcriptional corepressor complex with histone deacetylase (HDAC) to repress transcription (37–39).

Previous studies have suggested that TET proteins may have regulatory roles in adipocyte differentiation and function. Depletion of TET1 or TET2 substantially inhibits adipogenic differentiation of 3T3-L1 preadipocytes or mouse embryonic fibroblasts (40, 41). However, a recent study showed that TET1 is dispensable for adipogenesis of primary preadipocytes isolated from mice (42). Moreover, in mature adipocytes, TET proteins are involved in the PPAR $\gamma$ -regulated transcriptional program by being recruited to PPAR $\gamma$  response elements and inducing their demethylation to activate PPAR $\gamma$  target genes (40). In mice, all three TET proteins are expressed in various adipose depots, although at different levels (39), and TET1 suppresses thermogenesis by repressing *Ucp1* and *Ppargc1a* in a beige adipocyte-specific manner (39). As a result, *Tet1* knockout

mice are cold tolerant and partially protected from diet-induced obesity and metabolic dysfunction. In contrast, another recent report showed that *Tet1* haploinsufficiency promotes diet-induced obesity and aggravates glucose intolerance (42). Thus, the exact roles of TET proteins in adipocyte biology and metabolism remain unclear.

We show here that chromatin modification via TET-HDAC interaction constitutes a crucial regulatory component of adipocyte plasticity and adaptive thermogenesis by modulating  $\beta$ 3-AR expression and catecholamine sensitivity. TET proteins acted as pivotal epigenetic suppressors of  $\beta$ 3-AR expression in adipocytes, thereby reducing the sensitivity to  $\beta$ -adrenergic stimulation in vitro and in vivo. Thus, TET loss resulted in enhanced  $\beta$ -adrenergic responses, including browning, lipolysis, thermogenic gene induction, mitochondrial respiration, and fatty acid oxidation. Moreover, mice lacking all TET proteins in adipocytes resisted  $\beta$ 3-AR down-regulation and remained sensitive to  $\beta$ -AR stimuli during chronic high-fat diet (HFD) challenge. Consequently, the knockout mice maintained a higher capacity for fat lipolysis, thermogenesis, and energy expenditure, and were substantially resistant to diet-induced obesity and associated metabolic complications.

## Results

**TET Deficiency Increases  $\beta$ -Adrenergic Responsiveness by Up-Regulating  $\beta$ 3-AR Expression in Adipocytes.** It was previously reported that TET1 directly repressed the expression of crucial thermogenic genes, including *Ucp1* and *Ppargc1a*, in beige adipocytes (39). As a result, its loss increased energy expenditure and partially protected mice from diet-induced obesity and related metabolic comorbidities.  $\beta$ 3-AR is the principal regulator of lipolysis and thermogenesis that acts upstream of *Ucp1* and *Ppargc1a* (1, 2). Thus, we aimed to investigate whether TET proteins could control the expression of  $\beta$ 3-ARs, thereby modulating  $\beta$ -adrenergic responsiveness to indirectly control the downstream thermogenic program. To test this, we established immortalized stromal vascular fraction cells isolated from the subcutaneous inguinal WAT (iWAT) of *Tet1<sup>fl/fl</sup> Tet2<sup>fl/fl</sup> Tet3<sup>fl/fl</sup> Cre-ERT2* mice (*SI Appendix, Fig. S1A*). All three *Tet* genes were successfully deleted after 48 h of 4-hydroxytamoxifen (4-OHT) treatment that activated the Cre-ERT2 recombinase (*SI Appendix, Fig. S1B*). Notably, deletion of all *Tet* genes at the early phase of adipogenic differentiation (achieved by treating preadipocytes with 4-OHT at day  $-3$  or day 0) almost completely blocked adipogenesis in vitro, as assessed by quantification of accumulated lipids and expression of adipogenic marker genes such as *Pparg* and *Fabp4* (*SI Appendix, Fig. S1 C–E*). However, *Tet* deletion at a later stage (achieved by treating cells with 4-OHT at day 2 of differentiation) did not significantly affect adipogenesis (*SI Appendix, Fig. S1 C–E*), thus indicating a stage-specific requirement for TET proteins in adipogenesis. Based on these results, we used WT and *Tet1*, *Tet2*, *Tet3* triple knockout (hereafter, *Tet* TKO) adipocytes under similar differentiation states for subsequent studies (Fig. 1A), where *Tet* deletion was also monitored by 5hmC loss using a dot blot assay (43) (Fig. 1B). Importantly, the  $\beta$ 3-AR mRNA and protein levels were significantly elevated in *Tet* TKO adipocytes (Fig. 1 C and D and *SI Appendix, Fig. S1F*). Among the three  $\beta$ -AR subtypes,  $\beta$ 3-AR up-regulation was most prominent upon *Tet* deletion (*SI Appendix, Fig. S1G*). As expected, both mRNA and protein levels of Pgc-1 $\alpha$  and *Ucp1* were also increased in *Tet* TKO adipocytes (Fig. 1 C and D).

Stimulation of  $\beta$ -ARs activates the cAMP/PKA signaling cascade that ultimately triggers lipolysis by activating key lipases, including HSL (1–4). Furthermore, activated  $\beta$ -ARs also stimulate the transcription of key thermogenic genes, including *Ppargc1a*, *Ucp1*, and various genes implicated in mitochondrial respiration

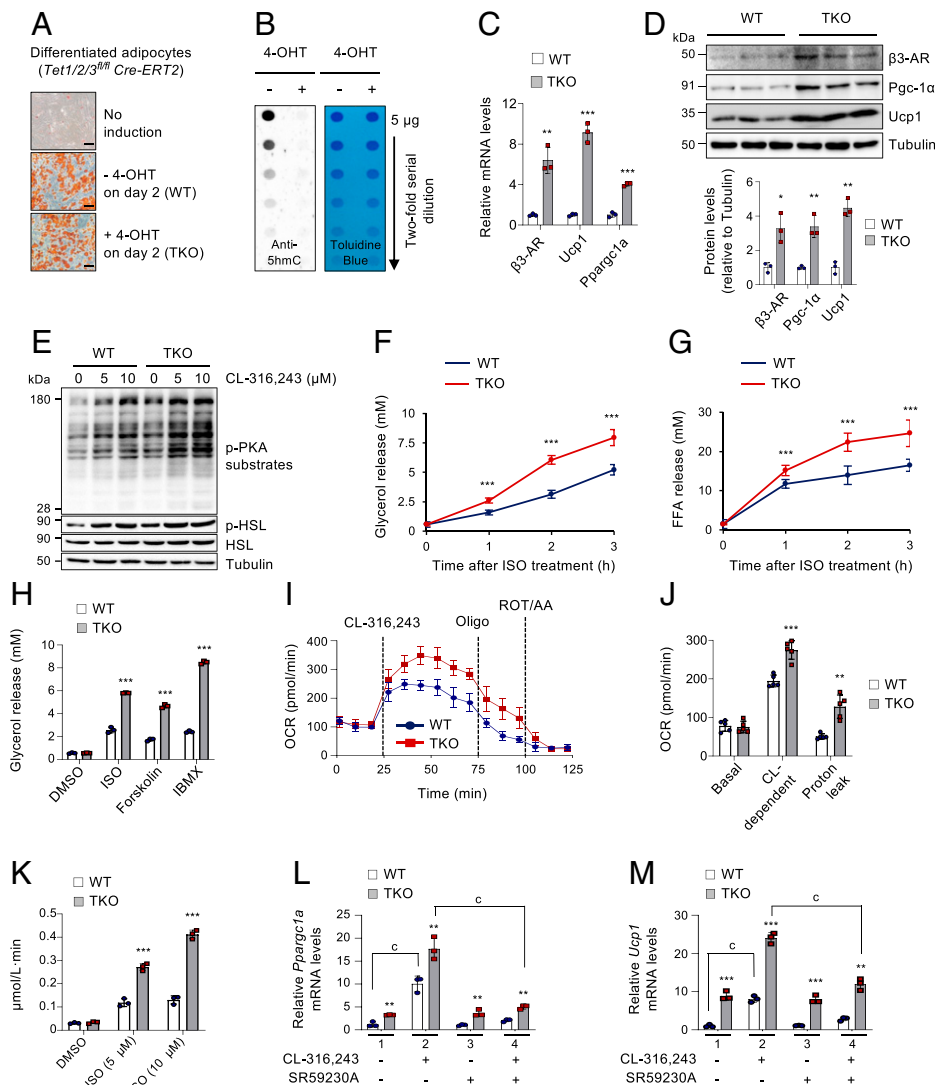


**Fig. 1.** TET deficiency increases  $\beta$ -adrenergic responsiveness by up-regulating  $\beta$ 3-AR expression in adipocytes. (A) Oil Red O staining of differentiated WT and *Tet* TKO adipocytes. Pre-adipocytes were treated with or without 4-OHT on day 2 of differentiation.  $n = 3$ . (Scale bar, 100  $\mu$ m.) (B) Dot blot analysis to quantify genomic 5hmC in WT and *Tet* TKO adipocytes shown in A. Toluidine blue staining confirmed blotting of equal amounts of DNA. (C) mRNA expression of  $\beta$ 3-AR, *Ucp1*, and *Pparg1a* relative to *Gapdh* in WT and *Tet* TKO adipocytes.  $n = 3$ . (D) Immunoblot analysis (Top) and quantification (Bottom) of  $\beta$ 3-AR, *Pgc-1 $\alpha$* , and *Ucp1* proteins in WT and *Tet* TKO adipocytes.  $\alpha$ -Tubulin served as a loading control.  $n = 3$ . (E) Immunoblot analysis of p-PKA substrates, p-HSL, and total HSL proteins in WT and *Tet* TKO adipocytes stimulated with or without CL-316,243 for 5 min at the indicated concentrations.  $\alpha$ -Tubulin served as a loading control.  $n = 3$ . (F and G) In vitro lipolysis in WT and *Tet* TKO adipocytes. The released glycerol (F) and free fatty acid (G) were quantified at the indicated time points after stimulation with ISO (5  $\mu$ M).  $n = 3$ . (H) In vitro lipolysis in WT and *Tet* TKO adipocytes stimulated with ISO (5  $\mu$ M), forskolin (20  $\mu$ M), or isobutylmethylxanthine (IBMX) (0.2 mM).  $n = 3$ . (I and J) Oxygen consumption rate (OCR) (I) and average OCR (J) in WT and *Tet* TKO adipocytes sequentially stimulated with CL-316,243 (10  $\mu$ M), oligomycin (oligo; 1.25  $\mu$ M), and rotenone/antimycin A (ROT/AA, 1  $\mu$ M).  $n = 5$ . (K) In vitro fatty acid oxidation in WT and *Tet* TKO adipocytes stimulated with ISO at the indicated concentrations.  $n = 3$ . (L and M) mRNA expression of *Pparg1a* (L) and *Ucp1* (M) relative to *Gapdh* in WT and *Tet* TKO adipocytes stimulated with or without CL-316,243 (1  $\mu$ M, 24 h). Cells were either untreated or pretreated for 1 h with SR59230A (10  $\mu$ M), a  $\beta$ 3-AR antagonist, prior to CL-316,243 treatments.  $n = 3$ . All data are presented as the mean  $\pm$  SD. The  $P$  values were determined by unpaired Student's  $t$  test. \*\* $P < 0.005$ , \*\*\* $P < 0.0005$  versus WT;  $^{\circ}P < 0.0005$  versus WT;  $^{\circ}P < 0.0005$  versus WT; CL, CL-316,243.

(1–4). Therefore, we next asked whether elevated  $\beta$ 3-AR expression by TET deficiency influenced adipocyte sensitivity to  $\beta$ -adrenergic stimuli. Treatment of WT and *Tet* TKO adipocytes with CL-316,243, a selective  $\beta$ 3-AR agonist, revealed that the intracellular  $\beta$ -adrenergic signaling was more potently activated in *Tet* TKO adipocytes compared to WT controls, as determined by higher levels of phosphorylated forms of PKA substrates and HSL in the stimulated *Tet* TKO adipocytes (Fig. 1E). Consistent with these results, *Tet* TKO significantly increased the rate of lipolysis stimulated by isoproterenol (ISO), a pan- $\beta$ -AR agonist, as assessed by the increased release of ISO-stimulated glycerol and free fatty acids in the *Tet* TKO adipocytes, when compared to WT controls (Fig. 1F and G). TET deficiency also significantly promoted lipolysis in adipocytes stimulated with forskolin or isobutylmethylxanthine (IBMX) that increased the concentration of intracellular cAMP (Fig. 1H), presumably due to the enhancement of pre-coupled stable complexes between the  $\beta$ 3-AR and adenylyl cyclase as a result of  $\beta$ 3-AR up-regulation (7). Furthermore, the oxygen consumption rate remained comparable between WT and *Tet* TKO adipocytes under basal conditions, but the CL-316,243-dependent oxygen consumption rate and proton leak were significantly increased in *Tet* TKO adipocytes, when compared to WT controls (Fig. 1I and J). TET deficiency also substantially enhanced fatty acid oxidation in ISO-stimulated adipocytes (Fig. 1K). Thus,

these results suggest that TET deficiency renders adipocytes more sensitive to  $\beta$ 3-AR signals by up-regulating  $\beta$ 3-AR expression.

We next determined whether TET deficiency elicited enhanced thermogenic gene expression by up-regulating  $\beta$ 3-AR expression. In agreement with a previous report (39), TET deficiency alone could significantly up-regulate a broad panel of thermogenesis-related genes (*SI Appendix*, Fig. S2A; *control*), confirming that TET proteins directly regulated their expression. Indeed, *Tet* TKO adipocytes possessed approximately fourfold higher *Pparg1a* promoter-driven reporter activity than did WT adipocytes (*SI Appendix*, Fig. S3A). TET proteins suppressed *Pparg1a* promoter activity through the CREB-binding element (CRE) that was previously shown to be responsive to  $\beta$ -AR signaling (*SI Appendix*, Fig. S3A and B) (44), and this suppression did not require their catalytic activities (*SI Appendix*, Fig. S3C). Instead, chromatin immunoprecipitation followed by qRT-PCR (ChIP-qPCR) showed that TET deficiency blocked the recruitment of HDAC1 to the *Pparg1a* and *Ucp1* gene loci, leading to an accumulation of acetylated H3K27, the active histone mark (*SI Appendix*, Fig. S3D and E). In both WT and *Tet* TKO adipocytes, forskolin considerably up-regulated *Pparg1a*, *Ucp1*, *Ppara*, *Elovl3*, and *Cidea*; however, this up-regulation was more robust in *Tet* TKO cells (*SI Appendix*, Fig. S2A). Neither *Tet* deficiency nor forskolin affected the expression of adipogenic *Pparg* and *Fabp4* marker

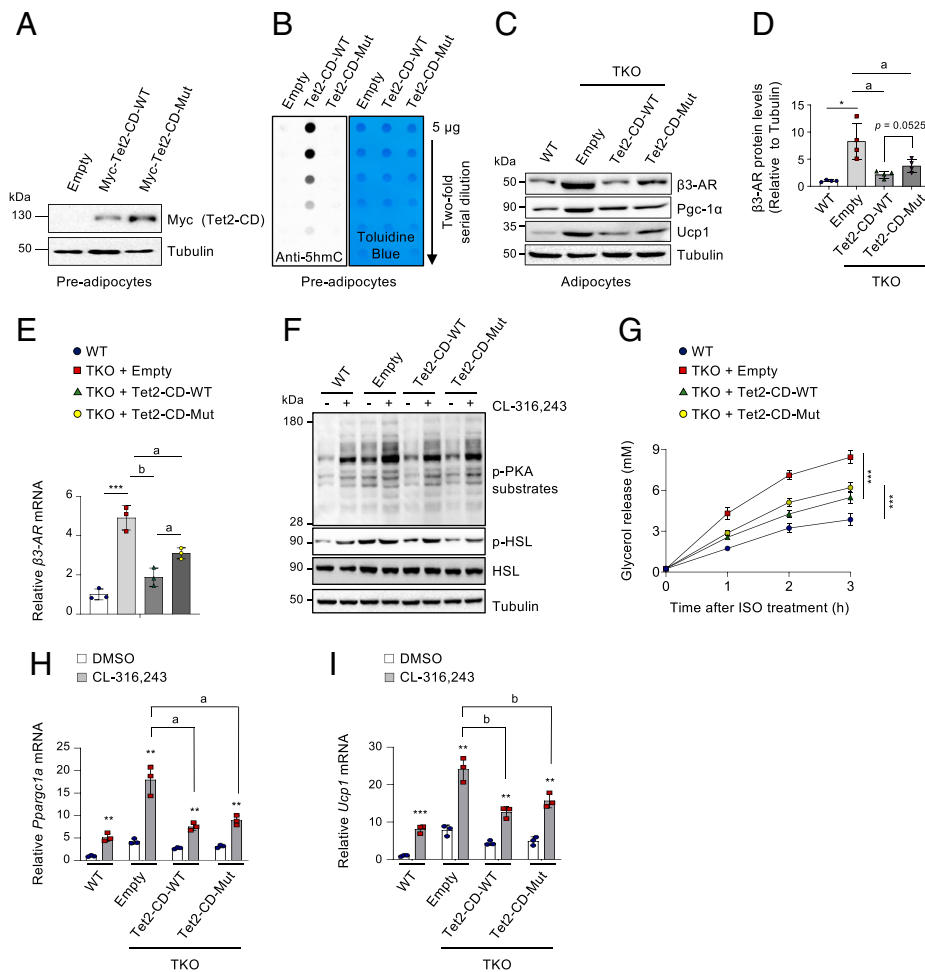


**Fig. 2.** TET proteins control  $\beta$ 3-AR expression and signaling in an enzymatic activity-independent manner. (A) Immunoblot analysis of Myc-tagged WT and mutant (Mut) Tet2 catalytic domain (Tet2-CD) in preadipocytes derived from iWAT of *Tet1<sup>fl/fl</sup> Tet2<sup>fl/fl</sup> Tet3<sup>fl/fl</sup> Cre-ERT2* mice.  $\alpha$ -Tubulin served as a loading control. *n* = 3. (B) Dot blot analysis to quantify genomic 5hmCs in cells shown in A. Toluidine blue staining confirmed blotting of equal amounts of DNA. *n* = 3. (C) Immunoblot analysis of  $\beta$ 3-AR, Pgc-1 $\alpha$ , and Ucp1 proteins in differentiated WT adipocytes or *Tet* TKO adipocytes expressing empty vector, WT, or mutant Tet2-CD.  $\alpha$ -Tubulin served as a loading control. *n* = 4. (D) Quantification of  $\beta$ 3-AR proteins presented in C. *n* = 4. (E) mRNA levels of  $\beta$ 3-AR relative to *Gapdh* in adipocytes shown in C. *n* = 3. (F) Immunoblot analysis of phosphorylated (p)-PKA substrates, p-HSL, and total HSL proteins in adipocytes shown in C after stimulation with or without CL-316,243 (10  $\mu$ M, 5 min).  $\alpha$ -Tubulin served as a loading control. (G) In vitro lipolysis in adipocytes shown in C. Plasma glycerol was quantified after stimulation with or without ISO (5  $\mu$ M) at the indicated time points. *n* = 6. (H and I) mRNA levels of *Pparg1a* (H) and *Ucp1* (I) relative to *Gapdh* in adipocytes shown in C after stimulation with or without CL-316,243 (1  $\mu$ M, 24 h). *n* = 3. All data are presented as the mean  $\pm$  SD. The *P* values were determined by unpaired Student's *t* test. \**P* < 0.05, \*\**P* < 0.005, \*\*\**P* < 0.0005 versus WT; <sup>a</sup>*P* < 0.05, <sup>b</sup>*P* < 0.005.

gene expressions (*SI Appendix, Fig. S2B*). Furthermore, acute stimulation with CL-316,243 also increased the mRNA levels of these thermogenic genes in WT adipocytes, and this was further enhanced in *Tet* TKO adipocytes (Fig. 1 *L* and *M* and *SI Appendix, Fig. S3F, panels 1 and 2*). Notably, pretreatment with SR59230A, a  $\beta$ 3-AR antagonist, substantially blocked the stimulatory effect of CL-316,243 in both WT and *Tet* TKO adipocytes (Fig. 1 *L* and *M* and *SI Appendix, Fig. S3F, compare panels 2 and 4*), confirming that  $\beta$ 3-AR up-regulation by TET deficiency was mainly responsible for the increased thermogenic gene expression during  $\beta$ -adrenergic stimulation.

**TET Proteins Suppress  $\beta$ 3-AR Expression and Signaling, Which Is Mainly Independent of Enzymatic Activity.** To further confirm whether the enzymatic activities of TET proteins were implicated in the control of thermogenic gene expression, the immortalized preadipocytes derived from iWAT of *Tet1<sup>fl/fl</sup> Tet2<sup>fl/fl</sup> Tet3<sup>fl/fl</sup> Cre-ERT2* mice were transduced with lentiviruses expressing WT or a catalytically inactive mutant version of the Myc-tagged Tet2 catalytic domain (Tet2-CD), which was previously shown to reverse loss of 5hmC and the effects by TET deficiency (45–47). Immunoblotting and dot blot assays validated appropriate Tet2 expression and activity (Fig. 2 *A* and *B*). As previously shown, both mRNA and protein levels of  $\beta$ 3-AR were up-regulated in differentiated adipocytes after induction of *Tet* deletion at day 2 of differentiation (Fig. 2 *C–E*). However, this up-regulation was substantially inhibited by ectopic expression of both WT and mutant Tet2-CD, although the catalytic mutant exhibited slightly weaker inhibitory

effects (Fig. 2 *C–E*). Consistently, both WT and mutant Tet2-CD similarly attenuated intracellular  $\beta$ -adrenergic signaling (Fig. 2*F*), lipolysis (Fig. 2*G*), and thermogenic gene induction (Fig. 2 *H* and *I* and *SI Appendix, Fig. S4 A–C*) in *Tet* TKO adipocytes upon  $\beta$ -agonist treatment. As expected, the Pgc-1 $\alpha$  and Ucp1 protein levels were also significantly down-regulated by Tet2-CD regardless of its enzymatic activity (Fig. 2*C* and *SI Appendix, Fig. S4 D–F*).

**Adipocyte-Specific TET Ablation Increases the Responsiveness to  $\beta$ 3-AR Signals In Vivo.**  $\beta$ 3-AR stimulation triggers beige adipocyte induction and activation in both murine and human ATs (6–8). To test whether elevated levels of  $\beta$ 3-AR in *Tet* TKO adipocytes affect fat browning under adrenergic stimulation, we generated adipose-specific *Tet* TKO mice by crossing *Tet1<sup>fl/fl</sup> Tet2<sup>fl/fl</sup> Tet3<sup>fl/fl</sup>* mice with *Adiponectin-Cre* mice (48). We deleted all three *Tet* genes to exclude potential functional compensation among TET family members that is commonly observed in various tissues (32, 49, 50). We verified successful *Tet* deletion and the resulting 5hmC diminution specifically in adipose tissues but not in the liver, kidney, pancreas, and other nonadipose tissues (*SI Appendix, Fig. S5 A–C*). Furthermore, *Tet* deletion was induced only in mature adipocytes within adipose depots and not in stromal vascular fraction cells containing preadipocytes and leukocytes (*SI Appendix, Fig. S5 D and E*).

To assess whether TET proteins influence  $\beta$ 3-AR agonist-triggered browning in vivo, WT and *Tet* TKO mice were administered CL-316,243 daily for three consecutive days, a condition

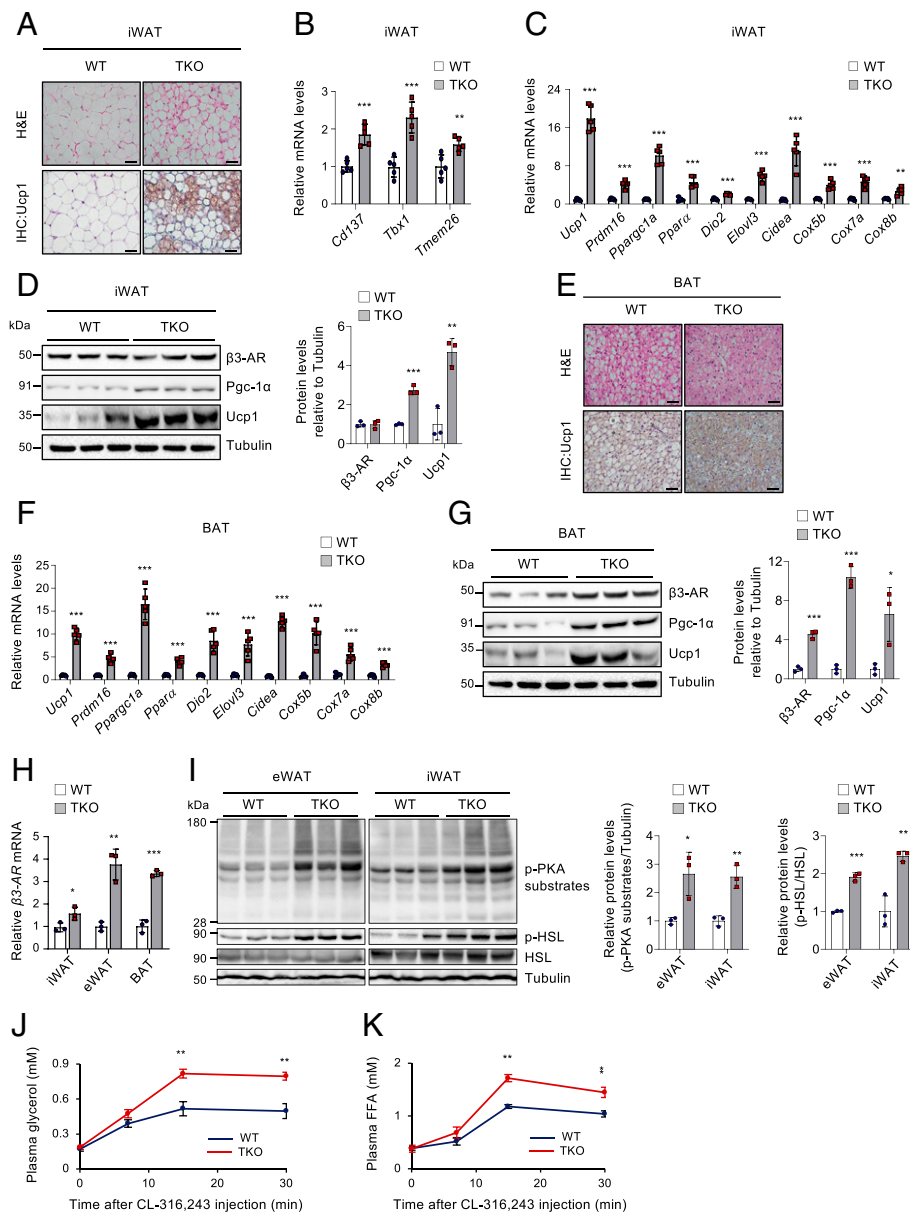


**Fig. 3.** Adipose TET deficiency increases the responsiveness to  $\beta$ 3-AR agonist in vivo. WT and *Tet* TKO mice were administered CL-316,243 (1 mg/kg body weight/d) intraperitoneally daily for three consecutive days. (A) Representative hematoxylin and eosin (H&E) (Top) and immunohistochemical staining for Ucp1 (Bottom) in iWAT of CL-316,243-treated mice.  $n = 4$ . (Scale bar, 50  $\mu$ m.) (B and C) mRNA levels of beige adipocyte-selective genes (B) or thermogenesis-related genes (C) relative to *Gapdh* in iWAT of CL-316,243-treated mice.  $n = 5$ . (D) Immunoblot analysis (Left) and quantification (Right) of  $\beta$ 3-AR, Pgc-1 $\alpha$ , and Ucp1 proteins in iWAT of CL-316,243-treated mice.  $\alpha$ -Tubulin served as a loading control.  $n = 3$ . (E) Representative H&E (Top) and immunohistochemical staining for Ucp1 (Bottom) in BAT of CL-316,243-treated mice.  $n = 4$ . (Scale bar, 50  $\mu$ m.) (F) mRNA levels of thermogenesis-related genes relative to *Gapdh* in BAT of CL-316,243-treated mice.  $n = 5$ . (G) Immunoblot analysis (Left) and quantification (Right) of  $\beta$ 3-AR, Pgc-1 $\alpha$ , and Ucp1 proteins in BAT of CL-316,243-treated mice.  $\alpha$ -Tubulin served as a loading control.  $n = 3$ . (H)  $\beta$ 3-AR mRNA levels relative to *Gapdh* in ATs (iWAT, eWAT, or BAT) of CL-316,243-treated mice.  $n = 3$ . (I) Immunoblot analysis (Left) and quantification (Right) of phosphorylated (p)-PKA substrates, p-HSL, and total HSL proteins in eWAT or iWAT of CL-316,243-treated mice.  $\alpha$ -Tubulin served as a loading control.  $n = 3$ . (J and K) In vivo lipolysis assay in WT and *Tet* TKO mice stimulated with CL-316,243. Plasma glycerol (J) and free fatty acid (FFA) (K) levels were quantified at the indicated time points.  $n = 3$ . All data are presented as the mean  $\pm$  SD. The  $P$  values were determined by unpaired Student's  $t$  test. \* $P < 0.05$ , \*\* $P < 0.005$ , \*\*\* $P < 0.0005$  versus WT. IHC, immunohistochemistry.

that induces mild fat browning (6). Histological analyses revealed that the iWAT of *Tet* TKO mice possessed more abundant Ucp1<sup>+</sup> multilocular adipocytes following CL-316,243 treatment compared to WT control (Fig. 3A). The iWAT of *Tet* TKO mice also displayed higher mRNA levels of genes associated with beiging (namely, *Cd137*, *Tbx1*, and *Tmem26*), thermogenesis (e.g., *Ucp1*, *Ppargc1a*, *Ppar $\alpha$* ), lipolysis (e.g., *Pnpl2*, *Lipe*), and fatty acid oxidation (e.g., *Acadm*, *Acadl*, *Acox1*) (Fig. 3B and C and SI Appendix, Fig. S6 A and B). Levels of Pgc-1 $\alpha$  and Ucp1 proteins were also higher in the iWAT of *Tet* TKO mice (Fig. 3D). A previous report showed that mice with *Fabp4-Cre*-mediated deletion of *Tet1* exhibited a depot-specific effect; they displayed increased thermogenic gene expression only in iWAT but not in BAT (39). However, the interscapular BAT of *Tet* TKO mice showed similar phenotypes as those observed in iWAT, including enhanced browning (Fig. 3E) and an elevated expression of  $\beta$ 3-AR and genes associated with thermogenesis, lipolysis, and fatty acid oxidation (Fig. 3F and G and SI Appendix, Fig. S6 C and D). Furthermore, both iWAT and BAT from *Tet* TKO mice contained higher amounts of mitochondrial DNAs compared to those from WT controls (SI Appendix, Fig. S6 E and F).

Together, these results suggest that TET loss promotes BAT activation as well as WAT browning. Notably, the mRNA levels of  $\beta$ 3-AR were higher in adipose depots (i.e., iWAT, eWAT, and BAT) from *Tet* TKO mice, more prominently in the latter two, when compared to WT controls (Fig. 3H). Consistently, *Tet* TKO mice displayed enhanced  $\beta$ -adrenergic signaling and in vivo lipolytic responses upon  $\beta$ 3-AR agonist treatment, as determined by increased phosphorylation of PKA substrates and HSL (Fig. 3I), and more robust release of plasma glycerol and free fatty acids (Fig. 3J and K). Collectively, these results suggest that adipose TET deficiency leads to elevated  $\beta$ 3-AR expression and increases the sensitivity to  $\beta$ 3-AR stimulation in vivo.

**Adipocyte-Specific *Tet* TKO Mice Are Resistant to Diet-Induced Obesity.**  $\beta$ 3-AR is substantially repressed in various animal models of obesity, and this  $\beta$ 3-AR down-regulation has been considered a key contributing factor that causes catecholamine resistance in obesity (16–18). As TET proteins negatively regulated  $\beta$ 3-AR, we next asked whether *Tet* expression was altered under persistent nutrient surplus. Notably, levels of *Tet1*, *Tet2*, and *Tet3* mRNAs (Fig. 4A) and those of 5hmCs (Fig. 4B and C) were significantly

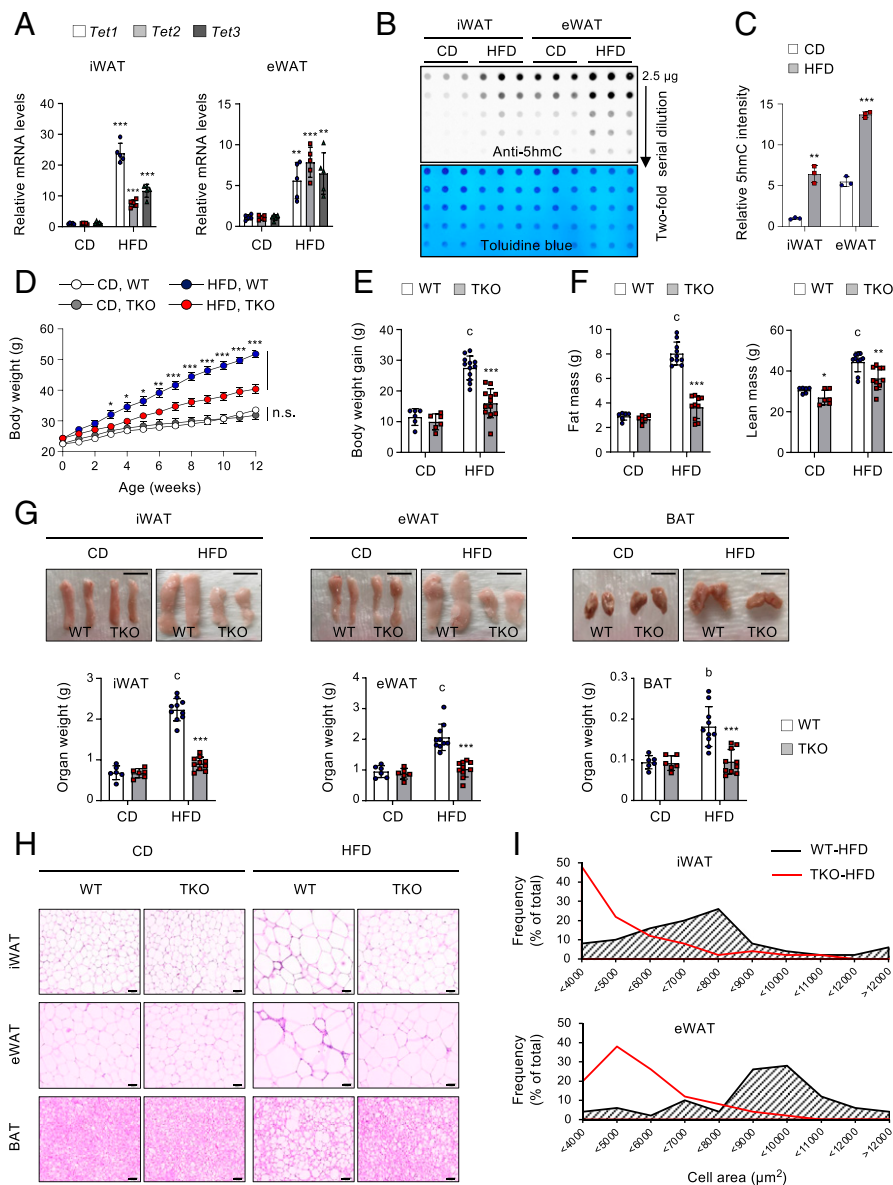


**Fig. 4.** Adipocyte *Tet* expression is elevated in obesity, and *Tet* TKO mice resist diet-induced obesity. (A) *Tet1*, *Tet2*, and *Tet3* mRNA levels relative to *Gapdh* in iWAT and eWAT from C57BL/6 male mice fed either CD or HFD for 12 wk. *n* = 5. (B) Genomic 5hmC levels in iWAT and eWAT from the mice shown in A. Toluidine blue staining confirmed blotting of equal amounts of DNAs. (C) Quantification of relative 5hmC intensity from the image shown in B. (D) Changes in body weight of WT and *Tet* TKO mice fed either CD or HFD. *n* = 6–12. (E) Summary of body weight gain in WT and *Tet* TKO mice fed either CD (*n* = 6) or HFD (*n* = 12) for 12 wk. (F) Absolute amount of fat mass (Left) and lean mass (Right) from WT and *Tet* TKO mice fed either CD (*n* = 6) or HFD (*n* = 10). (G) Representative photographs of iWAT, eWAT, and BAT of WT and *Tet* TKO mice fed either CD or HFD (Top). A summary of the weights of each fat pad is also shown (Bottom). *n* = 6 mice fed CD; *n* = 10 mice fed HFD. (Scale bar, 1 cm.) (H and I) Hematoxylin and eosin staining (H; *n* = 10) and frequency distribution of adipocyte cell size (I) in iWAT and eWAT of WT and *Tet* TKO mice fed either CD or HFD. (Scale bar, 100  $\mu$ m.) All data are presented as the mean  $\pm$  SD. The *P* values were determined by unpaired Student's *t* test. \**P* < 0.05, \*\**P* < 0.005, \*\*\**P* < 0.0005 versus WT; <sup>b</sup>*P* < 0.005, <sup>c</sup>*P* < 0.0005 versus CD. n.s., not significant.

elevated in iWAT and epididymal WAT (eWAT) of mice fed a HFD (60% energy as fat) compared to the levels in mice fed a chow diet (CD; 10% energy as fat). *TET1*, *TET2*, and *TET3* mRNA levels also tended to increase in patients with obesity or diabetes, compared to lean individuals, although this difference did not reach statistical significance, possibly due to negative feedback on TET expression in humans under obese or diabetic conditions (SI Appendix, Fig. S7A). These results suggest that *Tet* expression and function are nutritionally regulated in ATs and that TET proteins may play a role in diet-induced obesity.

To clarify the physiological function of TET proteins in the development of obesity, *Tet* TKO and WT littermate mice were fed either a CD or HFD for 12 wk, starting at 8 wk of age. There was no difference in weight gain in response to the CD (Fig. 4D and E and SI Appendix, Fig. S7B). However, *Tet* TKO mice were more resistant to weight gain in response to a HFD than were WT mice, despite comparable food intakes (Fig. 4D and E and SI Appendix, Fig. S7B and C). The lower body weight of *Tet* TKO mice primarily resulted from a reduction in fat mass with only a marginal alteration in lean body mass (Fig. 4F and SI Appendix, Fig. S7D and E). Examination of dissected fat tissues confirmed that iWAT, eWAT, and BAT

were significantly smaller in these mice (Fig. 4G). Histologically, both WAT and BAT from HFD-fed *Tet* TKO mice contained adipocytes possessing smaller lipid droplets compared with those of WT controls, whereas there was no discernible difference in adipocyte size of mice fed a CD (Fig. 4H and I). Upon HFD feeding, the average adipocyte size increased by  $\sim 3.56$ -fold in iWAT of WT mice but only  $\sim 1.68$ -fold in *Tet* TKO mice, and similar reductions were also observed in eWAT (by  $\sim 1.41$ -fold) and BAT (by  $\sim 3.25$ -fold) of *Tet* TKO mice (SI Appendix, Fig. S7F). These data indicate that adipose TET deficiency robustly inhibits the development of obesity and obesity-induced adipocyte hypertrophy. Previous reports suggested that TET proteins were required for early adipogenic differentiation in vitro (40, 41). However, the observed difference in body weight change was not attributable to impaired adipogenesis in vivo because mRNA levels of known markers or regulators of adipogenesis were comparable between WT and *Tet* TKO mice on either diet, consistent with the fact that adiponectin-Cre we used was active in mature adipocytes (48) (SI Appendix, Fig. S7G–J). Furthermore, we confirmed that *Tet* TKO female mice were also resistant to diet-induced obesity, mainly due to a reduction in fat mass (SI Appendix, Fig. S8).

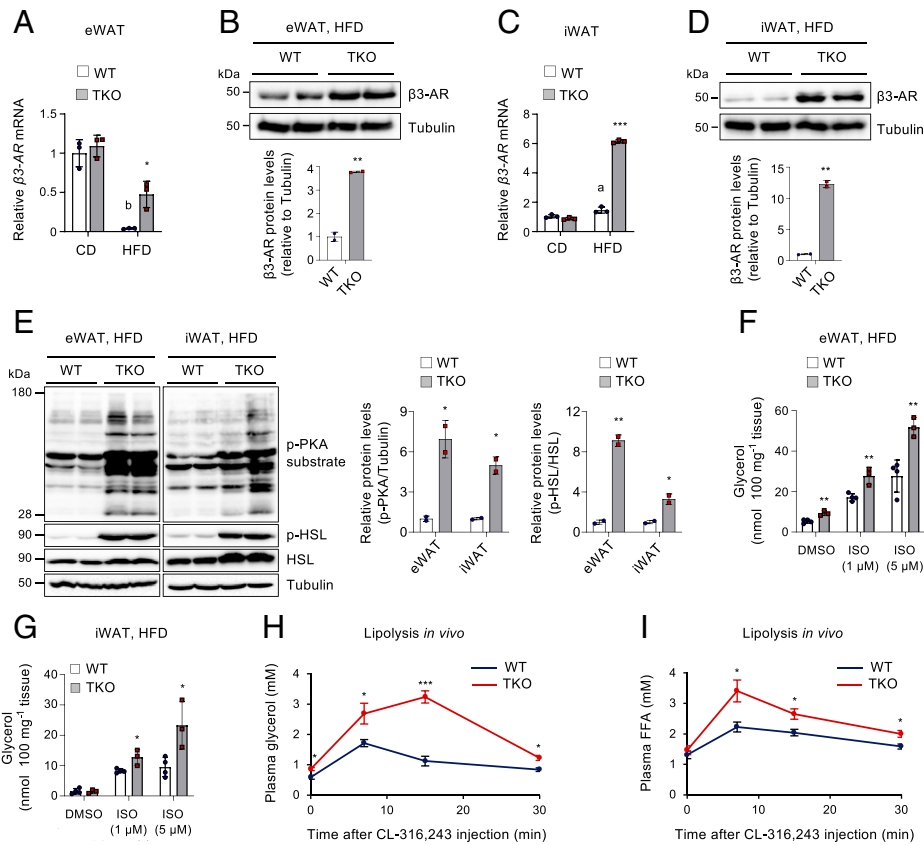


**Fig. 5.** TET deficiency resists obesity-associated catecholamine resistance by blocking  $\beta_3$ -AR reduction during diet-induced obesity. (A)  $\beta_3$ -AR mRNA levels relative to *Gapdh* in eWAT from WT and *Tet* TKO mice fed either CD or HFD.  $n = 3$ . (B) Immunoblot analysis (Top) and quantification (Bottom) of  $\beta_3$ -AR proteins in eWAT from WT and *Tet* TKO mice fed an HFD.  $\alpha$ -Tubulin served as a loading control. (C)  $\beta_3$ -AR mRNA levels relative to *Gapdh* in iWAT from WT and *Tet* TKO mice fed either CD or HFD.  $n = 3$ . (D) Immunoblot analysis (Top) and quantification (Bottom) of  $\beta_3$ -AR proteins in iWAT from WT and *Tet* TKO mice fed an HFD.  $\alpha$ -Tubulin served as a loading control. (E) Immunoblot analysis (Left) and quantification (Right) of phosphorylated (p)-PKA substrates, p-HSL, and total HSL proteins in eWAT or iWAT from HFD-fed WT and *Tet* TKO mice.  $\alpha$ -Tubulin served as a loading control. (F and G) Ex vivo lipolysis in eWAT (F) and iWAT (G) isolated from HFD-fed WT and *Tet* TKO mice after stimulation with or without ISO at the indicated concentrations.  $n = 3-4$ . (H and I) In vivo lipolysis in HFD-fed WT and *Tet* TKO mice. Plasma glycerol (H) and free fatty acid (I) levels were quantified after administration of CL-316,243.  $n = 3-4$ . All data are presented as the mean  $\pm$  SD. The  $P$  values were determined by unpaired Student's  $t$  test. \* $P < 0.05$ , \*\* $P < 0.005$ , \*\*\* $P < 0.0005$  versus WT; <sup>a</sup> $P < 0.05$ , <sup>b</sup> $P < 0.005$  versus CD. DMSO, dimethyl sulfoxide.

**Adipocyte-Specific *Tet* TKO Mice Resist  $\beta_3$ -AR Reduction and Catecholamine Resistance during Diet-Induced Obesity.** Activation of the  $\beta_3$ -adrenergic signaling increases energy expenditure by triggering lipolysis, fatty acid oxidation, and thermogenesis, ultimately leading to a decline in fat accumulation and obesity resistance (1, 2). Thus, we next sought to determine whether the restricted AT hypertrophy in the HFD-fed *Tet* TKO mice resulted from increased  $\beta$ -adrenergic responsiveness through enhanced  $\beta_3$ -AR expression.  $\beta_3$ -AR was substantially suppressed in eWAT of WT mice after 12 wk on a HFD, but this was substantially blocked in *Tet* TKO mice (Fig. 5A). Protein levels of  $\beta_3$ -AR also remained significantly higher in HFD-fed *Tet* TKO mice (Fig. 5B). HFD feeding did not affect  $\beta_3$ -AR mRNA levels in iWAT and BAT of WT mice, but TET deficiency led to an elevated  $\beta_3$ -AR expression in these ATs following HFD feeding (Fig. 5C and D and *SI Appendix*, Fig. S9A). Consistent with the higher levels of  $\beta_3$ -AR expression, both eWAT and iWAT of HFD-fed *Tet* TKO mice displayed significantly enhanced  $\beta$ -AR signaling, as determined by increased phosphorylation of PKA substrates and HSL (Fig. 5E).

To further confirm whether increased  $\beta_3$ -AR expression and signaling affect lipolytic responses, eWAT and iWAT were isolated from HFD-fed WT or *Tet* TKO mice and treated with ISO. The ISO-stimulated lipolysis, as assessed by the release of glycerol and free fatty acids, was significantly enhanced in these explants of *Tet* TKO mice compared to those from WT mice (Fig. 5F and G and *SI Appendix*, Fig. S9B). Moreover, TET deficiency also significantly promoted lipolysis in isolated primary ATs treated with forskolin or IBMX (*SI Appendix*, Fig. S9C). We also observed a mild increase in lipolytic responses in the BAT from *Tet* TKO mice (*SI Appendix*, Fig. S9D and E). To further confirm the lipolytic activity in vivo, we injected mice intraperitoneally with CL-316,243. Consistent with data obtained in vitro, the serum glycerol and free fatty acid levels

were significantly higher in *Tet* TKO mice than in WT mice (Fig. 5H and I). Together, these results suggest that TET deficiency resisted  $\beta_3$ -AR reduction during chronic HFD challenges and thereby rendered adipocytes more sensitive to catecholamines. This may have contributed to the maintenance of higher levels of  $\beta$ -agonist-stimulated lipolytic capacity and resistance to adipocyte hypertrophy.

**Adipose TET Deficiency Leads to the Maintenance of Higher Capacity for Thermogenesis and Energy Expenditure during Chronic Overnutrition.** Excess caloric intake activates thermogenesis as a means to increase energy expenditure to prevent excess fat accumulation and obesity (3, 4). This diet-induced thermogenesis is critically dependent on  $\beta$ -AR signaling (3, 4). However, energy expenditure fails to fully compensate for chronic overnutrition during the development of obesity. Indeed, consistent with  $\beta$ -AR reduction and decreased  $\beta$ -AR responses, obese humans and animals display diminished adipose thermogenesis (51). As  $\beta_3$ -AR expression and  $\beta$ -adrenergic responsiveness were maintained at higher levels in *Tet* TKO mice fed an HFD, we next examined whether TET deficiency resists the reduction of energy expenditure and thermogenesis during chronic overnutrition. To test this possibility, we first performed indirect calorimetry on HFD-fed WT and *Tet* TKO mice maintained at different ambient temperatures (30 °C, 22 °C, and 4 °C). HFD-fed *Tet* TKO mice exhibited significantly higher rates of oxygen consumption ( $V_{O_2}$ ), carbon dioxide production ( $V_{CO_2}$ ), and heat dissipation under all conditions, and these alterations became more pronounced as the temperature dropped (Fig. 6A–D and *SI Appendix*, Fig. S10A and B). However, the levels of motor activity were comparable between both groups of mice (*SI Appendix*, Fig. S10C). The respiratory exchange rate ( $V_{CO_2}/V_{O_2}$ ) indicated that a greater proportion of carbohydrate metabolism was preserved in HFD-fed *Tet* TKO mice during dark periods at 22 °C

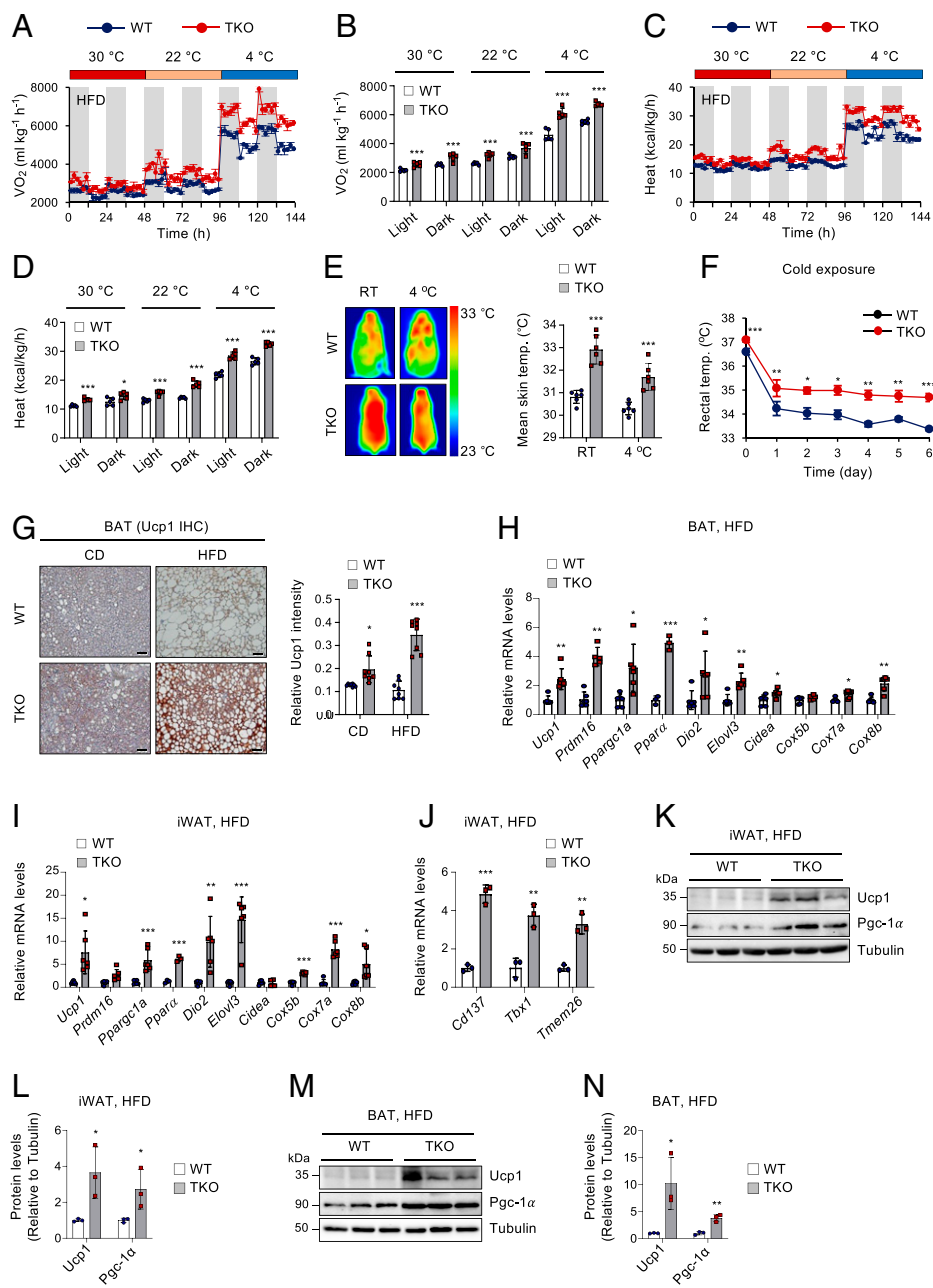


**Fig. 6.** TET deficiency leads to the maintenance of a higher capacity for thermogenesis and energy expenditure under chronic overnutrition. (A–D) Indirect calorimetry of HFD-fed WT and *Tet* TKO mice maintained at 30°C, 22°C, and 4°C to obtain  $VO_2$  (A), average  $VO_2$  (B), heat production (C), and average heat production (D) data.  $n = 5$ . (E) Representative dorsal infrared thermal images (Left) and mean skin temperature (Right) of HFD-fed WT and *Tet* TKO mice housed at room temperature (RT) or 4°C for 1 wk.  $n = 6$ . (F) Changes in rectal temperatures of HFD-fed WT and *Tet* TKO mice during cold exposure.  $n = 7$  WT mice;  $n = 9$  *Tet* TKO mice. (G) Representative immunohistochemical staining for Ucp1 ( $n = 6$ ; Left) in BAT sections from WT and *Tet* TKO mice fed either CD or HFD for 12 wk. Quantification results are also shown (Right).  $n = 8$ . (Scale bar, 100  $\mu m$ .) (H and I) mRNA levels of thermogenesis-related genes relative to *Gapdh* in BAT (H) or iWAT (I) from HFD-fed WT and *Tet* TKO mice.  $n = 5$ –6 (except *Ppar $\alpha$* ,  $n = 3$ ). (J) mRNA levels of beige adipocyte-selective genes relative to *Gapdh* in iWAT from HFD-fed WT and *Tet* TKO mice.  $n = 8$ . (K–N) Immunoblot analysis and quantification of Ucp1 and Pgc-1 $\alpha$  proteins in iWAT (K and L) or BAT (M and N) from WT and *Tet* TKO mice.  $n = 3$ . ( $\alpha$ -Tubulin served as a loading control.  $n = 3$ ). All data are presented as the mean  $\pm$  SD. The  $P$  values were determined by unpaired Student's  $t$  test. \* $P < 0.05$ , \*\* $P < 0.005$ , \*\*\* $P < 0.0005$  versus WT. IHC, immunohistochemistry.

and 4°C (SI Appendix, Fig. S10D), which was likely due to reduced fat deposition. To further correct metabolic rates for body mass, we performed regression-based ANCOVA using body weights as a covariate. We observed a group-specific effect between WT and *Tet* TKO mice, which was independent of a difference in body mass at 30°C and 4°C, whereas both genotypes fell on a similar regression line at 22°C (SI Appendix, Fig. S10E). It is possible that the effect was stronger at 4°C because levels of catecholamine released by sympathetic nerve terminals were up-regulated upon cold exposure. As *Tet*-deficient adipocytes express higher  $\beta_3$ -AR compared to WT cells, they would exhibit stronger responsiveness to the catecholamines. When we plotted ANCOVA-predicted metabolic rates at a given body mass of 40 g (kcal/h/40 g), as suggested previously as an alternative analysis when there is absolutely no overlap in the data from two groups on the mass axis (52, 53), as observed in our cases (Fig. 4), *Tet* TKO mice displayed significantly higher metabolic rates compared to WT mice under all conditions (SI Appendix, Fig. S10F).

Together, these results indicate that *Tet* TKO mice maintained a higher capacity of thermogenesis despite chronic overnutrition. Consistent with these observations, HFD-fed *Tet* TKO mice maintained significantly higher surface and core (rectal) temperatures than did WT littermates under basal conditions and after cold exposure (Fig. 6 E and F and SI Appendix, Fig. S10G). Thus, these results suggest that TET proteins restrict adaptive thermogenesis and energy expenditure during periods of chronic overnutrition.

Consistent with these observations, HFD-fed *Tet* TKO mice possessed smaller brown adipocytes with increased Ucp1 expression in BAT compared to WT controls (Fig. 6G) and exhibited elevated levels of thermogenic genes in both BAT and iWAT (Fig. 6 H and I). They also showed higher mRNA expressions of beige marker genes in iWAT (Fig. 6J). The levels of Ucp1 and Pgc-1 $\alpha$  proteins were also significantly higher in both iWAT and BAT of HFD-fed TKO mice (Fig. 6 K–N). Furthermore, HFD consumption significantly reduced the expression of *Ppargc1a*, a



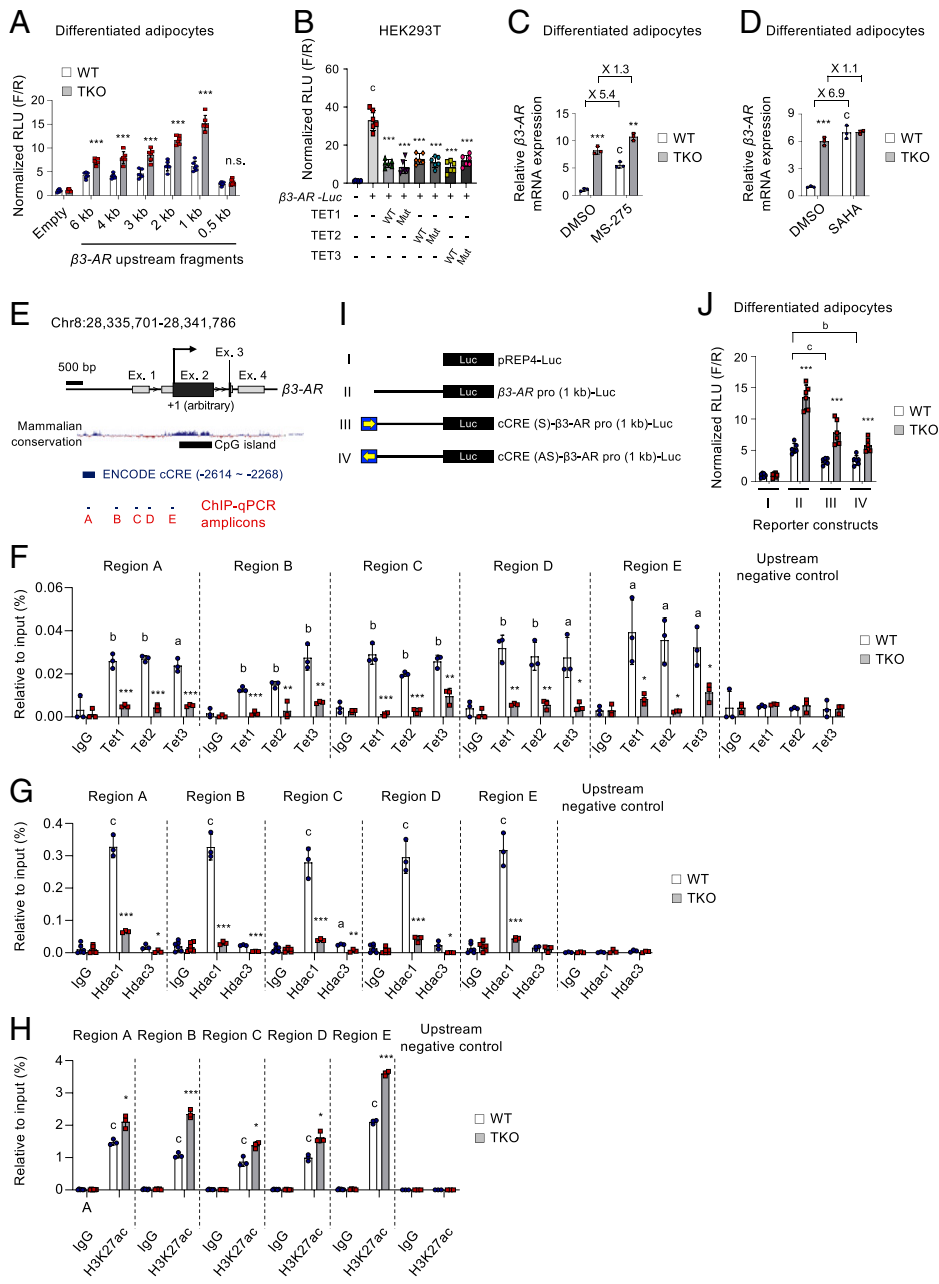


**Fig. 7.** TET proteins cooperate with HDACs to directly suppress  $\beta 3$ -AR transcription. (A) pREP4-based luciferase reporter activities driven by serially truncated  $\beta 3$ -AR promoters in WT and *Tet* TKO adipocytes. Results were normalized to Renilla luciferase activity.  $n = 6$ . (B) pREP4-based luciferase reporter activities driven by the  $\beta 3$ -AR (1 kb) promoter in HEK293T cells transfected with WT or mutant TET1, TET2, and TET3 plasmids.  $n = 6$ . (C and D) mRNA expression of  $\beta 3$ -AR relative to *Gapdh* in WT and *Tet* TKO adipocytes stimulated with or without MS-275 (10  $\mu$ M, 24 h) (C) or a pan-HDAC inhibitor, SAHA (20  $\mu$ M, 6 h) (D).  $n = 3$ . (E) The genomic configuration of the mouse  $\beta 3$ -AR gene locus. Locations of ChIP-qPCR amplicons, mammalian conservation, CpG islands, and Encyclopedia of DNA Elements (ENCODE) *cis*-CRE (cCRE) are shown. (F–H) ChIP-qPCR assays for Tet1, Tet2, and Tet3 (F); HDAC1 and HDAC3 (G); and acetylated H3K27 (H3K27ac) (H) for regions A–E shown in E. Enrichment at the nonbinding  $\beta 3$ -AR upstream region was used as a negative control.  $n = 3$ . (I) Schematic representation of the  $\beta 3$ -AR (1 kb) promoter-driven luciferase constructs. Yellow arrows indicate the direction of the incorporated ENCODE cCRE element shown in E. (J) pREP4-based luciferase reporter assay for the  $\beta 3$ -AR promoters shown in (I) in WT and *Tet* TKO adipocytes.  $n = 6$ . All data are presented as the mean  $\pm$  SD. The  $P$  values were determined by unpaired Student's  $t$  test. \* $P < 0.05$ , \*\* $P < 0.005$ , \*\*\* $P < 0.0005$  versus WT; <sup>a</sup> $P < 0.05$ , <sup>b</sup> $P < 0.005$ , <sup>c</sup> $P < 0.0005$  versus reporter only (B), dimethyl sulfoxide (DMSO) (C), immunoglobulin G (IgG) (F–H), and reporter II in WT (J). Ex, exon; Mut, catalytically inactive mutant; n.s., not significant; RLU, relative light units; F/R, firefly/renilla.

critical regulator of mitochondrial biogenesis and energy metabolism (54), in iWAT and eWAT, which was potentially blocked by TET deficiency (SI Appendix, Fig. S11A). *Ppargc1a* was also maintained at a higher level in BAT from HFD-fed *Tet* TKO mice. Consistently, various adipose depots from HFD-fed *Tet* TKO mice maintained higher mitochondrial DNA content and fatty acid oxidation capacity (SI Appendix, Fig. S11 B and C). Together, these data suggest that elevated TET expression in chronic overnutrition may promote obesity by limiting the energy expenditure and thermogenic potentials of both beige and BAT adipocytes.

**TET Proteins Cooperate with HDACs to Directly Repress  $\beta 3$ -AR Transcription in Adipocytes.** Given the inverse correlation between  $\beta 3$ -AR and *Tet* expressions, we assessed whether TET proteins could directly regulate  $\beta 3$ -AR promoter activity. We cloned serially truncated versions of the promoter regions (from 0.5 kb to 6 kb) of the mouse  $\beta 3$ -AR gene linked to a luciferase reporter ( $\beta 3$ -AR-*Luc*) into pREP4 plasmid that forms chromatin in mammalian cells (55, 56). Except for the 0.5-kb proximal

region, all fragments larger than 1 kb significantly stimulated reporter activities in WT adipocytes, and this was further enhanced in *Tet* TKO cells (Fig. 7A), indicating TET-mediated suppression of the  $\beta 3$ -AR promoter activity. In another reporter assay in HEK293T cells, both WT and catalytically inactive mutants of TET proteins were capable of suppressing the  $\beta 3$ -AR promoter activity, confirming that TET proteins controlled  $\beta 3$ -AR transcription, mainly in a catalytic activity-independent manner (Fig. 7B).

TET proteins often mediate transcriptional silencing through their incorporation into HDAC complexes (37–39). Thus, we next investigated whether HDACs are implicated in TET-mediated thermogenic gene regulation. MS-275, a selective inhibitor of HDAC1 and HDAC3, up-regulated various thermogenic genes in both WT and *Tet* TKO adipocytes; however, the fold induction by MS-275 was significantly decreased in *Tet* TKO cells compared to WT cells (Fig. 7C and SI Appendix, Fig. S12 A–C), suggesting the possible implication of HDACs, including HDAC1 and HDAC3, in TET-mediated  $\beta 3$ -AR suppression. However, upon MS-275 treatment, *Tet* TKO adipocytes

still expressed higher levels of thermogenic genes compared to WT controls. Thus, it is possible that additional HDACs other than class I HDACs may also be implicated in the TET-mediated suppression of these thermogenic genes. To test this possibility, we treated WT and *Tet* TKO adipocytes with suberoylanilide hydroxamic acid (SAHA; also known as vorinostat), a pan-HDAC inhibitor that potently inhibits class I and class II HDACs. SAHA exhibited little effects on thermogenic gene expression in *Tet* TKO adipocytes, whereas it robustly up-regulated it in WT controls (Fig. 7D and *SI Appendix*, Fig. S12 A and B). Furthermore, when treated with SAHA, both WT and *Tet* TKO adipocytes expressed thermogenic genes at comparable levels. Together, these results indicate that TET proteins directly repress  $\beta$ 3-AR and other thermogenic genes by modulating HDACs.

As previously reported (38, 39), we also confirmed that TET proteins physically associated with HDAC1 and HDAC3 (*SI Appendix*, Fig. S12 D–F). HDAC enzymes deacetylate histones and suppress transcription. ChIP-qPCR revealed that WT adipocytes exhibited a significant accumulation of all three TET proteins and HDAC1 on the upstream regulatory regions of the  $\beta$ 3-AR gene locus (Fig. 7 E–G). However, the occupancy of HDAC3 was very low and not significant when compared with enrichment by immunoglobulin G controls (Fig. 7G). Notably, *Tet* TKO adipocytes exhibited a diminished occupancy of both TET and HDAC1 proteins in the  $\beta$ 3-AR gene locus and thus possessed increased levels of acetylated H3K27, the active histone marker (Fig. 7 F–H). The immunoprecipitated genomic DNA samples showed no enrichment at the nonbinding region upstream of  $\beta$ 3-AR. These results suggest that TET proteins recruit HDAC1 to the  $\beta$ 3-AR gene promoter, ultimately leading to histone deacetylation for transcriptional suppression.

The Encyclopedia of DNA Elements project (57) predicted a 346-bp upstream DNA element located between  $-2,614$  and  $-2,268$  as one of the candidate *cis*-regulatory elements in the  $\beta$ 3-AR locus (Fig. 7E, *region A* and *SI Appendix*, Fig. S12G). This region is well conserved among mammalian species (Fig. 7E), and its histone acetylation was controlled by TET-HDAC interaction (Fig. 7 F–H, *region A*). To confirm the functionality of this element, we constructed additional reporters by incorporating this element upstream of the  $\beta$ 3-AR promoter (1 kb) in both orientations (Fig. 7I). The presence of this element significantly diminished  $\beta$ 3-AR promoter activity in adipocytes regardless of its orientation (Fig. 7J, *compare reporter activities in WT cells*), and this was significantly relieved by TET deficiency (Fig. 7J), confirming its silencer-like function. Together, these results indicate that TET proteins directly repress  $\beta$ 3-AR transcription by the epigenetic modification of its promoter via the recruitment of HDACs.

## Discussion

Here, we report that TET proteins are crucial epigenetic suppressors of  $\beta$ 3-AR expression and  $\beta$ -adrenergic responsiveness in adipocytes. A pan-TET deficiency significantly elevated  $\beta$ 3-AR expression and sensitivity to  $\beta$ -AR agonists in cultured cells and mice, thus potentiating the  $\beta$ 3-AR-triggered downstream responses, including lipolysis, thermogenic gene induction, mitochondrial respiration, and fat browning. Notably, adipose *Tet* expression was elevated by excess nutrient uptake. During the development of HFD-induced obesity, adipose-specific pan-TET deficiency led to the maintenance of higher  $\beta$ 3-AR expression and  $\beta$ -adrenergic responsiveness in both WAT and BAT. As a result, *Tet* TKO mice were strikingly resistant to diet-induced obesity, inflammation, and related metabolic defects.

Previous studies proposed the potential regulatory roles of TET proteins in adipocyte differentiation and function. However, knockdown of *Tet1* or *Tet2* exerts controversial effects on adipogenic differentiation in vitro (40–42). Our data show that TET proteins differentially affect adipogenesis in vitro, depending on the differentiation stage. Ablation of all TET proteins in preadipocytes or during adipogenic induction completely blocked the formation of mature adipocytes, but its loss at a later stage did not exhibit any significant antiadipogenic effects. TET proteins may be essential for the early adipogenic commitment of progenitor cells, presumably by regulating key adipogenic regulators, including PPAR $\gamma$ , as previously suggested (41, 58). However, they may be largely dispensable for adipogenesis after preadipocytes are committed to adipogenic lineage. Furthermore, a previous report showed that *Tet1* deletion in mice suppressed thermogenesis by repressing *Ucp1* and *Ppargc1a* in beige adipocytes (39). Thus, the *Tet1* knockout mice were partially protected from cold stress, diet-induced obesity, and associated metabolic dysfunctions. In contrast, another report showed that *Tet1* haploinsufficiency predisposed mice to diet-induced obesity and aggravated glucose intolerance (42). Thus, the exact roles of TET proteins in metabolism remain unclear. Here, we deleted all three *Tet* genes using *Adiponectin-Cre*, which is expressed in a highly adipocyte-specific manner (48, 59), and confirmed that triple TET deficiency substantially increases  $\beta$ 3-AR expression and function in both ATs and cultured adipocytes, and enhances fat lipolysis, browning, and thermogenic gene expression. The resulting phenotype was more pronounced than that of cells and mice rendered *Tet1*-deficient with *Fabp4-Cre* (39), which is expressed in both AT and nonadipose tissue (59). Furthermore, although *Tet1* deficiency was previously shown to increase thermogenic gene expression only in iWAT but not in BAT (39), our *Tet* TKO mice showed similar phenotypes in both WAT and BAT. The weaker phenotypes in *Tet1* knockout mice, compared to our *Tet* TKO mice, may be attributed to the functional redundancy among TET family members.

Our analysis identified  $\beta$ 3-AR as the direct target of TET proteins that, in turn, controlled downstream  $\beta$ -adrenergic responses. From a molecular standpoint, we showed that TET proteins recruited HDACs, particularly HDAC1, to the  $\beta$ 3-AR promoter to directly suppress its transcription. TET deficiency led to a dissociation of HDACs from the  $\beta$ 3-AR gene promoter, thereby switching the repressive chromatin state to the active state. Pharmacological inactivation of HDACs led to significant induction of various thermogenic genes in WT adipocytes, but its effect was decreased in *Tet* TKO adipocytes. Notably, this TET-HDAC cooperation occurred via a physical interaction between TET and HDAC enzymes, and functional cooperation did not require the catalytic activity of the TET proteins in reporter assays for  $\beta$ 3-AR promoter activities. HDACs, particularly class I HDACs, have recently emerged as promising molecular targets for treating obesity and type 2 diabetes (60). TET deficiency mimics the effects of HDAC inhibition in vitro and in vivo. Genetic or pharmacological inactivation of HDACs (particularly HDAC1 or HDAC3) simultaneously activates  $\beta$ 3-AR, *Ucp1*, and *Ppargc1a* by increasing histone acetylation at these gene loci (61–63). Consistently, HDAC inactivation in mice facilitates systemic energy expenditure by promoting WAT browning, lipolysis, thermogenesis, and oxidative metabolism, and thus prevents obesity and insulin resistance (61, 62, 64). All these phenotypes are recapitulated in our *Tet* TKO mice. Thus, TET proteins may control thermogenesis and energy expenditure by modulating the genomic distribution of HDACs. As TET deficiency resists the suppressive effects of chronic overnutrition on

$\beta$ 3-AR expression and function, targeting the TET-HDAC- $\beta$ 3-AR axis could provide a way to reprogram fat cell fates and functions to treat obesity and related metabolic diseases.

Our data also suggested that HFD-induced elevation of TET expression is causally linked to the initiation and development of diet-induced obesity.  $\beta$ 3-AR expression and  $\beta$ -adrenergic signaling are significantly suppressed during chronic nutrient overload, ultimately leading to catecholamine resistance in obesity (13–18). Despite chronic overnutrition, TET deficiency may allow for sustained catecholamine sensitivity by blocking  $\beta$ 3-AR down-regulation, thus enhancing  $\beta$ -adrenergic signaling, lipolysis, mitochondrial biogenesis, fatty acid oxidation, and thermogenesis. Ultimately, it may result in an overall increase in energy expenditure to prevent fat accumulation and obesity. Moreover, TET proteins seem to exert their primary effects at the level of lipolysis. TET loss leads to a remarkable increase in  $\beta$ -agonist-stimulated lipolysis *in vitro* and *in vivo*. The increased lipolysis may contribute to the maintenance of smaller and metabolically healthier adipocytes by robustly antagonizing fat storage and AT hypertrophy, despite excess nutrient uptake. AT expansion during periods of nutritional affluence promotes inflammation and adipocyte dysfunction (65). Consistent with reduced fat cell size, *Tet* TKO mice were markedly protected from inflammation and metabolic defects when fed an HFD (*SI Appendix, Figs. S13–S15*). Thus, it is likely that the improved metabolic phenotypes observed in the HFD-fed *Tet* TKO mice may primarily be attributable to the reduced AT hypertrophy and body weight gain. However, given the role of  $\beta$ 3-AR signals in antagonizing ectopic fat accumulation and obesity, our data suggest that TET-mediated modulation of catecholamine sensitivity may exert more fundamental effects on the metabolic phenotypes.  $\beta$ 3-ARs are abundantly expressed in murine ATs and serve as primary  $\beta$ -ARs. Agonists of  $\beta$ 3-ARs display antiobesity and antidiabetic effects in mice. However, low levels of  $\beta$ 3-AR expression in human white adipocytes (2, 66) seemed to limit the therapeutic efficacy of  $\beta$ 3-AR agonists in clinical trials (27). Thus, combined administration of selective  $\beta$ 3-AR agonists while boosting  $\beta$ 3-AR expression with pan-TET inhibitors may offer a therapeutic opportunity for treating human obesity and metabolic diseases.

It remains unknown how TET expression is up-regulated in ATs following HFD consumption. Recent studies have suggested that TET expression or function can be controlled by obesity- or type 2 diabetes-associated hyperglycemia (67–69). However, it was variably altered depending on the context and not directly assessed in ATs. In this regard, we note that 5hmC paradoxically accumulates more effectively under hypoxia (70–72), despite limited levels of oxygen, an essential cofactor for TET enzymes (32). HIF-1 $\alpha$  has been shown to activate *TET1*, *TET2*, and *TET3* transcription by directly binding to their promoters in various cells, including adipocytes

(70–72). As HFD-induced adipocyte expansion restricts oxygen availability within ATs (73), the subsequent HIF-1 $\alpha$  accumulation may stimulate *Tet* expression. Furthermore, recent studies showed that hypoxia-induced HIF-1 $\alpha$  triggers obesity-induced AT inflammation and adipocyte dysfunction, leading to insulin resistance (73). Notably, upon HFD feeding, mice lacking HIF-1 $\alpha$  in adipocytes largely phenocopied our *Tet* TKO mice, as both animal models exhibited resistance to diet-induced obesity, reduced macrophage accrual and inflammation, improved insulin sensitivity, glucose tolerance, and elevated energy expenditure and fatty acid oxidation (73–75). Together, these results suggest that adipose HIF-1 $\alpha$  and TET proteins may work in the same pathway to promote fat deposition and obesity in times of excessive nutrient uptake. More studies are warranted to determine whether and how the hypoxia–HIF-1 $\alpha$ –TET axis works to induce obesity and metabolic defects.

In summary, we identified TET proteins as pivotal epigenetic suppressors of  $\beta$ 3-AR in adipocytes that reduced the sensitivity to  $\beta$ -adrenergic stimulation *in vitro* and *in vivo*. Our findings shed light on the epigenetic control of  $\beta$ -adrenergic responses via TET–HDAC cooperation. Because loss of TET proteins in adipocytes robustly defended against the suppressive effects of chronic overnutrition on  $\beta$ -adrenergic sensitivity, thermogenesis, and energy expenditure, targeting the TET–HDAC– $\beta$ 3-AR axis may increase therapeutic options for treating obesity and related metabolic diseases.

## Materials and Methods

Mice carrying *LoxP*-targeted (floxed) *Tet1<sup>fl/fl</sup>*, *Tet2<sup>fl/fl</sup>*, and *Tet3<sup>fl/fl</sup>* have been described previously (76–78) and were provided by Dr. Anjana Rao (La Jolla Institute, CA, USA). *Adiponectin-Cre* (#010803) and *Cre-ERT2* (#8085) transgenic mice were obtained from the Jackson Laboratory. Detailed materials and methods can be found in *SI Appendix, SI Materials and Methods*.

**Data Availability.** RNA-sequencing datasets used in this study have been deposited in National Center for Biotechnology Information (NCBI) Gene Expression Omnibus (GEO) repository with the accession number [GSE178762](https://www.ncbi.nlm.nih.gov/geo/query/acc.cgi?acc=GSE178762).

**ACKNOWLEDGMENTS.** This work was supported by the National Research Foundation of Korea (Grants 2018R1D1A1B07049676, 2019R1F1A1063340, 2018R1A6A1A03025810, and 2017R1C1B2005604) and the Future-leading Project Research Fund of Ulsan National Institute of Science and Technology (Grant 1.220023.01). M.K. is also supported by the Center for Genomic Integrity, Institute for Basic Science (Grant IBS-R022-D1).

Author affiliations: <sup>a</sup>Department of Biological Sciences, Ulsan National Institute of Science and Technology, Ulsan 44919, Republic of Korea; <sup>b</sup>Department of Life Sciences, Jeonbuk National University, Jeonju 54896, Republic of Korea; <sup>c</sup>Department of Biomedical Engineering, Ulsan National Institute of Science and Technology, Ulsan 44919, Republic of Korea; and <sup>d</sup>Center for Genomic Integrity, Institute for Basic Science, Ulsan 44919, Republic of Korea

1. J. Robidou, T. L. Martin, S. Collins, Beta-adrenergic receptors and regulation of energy expenditure: A family affair. *Annu. Rev. Pharmacol. Toxicol.* **44**, 297–323 (2004).
2. B. A. Evans, J. Merlin, T. Bengtsson, D. S. Hutchinson, Adrenoceptors in white, brown, and brite adipocytes. *Br. J. Pharmacol.* **176**, 2416–2432 (2019).
3. E. T. Chouchani, S. Kajimura, Metabolic adaptation and maladaptation in adipose tissue. *Nat. Metab.* **1**, 189–200 (2019).
4. B. B. Lowell, B. M. Spiegelman, Towards a molecular understanding of adaptive thermogenesis. *Nature* **404**, 652–660 (2000).
5. A. Fedorenko, P. V. Lishko, Y. Kirichok, Mechanism of fatty-acid-dependent UCP1 uncoupling in brown fat mitochondria. *Cell* **151**, 400–413 (2012).
6. Y. Jiang, D. C. Berry, J. M. Graff, Distinct cellular and molecular mechanisms for  $\beta$ 3 adrenergic receptor-induced beige adipocyte formation. *eLife* **6**, e30329 (2017).
7. C. Cero *et al.*,  $\beta$ 3-Adrenergic receptors regulate human brown/beige adipocyte lipolysis and thermogenesis. *JCI Insight* **6**, e139160 (2021).
8. M. Ghorbani, S. Teimourian, R. Farzad, N. N. Asl, Apparent histological changes of adipocytes after treatment with CL 316,243, a  $\beta$ 3-adrenergic receptor agonist. *Drug Des. Devel. Ther.* **9**, 669–676 (2015).
9. E. Widén *et al.*, Association of a polymorphism in the beta 3-adrenergic-receptor gene with features of the insulin resistance syndrome in Finns. *N. Engl. J. Med.* **333**, 348–351 (1995).
10. K. Clément *et al.*, Genetic variation in the beta 3-adrenergic receptor and an increased capacity to gain weight in patients with morbid obesity. *N. Engl. J. Med.* **333**, 352–354 (1995).
11. E. S. Bachman *et al.*, betaAR signaling required for diet-induced thermogenesis and obesity resistance. *Science* **297**, 843–845 (2002).
12. V. S. Susulic *et al.*, Targeted disruption of the beta 3-adrenergic receptor gene. *J. Biol. Chem.* **270**, 29483–29492 (1995).
13. S. Reynisdottir, K. Ellerfeldt, H. Wahrenberg, H. Lithell, P. Arner, Multiple lipolysis defects in the insulin resistance (metabolic) syndrome. *J. Clin. Invest.* **93**, 2590–2599 (1994).
14. J. W. Jocken, E. E. Blaak, C. J. van der Kallen, M. A. van Baak, W. H. Saris, Blunted beta-adrenoceptor-mediated fat oxidation in overweight subjects: A role for the hormone-sensitive lipase gene. *Metabolism* **57**, 326–332 (2008).
15. T. Guo *et al.*, Adipocyte ALK7 links nutrient overload to catecholamine resistance in obesity. *eLife* **3**, e03245 (2014).

16. S. Collins *et al.*, Impaired expression and functional activity of the beta 3- and beta 1-adrenergic receptors in adipose tissue of congenitally obese (C57BL/6J ob/ob) mice. *Mol. Endocrinol.* **8**, 518–527 (1994).
17. P. Muzzin *et al.*, An adipose tissue-specific beta-adrenergic receptor. Molecular cloning and down-regulation in obesity. *J. Biol. Chem.* **266**, 24053–24058 (1991).
18. S. Collins, K. W. Daniel, E. M. Rohlf, Depressed expression of adipocyte beta-adrenergic receptors is a common feature of congenital and diet-induced obesity in rodents. *Int. J. Obes. Relat. Metab. Disord.* **23**, 669–677 (1999).
19. R. De Matteis *et al.*, Immunohistochemical identification of the beta(3)-adrenoceptor in intact human adipocytes and ventricular myocardium: Effect of obesity and treatment with ephedrine and caffeine. *Int. J. Obes. Relat. Metab. Disord.* **26**, 1442–1450 (2002).
20. S. K. Shenoy *et al.*, beta-arrestin-dependent, G protein-independent ERK1/2 activation by the beta2 adrenergic receptor. *J. Biol. Chem.* **281**, 1261–1273 (2006).
21. T. T. Cao, H. W. Deacon, D. Reczek, A. Bretscher, M. von Zaastrow, A kinase-regulated PDZ-domain interaction controls endocytic sorting of the beta2-adrenergic receptor. *Nature* **401**, 286–290 (1999).
22. M. Ghorbani, T. H. Claus, J. Himms-Hagen, Hypertrophy of brown adipocytes in brown and white adipose tissues and reversal of diet-induced obesity in rats treated with a beta3-adrenoceptor agonist. *Biochem. Pharmacol.* **54**, 121–131 (1997).
23. J. G. Granneman, P. Li, Z. Zhu, Y. Lu, Metabolic and cellular plasticity in white adipose tissue I: Effects of beta3-adrenergic receptor activation. *Am. J. Physiol. Endocrinol. Metab.* **289**, E608–E616 (2005).
24. X. Liu, F. Pérusse, L. J. Bukowiecki, Mechanisms of the antidiabetic effects of the beta 3-adrenergic agonist CL-316243 in obese Zucker-ZDF rats. *Am. J. Physiol.* **274**, R1212–R1219 (1998).
25. L. Hao *et al.*, Beneficial metabolic effects of mirabegron in vitro and in high-fat diet-induced obese mice. *J. Pharmacol. Exp. Ther.* **369**, 419–427 (2019).
26. J. R. Arch *et al.*, Atypical beta-adrenoceptor on brown adipocytes as target for anti-obesity drugs. *Nature* **309**, 163–165 (1984).
27. J. R. Arch, Challenges in  $\beta$ (3)-adrenoceptor agonist drug development. *Ther. Adv. Endocrinol. Metab.* **2**, 59–64 (2011).
28. B. S. Finlin *et al.*, The  $\beta$ 3-adrenergic receptor agonist mirabegron improves glucose homeostasis in obese humans. *J. Clin. Invest.* **130**, 2319–2331 (2020).
29. B. S. Finlin *et al.*, Human adipose beiging in response to cold and mirabegron. *JCI Insight* **3**, e121510 (2018).
30. A. E. O'Mara *et al.*, Chronic mirabegron treatment increases human brown fat, HDL cholesterol, and insulin sensitivity. *J. Clin. Invest.* **130**, 2209–2219 (2020).
31. A. M. Cypess *et al.*, Activation of human brown adipose tissue by a  $\beta$ 3-adrenergic receptor agonist. *Cell Metab.* **21**, 33–38 (2015).
32. W. A. Pastor, L. Aravind, A. Rao, TETonic shift: Biological roles of TET proteins in DNA demethylation and transcription. *Nat. Rev. Mol. Cell Biol.* **14**, 341–356 (2013).
33. H. Wu *et al.*, Dual functions of Tet1 in transcriptional regulation in mouse embryonic stem cells. *Nature* **473**, 389–393 (2011).
34. G. C. Hon *et al.*, 5mC oxidation by Tet2 modulates enhancer activity and timing of transcriptome reprogramming during differentiation. *Mol. Cell* **56**, 286–297 (2014).
35. A. Tsagaratou *et al.*, Dissecting the dynamic changes of 5-hydroxymethylcytosine in T-cell development and differentiation. *Proc. Natl. Acad. Sci. U.S.A.* **111**, E3306–E3315 (2014).
36. X. Wu, G. Li, R. Xie, Decoding the role of TET family dioxygenases in lineage specification. *Epigenetics Chromatin* **11**, 58 (2018).
37. K. Williams *et al.*, TET1 and hydroxymethylcytosine in transcription and DNA methylation fidelity. *Nature* **473**, 343–348 (2011).
38. Q. Zhang *et al.*, Tet2 is required to resolve inflammation by recruiting Hdac2 to specifically repress IL-6. *Nature* **525**, 389–393 (2015).
39. S. Damal Villivalam *et al.*, TET1 is a beige adipocyte-selective epigenetic suppressor of thermogenesis. *Nat. Commun.* **11**, 4313 (2020).
40. K. Fujiki *et al.*, PPAR $\gamma$ -induced PARylation promotes local DNA demethylation by production of 5-hydroxymethylcytosine. *Nat. Commun.* **4**, 2262 (2013).
41. L. Wihle *et al.*, Tet1 and Tet2 protect DNA methylation canyons against hypermethylation. *Mol. Cell. Biol.* **36**, 452–461 (2015).
42. Y. Yuan *et al.*, Vitamin C inhibits the metabolic changes induced by tet1 insufficiency under high fat diet stress. *Mol. Nutr. Food Res.* **65**, e2100417 (2021).
43. Y. Huang *et al.*, The behaviour of 5-hydroxymethylcytosine in bisulfite sequencing. *PLoS One* **5**, e8888 (2010).
44. S. Herzig *et al.*, CREB regulates hepatic gluconeogenesis through the coactivator PGC-1. *Nature* **413**, 179–183 (2001).
45. C. W. Lio *et al.*, Tet2 and Tet3 cooperate with B-lineage transcription factors to regulate DNA modification and chromatin accessibility. *eLife* **5**, e18290 (2016).
46. S. Montagner *et al.*, TET2 regulates mast cell differentiation and proliferation through catalytic and non-catalytic activities. *Cell Rep.* **15**, 1566–1579 (2016).
47. Y. Bao *et al.*, DNA demethylase Tet2 suppresses cisplatin-induced acute kidney injury. *Cell Death Discov.* **7**, 167 (2021).
48. J. Eguchi *et al.*, Transcriptional control of adipose lipid handling by IRF4. *Cell Metab.* **13**, 249–259 (2011).
49. J. An *et al.*, Acute loss of TET function results in aggressive myeloid cancer in mice. *Nat. Commun.* **6**, 10071 (2015).
50. M. M. Dawlaty *et al.*, Combined deficiency of Tet1 and Tet2 causes epigenetic abnormalities but is compatible with postnatal development. *Dev. Cell* **24**, 310–323 (2013).
51. R. T. Jung, P. S. Shetty, W. P. James, M. A. Barrand, B. A. Callingham, Reduced thermogenesis in obesity. *Nature* **279**, 322–323 (1979).
52. J. R. Speakman, Measuring energy metabolism in the mouse - Theoretical, practical, and analytical considerations. *Front. Physiol.* **4**, 34 (2013).
53. T. D. Müller, M. Klingenspor, M. H. Tschöp, Revisiting energy expenditure: How to correct mouse metabolic rate for body mass. *Nat. Metab.* **3**, 1134–1136 (2021).
54. J. Lin, C. Handschin, B. M. Spiegelman, Metabolic control through the PGC-1 family of transcription coactivators. *Cell Metab.* **1**, 361–370 (2005).
55. J. van der Vlag, J. L. den Blaauwen, R. G. Sewalt, R. van Driel, A. P. Otte, Transcriptional repression mediated by polycomb group proteins and other chromatin-associated repressors is selectively blocked by insulators. *J. Biol. Chem.* **275**, 697–704 (2000).
56. R. Liu *et al.*, Regulation of CSF1 promoter by the SWI/SNF-like BAF complex. *Cell* **106**, 309–318 (2001).
57. J. E. Moore *et al.*; ENCODE Project Consortium, Expanded encyclopaedias of DNA elements in the human and mouse genomes. *Nature* **583**, 699–710 (2020).
58. A. A. Sérandour *et al.*, Dynamic hydroxymethylation of deoxyribonucleic acid marks differentiation-associated enhancers. *Nucleic Acids Res.* **40**, 8255–8265 (2012).
59. E. Jeffery *et al.*, Characterization of Cre recombinase models for the study of adipose tissue. *Adipocyte* **3**, 206–211 (2014).
60. B. X. Ong *et al.*, Regulation of thermogenic adipocyte differentiation and adaptive thermogenesis through histone acetylation. *Front. Endocrinol. (Lausanne)* **11**, 95 (2020).
61. A. Galmozzi *et al.*, Inhibition of class I histone deacetylases unveils a mitochondrial signature and enhances oxidative metabolism in skeletal muscle and adipose tissue. *Diabetes* **62**, 732–742 (2013).
62. A. Ferrari *et al.*, HDAC3 is a molecular brake of the metabolic switch supporting white adipose tissue browning. *Nat. Commun.* **8**, 93 (2017).
63. F. Li *et al.*, Histone deacetylase 1 (HDAC1) negatively regulates thermogenic program in brown adipocytes via coordinated regulation of histone H3 lysine 27 (H3K27) deacetylation and methylation. *J. Biol. Chem.* **291**, 4523–4536 (2016).
64. Z. Gao *et al.*, Butyrate improves insulin sensitivity and increases energy expenditure in mice. *Diabetes* **58**, 1509–1517 (2009).
65. H. Xu *et al.*, Chronic inflammation in fat plays a crucial role in the development of obesity-related insulin resistance. *J. Clin. Invest.* **112**, 1821–1830 (2003).
66. C. Deng *et al.*, Respective degree of expression of beta 1-, beta 2- and beta 3-adrenoceptors in human brown and white adipose tissues. *Br. J. Pharmacol.* **118**, 929–934 (1996).
67. N. Dhillwyo, M. P. Sarras Jr., E. Luczkowski, S. M. Mason, R. V. Intine, Parp inhibition prevents ten-eleven translocase enzyme activation and hyperglycemia-induced DNA demethylation. *Diabetes* **63**, 3069–3076 (2014).
68. E. F. Yuan *et al.*, Hyperglycemia affects global 5-methylcytosine and 5-hydroxymethylcytosine in blood genomic DNA through upregulation of SIRT6 and TETs. *Clin. Epigenetics* **11**, 63 (2019).
69. D. Wu *et al.*, Glucose-regulated phosphorylation of TET2 by AMPK reveals a pathway linking diabetes to cancer. *Nature* **559**, 637–641 (2018).
70. M. M. Ali, S. A. Phillips, A. M. Mahmoud, HIF1 $\alpha$ /TET1 pathway mediates hypoxia-induced adipocytokine promoter hypomethylation in human adipocytes. *Cells* **9**, 134 (2020).
71. J. Z. Cao, H. Liu, A. Wickrema, L. A. Godley, HIF-1 directly induces TET3 expression to enhance 5-hmC density and induce erythroid gene expression in hypoxia. *Blood Adv.* **4**, 3053–3062 (2020).
72. R. Matuleviciute, P. P. Cunha, R. S. Johnson, I. P. Foskolou, Oxygen regulation of TET enzymes. *FEBS J.* **288**, 7143–7161 (2021).
73. Y. S. Lee *et al.*, Increased adipocyte O<sub>2</sub> consumption triggers HIF-1 $\alpha$ , causing inflammation and insulin resistance in obesity. *Cell* **157**, 1339–1352 (2014).
74. J. Krishnan *et al.*, Dietary obesity-associated Hif1 $\alpha$  activation in adipocytes restricts fatty acid oxidation and energy expenditure via suppression of the Sirt2-NAD<sup>+</sup> system. *Genes Dev.* **26**, 259–270 (2012).
75. C. Jiang *et al.*, Disruption of hypoxia-inducible factor 1 in adipocytes improves insulin sensitivity and decreases adiposity in high-fat diet-fed mice. *Diabetes* **60**, 2484–2495 (2011).
76. M. Ko *et al.*, Ten-eleven-translocation 2 (TET2) negatively regulates homeostasis and differentiation of hematopoietic stem cells in mice. *Proc. Natl. Acad. Sci. U.S.A.* **108**, 14566–14571 (2011).
77. M. Ko *et al.*, TET proteins and 5-methylcytosine oxidation in hematological cancers. *Immunol. Rev.* **263**, 6–21 (2015).
78. J. Kang *et al.*, Simultaneous deletion of the methylcytosine oxidases Tet1 and Tet3 increases transcriptome variability in early embryogenesis. *Proc. Natl. Acad. Sci. U.S.A.* **112**, E4236–E4245 (2015).

## Supplementary Information for

### Loss of adipose TET proteins enhances $\beta$ -adrenergic responses and protects against obesity by epigenetic regulation of $\beta$ 3-AR expression

Seongjun Byun<sup>1,†</sup>, Chan Hyeong Lee<sup>2,†</sup>, Hyeongmin Jeong<sup>1,†</sup>, Hyejin Kim<sup>1</sup>, Hyug Moo Kwon<sup>1</sup>, Sungho Park<sup>1</sup>, Kyungjae Myung<sup>3,4</sup>, Jungeun An<sup>2,\*</sup>, Myunggon Ko<sup>1,4,\*</sup>

Corresponding authors: Jungeun An (jan@jbnu.ac.kr), Myunggon Ko (mgko@uist.ac.kr)

#### **This PDF file includes:**

Supplementary Text

SI Materials and Methods

SI References

Figures S1 to S17

Table S1

## Supplementary Text

### Adipose TET deficiency protects against the detrimental metabolic effects of obesity.

Obesity is often accompanied by deleterious metabolic complications, including glucose intolerance and insulin resistance, which is reflected by hyperglycemia and hyperinsulinemia (1). As anticipated, an HFD substantially increased plasma glucose and insulin concentrations in WT mice, which were potently inhibited in *Tet* TKO mice (*SI Appendix*, Fig. 13 A and B). The Homeostatic Model Assessment of Insulin Resistance (HOMA-IR) score also indicated that adipose TET deficiency antagonized obesity-induced insulin resistance (*SI Appendix*, Fig. S14A). Consistently, glucose and insulin tolerance tests revealed that *Tet* TKO mice fed an HFD showed improved glucose tolerance and insulin sensitivity (*SI Appendix*, Fig. 13 C and D). These parameters were comparable between CD-fed mice groups (*SI Appendix*, Fig. S14 B and C). To directly analyze insulin signaling, we stimulated mice *in vivo* with insulin and then examined Akt phosphorylation in insulin-responsive tissues (i.e., adipose depots, liver, and muscle). HFD-fed *Tet* TKO mice displayed an enhanced Akt phosphorylation in all tissues tested compared to WT littermates, thus confirming more efficient insulin signaling (*SI Appendix*, Fig. 13 E and F and *SI Appendix*, Fig. S14 D-G); however, there was no difference in CD-fed mice (*SI Appendix*, Fig. S14H). In response to insulin resistance, a compensatory homeostatic mechanism in pancreatic  $\beta$ -cells causes islet hypertrophy and hyperinsulinemia (2). Consistent with metabolic improvements, the amplification of pancreatic islets and insulin-secreting  $\beta$ -cells was not observed in HFD-fed *Tet* TKO mice (*SI Appendix*, Fig. 13 G and *SI Appendix*, Fig. S14I).

Chronic HFD feeding causes hepatic steatosis and increased liver mass that are both associated with hepatic dysfunction (3). As expected, HFD-fed WT mice possessed enlarged livers exhibiting large LDs and high TG contents (*SI Appendix*, Fig. 13 H and I and *SI Appendix*, Fig. S15A), and elevated levels of circulating alanine aminotransferase, aspartate aminotransferase, cholesterol, low- and high-density lipoproteins, and TG (*SI Appendix*, Fig. 13J and *SI Appendix*, Fig. S15 B and C). All these alterations were dramatically mitigated in *Tet* TKO mice. Circulating free fatty acid concentrations were substantially increased in HFD-fed WT mice but not in *Tet* TKO mice (*SI Appendix*, Fig. 13J). Obesity also profoundly alters adipokine profiles, and this aggravates glucose homeostasis and insulin sensitivity (4). HFD-fed *Tet* TKO mice possessed significantly higher serum concentrations of antidiabetic adiponectin and elevated *adiponectin* mRNA levels in eWAT (*SI Appendix*, Fig. 13K). Feeding a HFD significantly increased the serum leptin concentrations in WT mice, as

reflected by the upregulation of *leptin* mRNA levels in eWAT. However, circulating leptin concentrations and adipose *leptin* mRNA levels remained low in the HFD-fed TKO mice, reflecting reduced fat mass (*SI Appendix*, Fig. 13L).

Chronic low grade inflammation is a hallmark of obesity that is initiated early during AT expansion, particularly in eWAT, and it progresses during the development of obesity to permanently skew the inflammatory balance toward a pro-inflammatory status that impairs insulin signaling (5). As expected, macrophage infiltration was substantially blocked in eWAT of HFD-fed *Tet* TKO mice, as assessed by a marked decrease in the frequency of crown-like structures and CD11b<sup>+</sup> F4/80<sup>+</sup> macrophages (*SI Appendix*, Fig. 13M and *SI Appendix*, Fig. S15 D and E). Consistent with these observations, the mRNA levels of inflammatory chemokines (e.g., *Ccl2*, *Ccl5*, etc.), proinflammatory molecules (e.g., *Tnf- $\alpha$* , *Il-1b*, *Il6*, and *Nos*), and macrophage markers (e.g., *F4/80*, *Ccr2*, and *Ccr5*) were also dramatically reduced (*SI Appendix*, Fig. 13N and *SI Appendix*, Fig. S15 F and G). Taken together, these data indicate that ablation of adipose TET proteins substantially protects mice from obesity-associated metabolic complications.

### **TET deficiency prevents HFD-induced transcriptional alterations in visceral adipose tissues.**

To further analyze the mechanism of TET-mediated metabolic regulation, we performed RNA sequencing of eWAT from CD- or HFD-fed WT and TKO mice. There was no significant variation among triplicate samples (*SI Appendix*, Fig. S16A). Comparisons of gene expression levels in four different conditions revealed that 3,898 genes were differentially expressed in at least one condition, and these genes could be clustered into 10 distinct groups based on their expression patterns (*SI Appendix*, Fig. S16B). In WT mice, 2,162 genes (clusters 1, 2, 3, and 5) were significantly upregulated after HFD feeding (*SI Appendix*, Fig. S16 B–D). Strikingly, 2,030 (~ 93.89%) of these genes (clusters 1, 2, and 3) were not upregulated or remained at lower levels in *Tet* TKO mice. Gene ontology (GO) enrichment analysis revealed that these genes are involved in hypoxia, inflammation, TNF signaling via NF- $\kappa$ B, interferon response, and KRAS and E2F signaling (*SI Appendix*, Fig. S16B). In contrast, 1,250 genes (clusters 7, 8, and 9) were significantly downregulated in WT mice after HFD feeding. Of these, 753 (60.24%) genes (clusters 7 and 8) were not downregulated or expressed at higher levels in *Tet* TKO mice (*SI Appendix*, Fig. S16 B–D). These genes were enriched for GO terms related to

adipogenesis, fatty acid metabolism, oxidative phosphorylation, and xenobiotic metabolism. Thus, these data suggest that TET proteins are required for HFD-induced transcriptional reprogramming in eWAT during the development of obesity.

To further analyze the cellular pathways, we categorized genes differentially expressed in HFD-fed WT and *Tet* TKO mice into two main classes. Ingenuity pathway analysis (IPA) indicated that genes expressed at lower levels in TKO cells (class 1; clusters C1, 2, 3, and 4) were primarily implicated in the innate or adaptive immune cell infiltration, signaling, differentiation, or activation (*SI Appendix*, Fig. S17A). In contrast, IPA of genes that were expressed at higher levels in TKO cells (class 2; clusters 6, 7, and 8) indicated that TET deficiency blocked HFD-induced suppression of genes affiliated with WAT browning, fat lipolysis, fatty acid oxidation, reactive oxygen species detoxification, AMPK signaling, and epigenetic gene regulation (*SI Appendix*, Fig. S17B). RNA-seq also confirmed that TET deficiency resisted HFD-induced reduction of  $\beta$ 3-AR expression (*SI Appendix*, Fig. S17C). Thus, these results suggest that TET proteins are critical mediators of HFD-induced alterations in gene expression programs in adipose tissues during promotion of diet-induced obesity.



## SI Materials and Methods

### Animals

Mice carrying *LoxP*-targeted (floxed) *Tet1*, *Tet2*, and *Tet3* genes (*Tet1<sup>fl/fl</sup>*, *Tet2<sup>fl/fl</sup>*, and *Tet3<sup>fl/fl</sup>*) have been described previously (6-8), and kindly provided by Dr. Anjana Rao (La Jolla Institute, CA, USA). *Adiponectin-Cre* (#010803) and *Cre-ERT2* (#8085) transgenic mice were obtained from the Jackson Laboratory. To delete all *Tet-floxed* alleles in adipose tissues, *Tet1<sup>fl/fl</sup> Tet2<sup>fl/fl</sup> Tet3<sup>fl/fl</sup>* mice were crossed with *Adiponectin-Cre* mice. For inducible excision of *Tet-floxed* alleles, *Tet1<sup>fl/fl</sup> Tet2<sup>fl/fl</sup> Tet3<sup>fl/fl</sup>* mice were crossed with *Cre-ERT2* transgenic mice. Male mice on a C57BL/6J background used for all studies unless stated otherwise. Mice were maintained in a temperature-controlled ( $22 \pm 2$  °C) facility under a 12-hr light/dark cycle. Mice were bred and housed in the In Vivo Research Center (IVRC) at Ulsan National Institute of Science and Technology (UNIST, Ulsan, Korea) under specific pathogen-free conditions. All animal experiments were approved by the Institutional Animal Care and Use Committee of the UNIST (UNISTACUC-17-35, 20–23), and performed in accordance with the institutional guidelines.

### Cell Lines

HEK293T cells from American Type Culture Collection were maintained in Dulbecco's Modified Eagle's medium (Life Technologies) supplemented with 10% heat-inactivated fetal bovine serum (Hyclone, Utah, USA), 2 mM L-glutamine, and 1X penicillin/streptomycin (Invitrogen). Immortalized preadipocytes from iWAT of 4–6-week-old *Tet1<sup>fl/fl</sup> Tet2<sup>fl/fl</sup> Tet3<sup>fl/fl</sup> ERT2-Cre* mice were maintained and differentiated in DMEM/F12 (Thermo Fischer Scientific) supplemented with 10% FBS and 1X penicillin/streptomycin (Invitrogen) at 37 °C in an incubator with 5% CO<sub>2</sub>.

### Establishment of Immortalized Preadipocytes

The stromal vascular fraction (SVF) was isolated from iWAT of 4–6-week-old *Tet1<sup>fl/fl</sup> Tet2<sup>fl/fl</sup> Tet3<sup>fl/fl</sup> ERT2-Cre* mice. Briefly, iWAT was washed with phosphate-buffered saline (PBS), minced in HBSS (Gibco, #14175-095), and digested with 1.5 mg/mL collagenase type II (Sigma, C6885) for 40 min at 37 °C with gentle shaking. After incubation, digestion was stopped by adding the same volume of DMEM/F12 medium supplemented with 10% FBS and 1X penicillin/streptomycin (Invitrogen), and the digested tissue was filtered through a 100 μm nylon cell strainer (BD Falcon). After centrifugation at 700 g for 5 min, the pellet was resuspended in ACK lysis buffer (150 mM NH<sub>4</sub>Cl, 10 mM KHCO<sub>3</sub>, 0.1 mM Na<sub>2</sub>-EDTA) for 1 min at room temperature to remove red blood cells. After centrifugation, cells were plated onto

dishes, and the medium was aspirated after 1–2 h to remove immune cells and other contaminants. Then, cells were further washed with PBS twice and cultured in fresh medium at 37 °C in an incubator with 5% CO<sub>2</sub>. An immortalized preadipocyte cell line was established by transducing cells with retroviruses expressing SV40 large T antigen, followed by selection with geneticin (G418, 500 µg/mL).

### **Adipogenic Differentiation *in vitro***

Immortalized preadipocytes were maintained and differentiated in DMEM/F12 supplemented with 10% FBS and 1X penicillin/streptomycin (Invitrogen) at 37 °C in an incubator with 5% CO<sub>2</sub>. Two days after cell confluency, adipogenic differentiation was induced with an adipogenic cocktail consisting of 5 mg/mL insulin (Sigma, #I6634), 1 nM T3 (Sigma, #T2877), 125 µM indomethacin (Sigma, #I7378), 1 µM dexamethasone (Sigma, #D1756), 0.5 mM IBMX (Sigma, #I5879), and 0.5 µM rosiglitazone (Sigma, #R2408). After 2 days, cells were maintained in culture medium in the presence of insulin and T3, and the media was replaced every two days. To induce *Tet* gene deletion in cells derived from *Tet1<sup>fl/fl</sup> Tet2<sup>fl/fl</sup> Tet3<sup>fl/fl</sup> ERT2-Cre* mice, the cells were treated with 4-hydroxytamoxifen (1 µM, Sigma, #H7904) dissolved in ethanol at the indicated points until day 6. For Oil Red O staining, the cells were washed twice with 1X PBS, fixed with 10% neutral buffered formalin (MEDILAB, #0151) for 30 min, washed twice with distilled water, and then stained with 0.2% Oil Red O dye (Sigma, #O0623) in isopropanol and water (6:4) for 1 h at room temperature. The cells were then washed with distilled water ten times. The stained cells were visualized under a microscope and de-stained with 100% isopropanol for 10 min under gentle shaking. Optical density was measured by spectrometry at a wavelength of 492 nm. For the majority of the experiments involving *in vitro* differentiated adipocytes, WT and *Tet* TKO adipocytes were generated by treating differentiating cells with either ethanol or 4-OHT (1 µM) at day 2, followed by further differentiation until day 6. Differentiated adipocytes were treated with HDAC inhibitors including SAHA (Selleckchem, #S1047) and MS-275 (Cayman, #13284).

### **Lentivirus transduction**

Lentiviral particles were generated by co-transfection of HEK293T cells with the lentiviral vector together with packaging vectors psPAX2 (Addgene #12260) and pMD2.G (Addgene #12259) using PEI transfection reagent (Polyscience, #23966). The Myc-tagged WT (Addgene #79554) or mutant (Addgene #79611) Tet2 catalytic domain (Tet2-CD) in pScalps\_Puro lentiviral plasmid was provided by Dr. Silvia Moticelli (Institute for Research in Biomedicine,

Switzerland). The virus-containing medium was collected, filtered through 0.45  $\mu\text{m}$  filter, and added to the cell culture together with 8  $\mu\text{g}/\text{ml}$  polybrene (Millipore, PR-1003) for 2 days, followed by selection with 2  $\mu\text{g}/\text{ml}$  puromycin (Gibco, A1113803) for 2–3 days. Stable expression of WT or Mut Tet2-CD was validated by immunoblot analysis.

### **Diet-Induced Obesity, Cold Exposure, and CL-316,243-Induced Browning**

To induce diet-induced obesity, all mice were fed a regular diet (13.5% fat; #R03-10, SAFE, Rosenberg, Germany) until 8 weeks of age. Subsequently, mice were randomly divided into two groups and fed either a chow diet (CD, 10% fat, Research Diets, NJ, USA) or a high-fat diet (HFD, 60% fat, Research Diets, NJ, USA) for 12 weeks, and water was provided *ad libitum*. Individual animals were weighed weekly. At the end of the study, blood samples were collected from the orbital venous plexus. Tissues were immediately frozen in liquid nitrogen and stored at  $-80\text{ }^{\circ}\text{C}$  for further analyses. For cold exposure, mice were housed at  $4\text{ }^{\circ}\text{C}$  for 7 days with access to food and water. Rectal temperatures were measured at different time intervals during the cold challenge using a digital thermometer (TD-300, Shibaura Electronics, Tokyo, Japan). Thermal images of the dorsal view were acquired using a thermal camera (Fortric, #226) and analyzed using AnalyzIR software (Fortric). In addition, the  $\beta$ 3-AR agonist CL-316,243 (Tocris, Catalog #1499, 1 mg/kg body weight/d) was administered intraperitoneally daily to 8-week-old WT and *Tet* TKO mice for 3 consecutive days.

### **Glucose Tolerance Test (GTT) and Insulin Tolerance Test (ITT)**

For the oral glucose tolerance test (OGTT), mice were administered an oral injection of D-glucose (1 g/kg body weight; ThermoFischer, #15023–021) after overnight fasting, and serum glucose concentrations were measured at the indicated time points using a glucometer (Accu-check Performa, Roche). For insulin tolerance tests (ITT), mice were fasted for 6 h before intraperitoneal injection of insulin (0.75 unit/kg body weight; Sigma, #91077C), and blood glucose concentrations were measured at the indicated time points. HOMA-IR (homeostatic model assessment of insulin resistance) was calculated as fasting blood glucose ( $\text{mg dL}^{-1}$ )  $\times$  fasting plasma insulin ( $\text{mU mL}^{-1}$ )/405 (9).

### **Metabolic Analyses**

For indirect calorimetry, mice were individually housed for 3 days prior to measurements to allow them to acclimate to the housing conditions. Animals were weighed before being placed in designated cages. Mice in each chamber had free access to food and water. Oxygen

consumption (VO<sub>2</sub>), carbon dioxide production (VCO<sub>2</sub>), and heat production were measured using the Comprehensive Lab Animal Monitoring System (CLAMS; Columbus Instruments, Columbus, OH, USA) and calculated using built-in software (Oxymax). The raw data were normalized to body weight. Movement was measured by counting horizontal beam breaks. Ambient temperatures were set to automatically drop from 30 °C to 22 °C to 4 °C at 2-day intervals. Recording was performed at regular intervals throughout the duration of the experiment.

### **ELISA and Lipid Analyses**

Blood glucose levels were measured using a glucometer (Accu-check Performa, Roche). Plasma levels of insulin (Cayman, #589501), adiponectin (Cayman, #10007620), leptin (Cayman, #10007609), and hepatic TG (Cayman, #10010303) were determined by ELISA using commercial kits. Serum ALT, AST, cholesterol, low and high-density lipoprotein (LDL, HDL), triglycerides, and free fatty acids were analyzed using a BS-390 Automated Chemistry Analyzer (POHANG TECHNOPARK, Bioengineering Center, Pohang, Korea). Plasma samples were stored at -80 °C until analysis.

### **Histology**

Tissue biopsies were fixed at 4 °C overnight in 10% neutral buffered formalin (MEDILAB, #0151), dehydrated, and then embedded in paraffin according to the standard laboratory protocol. Paraffin blocks were sectioned at 5 µm thickness, deparaffinized, rehydrated, and stained with hematoxylin and eosin (H&E) following the standard protocol. Adipocyte cell area was determined from H&E-stained sections using the virtual microscopy (Olympus). Adipocyte size was analyzed using built-in software (imaging software). For immunohistochemistry, specimens were deparaffinized and endogenous peroxidase was blocked in 0.3% H<sub>2</sub>O<sub>2</sub>. Heat-induced antigen retrieval with sodium citrate buffer (10 mM, pH 6.0) was performed before blocking with PBS containing 1% bovine serum albumin for 30 min at room temperature in a humidifying chamber. Then, tissue sections were stained with anti-Ucp1 (Abcam, #ab10983, 1:500), anti-F4/80 (Abcam, #ab6640, 1:500), or anti-insulin (Abcam, #ab181547, 1:200) at 4 °C overnight. After washing with PBS, tissue sections were incubated with horseradish peroxidase (HRP)-conjugated goat anti-rabbit IgG for 1 h, followed by incubation in 3,3-diamino-benzidine (DAB) solution (Dako, #L346811) and subsequent imaging by microscopy. The relative Ucp1 intensity was quantified using ImageJ (ij150, USA). For the immunofluorescence assay, Alexa Fluor 594-conjugated goat anti-rat secondary antibodies

were used, and imaging was performed using a LSM880 confocal microscope (ZEISS).

### **Lipolysis Assays**

For the *in vivo* lipolysis assay, mice were injected intraperitoneally with CL316,243 (Tocris Bioscience, #1499) at 1 mg/kg body weight. Plasma samples were collected before injection and at 7.5, 15, and 30 min after injection. For *ex vivo* and *in vitro* assays, small pieces of adipose tissue explants (0.5 ~ 1 cm<sup>2</sup>) or *in vitro* differentiated adipocytes were stimulated with isoproterenol (Sigma, #I2760, 1–10 μM), forskolin (Selleckchem, #S2449, 20 μM), or isobutylmethylxanthine (IBMX) (Sigma, #I5879, 0.2 mM) for 90 min. Concentrations of glycerol or free fatty acids were measured using an EZ-free Glycerol Assay kit (Dogenbio, #DG-FGC100, Seoul, Korea) or a Free Fatty Acid Assay kit (Dogenbio, #DG-FFA100, Seoul, Korea), respectively, according to the manufacturer's instructions. For *ex vivo* samples, the quantification results were normalized to tissue weights as an index of lipolysis.

### **Fatty Acid Oxidation**

Fatty acid oxidation (FAO) was measured using the Fatty Acid Oxidation kit (Biomedical Research Service, E-141, New York, USA) following the manufacturer's instructions. Briefly, tissues or cells were homogenized or resuspended in ice-cold lysis solution and centrifuged at 14,000 rpm for 5 min at 4 °C, and supernatants were then transferred to new tubes. Twenty microliters of each supernatant were added into each well of a 96-well plate and mixed with 50 μL of FAO Assay solution or control solution. After incubation at 37 °C for 60 min, the plate was read at an optical density of 492 nm (OD492) using a spectrophotometer (SpectraMax 190, Molecular Devices).

### **Assessment of oxygen consumption rate (OCR)**

OCR was measured using a Seahorse XF-24 analyzer (Seahorse Bioscience, Billerica, MA, USA), according to the manufacturer's instructions. For OCR measurements, SVF cells (20,000 cells) were seeded in a 24-well Seahorse assay plate (Agilent, San Jose, CA, USA) and differentiated into adipocytes as described above. One day before measurement, the sensor cartridge was placed into calibration buffer (XF calibrant, pH 7.4) and incubated in a non-CO<sub>2</sub> incubator at 37°C. After 6 days of differentiation, adipocytes were washed twice and pre-incubated in pre-warmed XF assay media (pH 7.4), supplemented with 25 mM glucose, 2 mM glutamine, 1 mM sodium pyruvate, and 2% bovine serum albumin in a non-CO<sub>2</sub> incubator for 30 min. During measurements, adipocytes were sequentially treated with CL316,243 (10 μM),

oligomycin (1.25  $\mu$ M), and rotenone/antimycin A (1  $\mu$ M). The basal OCR was measured three times, and three readings were taken after the addition of each mitochondrial OXPHOS inhibitor. The OCR was automatically recorded and calculated by the sensor cartridge and Seahorse XF-24 software.

### **Mitochondrial DNA quantification**

Tissues were digested with 200  $\mu$ g/mL proteinase K (Roche, Basel, Switzerland) overnight at 55°C with gentle agitation. Then, genomic DNA was isolated sequentially with equal volumes of phenol, phenol:chloroform:isoamyl alcohol (25:24:1), and chloroform:isoamyl alcohol (24:1), followed by precipitation with two volumes of ethanol. Total DNA was quantified using a Nanodrop 1000 (Thermo Fisher Scientific, Waltham, MA, USA). Mitochondrial DNA was quantified by measuring the abundance of DNA regions corresponding to mitochondrial cytochrome *c* oxidase subunit 2 (Cox2), NADH dehydrogenase subunit 1, and cytochrome *c*, relative to that of the intronic regions of nuclear-encoded  $\beta$ -actin,  $\beta$ -globin, and glucagon using SYBR Green real-time PCR. Primer sequences are listed in Table S1.

### **mRNA Sequencing (RNA-Seq)**

Total RNA was extracted from three biological replicates of eWAT from CD- or HFD-fed WT or *Tet* TKO mice using a Purelink RNA Micro kit (Invitrogen). Total RNA integrity was assessed using an Agilent Technologies 2100 Bioanalyzer with an RNA Integrity Number (RIN) value. mRNA sequencing libraries were prepared using the Truseq stranded mRNA library prep kit (Illumina) according to the manufacturer's instructions. The quality of the libraries was verified by capillary electrophoresis (Bioanalyzer, Agilent). High-throughput sequencing (100 bp, paired end) was performed using a NovaSeq 6000 sequencing system (Illumina).

### **Analysis of RNA Sequencing Data**

After quality filtering according to the Illumina pipeline, paired-end reads were mapped to the reference mouse genome (mm10 assembly) using STAR aligner version 2.7.3a with default parameters. Differentially expressed genes (DEGs) were identified using DESeq2 1.30.0. Read counts for DESeq2 analysis were obtained using featureCounts v2.0.0. After eliminating absent and low features (zero or < 1 CPM), the raw counts were normalized using DESeq2, followed by differential expression analysis. Differentially expressed genes were identified according to a P-value of  $\leq 0.01$  and fold change thresholds of  $\geq 2$  or  $\leq 0.5$ . To generate the heatmap of K-mean clusters using RNA-seq, we used the Morpheus

(<https://software.broadinstitute.org/morpheus/>) K-means algorithm. K was chosen at 10, as lower values failed to identify all meaningful clusters and higher values subdivided meaningful clusters. Clusters were further grouped into two classes based on gene expression levels in HFD-fed WT and TKO mice. The canonical pathway was determined according to the IPA canonical pathway analysis of genes within classes 1 and 2. One representative category based on *P*-value was presented if more than one similar category was identified. Principal component analysis (PCA) was conducted using R tools, and RNA-seq data were visualized by preparing custom tracks for the UCSC Genome Browser.

### **Flow Cytometry**

Stromal vascular fraction (SVF) cells were harvested as described and washed with 1X PBS. The cells were then suspended in FACS buffer (1X PBS containing 0.2% heat-inactivated FBS and 0.1% sodium azide), blocked with purified rat anti-mouse CD16/CD32 (Mouse BD Fc Block™), and stained with anti-mouse monoclonal antibodies (BioLegend), including APC-Cy7-conjugated CD45.2 (104), APC-conjugated CD11b (M1/70), and PE-Cy7-conjugated F4/80 (BM8), at 4 °C for 30 min in the dark. The cells were then washed and resuspended in FACS buffer for flow cytometry. Flow cytometric analyses were performed using a FACS LSR Fortessa (BD Biosciences), and the data were analyzed using FlowJo software (BD Biosciences).

### **Cloning of TET Expression Vectors and Co-Immunoprecipitation**

The open reading frame (ORF) of full-length (FL), N-terminal region lacking catalytic domain ( $\Delta$ CD), or C-terminal catalytic domain (CD) of human TET1, TET2, and TET3 was amplified by polymerase chain reaction (PCR) and cloned into pOZ-FH-N vector that adds Flag-HA (FH) tandem tag to the N-terminal region of the inserted protein. Then, FH-tagged FL, CD,  $\Delta$ CD of each TET was amplified by PCR using FH-TET1,2,3 in pOZ-FH-N vector as templates, followed by insertion into pEF1/V5 vector (Invitrogen). The amino acid numbers of the cloned regions are shown in Fig. S16 *D-F*. HEK293T cells were transfected with FH-tagged TET1, TET2, and TET3 plasmids described above. After 48 h, cells were harvested and washed twice with 1X PBS. Cells were then lysed with lysis buffer (50 mM Tris-HCl, pH 7.4, 150 mM NaCl, 1 mM EDTA, and 1% Triton X-100) supplemented with protease/phosphatase inhibitor cocktail (10 mM sodium pyrophosphate, 20 mM  $\beta$ -glycerophosphate, 1 mM sodium orthovanadate, 10  $\mu$ M leupeptin, 10  $\mu$ g/mL aprotinin, and 1 mM phenylmethylsulphonyl fluoride (PMSF)), incubated on ice for 20 min, and centrifuged at 12,000 rpm for 15 min at 4 °C. Co-

immunoprecipitation was performed using an anti-FLAG<sup>®</sup> M2 affinity gel (Sigma). Whole-cell lysate (500 µg) in a final 500 µL volume of lysis buffer was incubated with protein A/G agarose for 1 h at 4 °C with gentle rotation, followed by centrifugation for 2 min at 1,400 rpm. The supernatant was transferred to a tube containing 40 µL of anti-FLAG<sup>®</sup> M2 affinity gel and incubated overnight at 4 °C with gentle rotation. The protein-bead complexes were washed with 1X wash buffer (50 mM Tris-HCl, pH 7.4, 150 mM NaCl, 0.05% Triton X-100) six times at 4 °C. Each wash consisted of a 5 min incubation at 4 °C with gentle rotation. The bound proteins were eluted by boiling in a sample buffer and then visualized by electrophoresis on SDS-PAGE and subsequent immunoblotting.

### **Chromatin Immunoprecipitation Coupled with qPCR**

ChIP assays were performed using the Chromatin Immunoprecipitation (ChIP) Assay kit (Merck, #17–295) according to the manufacturer’s instructions. Briefly, cells were cross-linked using 1% (w/v) formaldehyde for 10 min at 37 °C. After washing twice with cold PBS, cells were collected and resuspended in SDS lysis buffer (Merck, #20–163). Lysates were sonicated to shear DNA to lengths that were between 200 and 500 bp using a Q800R3 sonicator (Qsonica). The sonicated cell supernatants were diluted 10-fold in ChIP Dilution Buffer and immunoprecipitated with 2 µg of anti-H3K27Ac (Abcam, #ab4729) or 10 µg of anti-HDAC1 (GeneTex, #GTX100513), anti-HDAC3 (Abcam, #ab7030), anti-Tet1 (GeneTex, #GTX125888), anti-Tet2 (Abcam, #ab94580), anti-Tet3 (GeneTex, #GTX121453), or IgG (Cell Signaling Technology, #2729). After washing, the immunoprecipitated DNA was recovered using phenol/chloroform extraction and analyzed via qPCR with TOPreal<sup>™</sup> qPCR 2X PreMIX (Enzynomics) and QuantStudio 5 and 6 real-time PCR systems. Percentages of input recovery were calculated. The primer sequences are listed in Table S1.

### **Dot Blot Analysis**

Cells and tissues were digested by incubation with 200 µg/mL proteinase K (Roche) overnight at 55 °C, followed by isolation of genomic DNA by phenol-chloroform extraction as described above. DNA samples were denatured in 0.4 M NaOH, 10 mM EDTA at 95 °C for 10 min, and then neutralized with cold 2 M ammonium acetate (pH 7.0). Two-fold serial dilutions of the denatured DNAs were spotted on a nitrocellulose membrane in an assembled Bio-Dot apparatus (Bio-Rad) according to the manufacturer’s instructions. The membrane was washed with 2X SSC buffer, air-dried, and vacuum-baked at 80 °C for 2 h, then blocked with 5% non-fat milk for 1 h and incubated with anti-5hmC (1:6,000, gifted from Dr. Anjana Rao) overnight at 4 °C.



After incubating with horseradish peroxidase (HRP)-conjugated anti-rabbit IgG secondary antibody, the membrane was visualized by chemiluminescence (Biorad). To ensure equal loading of DNAs on the membrane, the same blot was stained with 0.04% toluidine blue in 0.3 M sodium acetate (pH 5.2).

### **RNA Purification, Reverse Transcription, and Real-Time RT-PCR**

Total RNA was extracted from cells or tissues using TRIzol reagent (Invitrogen) and reverse transcription was performed using SuperScript IV (Invitrogen), according to the manufacturer's instructions. Diluted cDNAs were analyzed by real-time PCR using QuantStudio 5, 6, or 7 Flex (Applied Biosystems) and TOPreal™ qPCR 2X PreMIX (Enzynomics). Data were analyzed by QuantStudio 5, 6, or 7 real-time PCR software (Applied Biosystems). Levels of gene expression were normalized to *Gapdh*. Primer sequences are listed in Table S1.

### **Immunoblot Analysis**

Cells and tissues were lysed using RIPA buffer (150 mM NaCl, 50 mM Tris-HCl, pH 8.0, 1% Triton X-100, 0.5% sodium deoxycholate, and 0.1% SDS) supplemented with protease/phosphatase inhibitor (20 mM  $\beta$ -glycerophosphate, 10 mM sodium pyrophosphate, 1 mM sodium o-vanadate, 10  $\mu$ M leupeptin, 10  $\mu$ g/mL aprotinin, 1 mM freshly prepared phenylmethylsulphonyl fluoride (PMSF) and incubated on ice for 15 min. Adipose tissues were lysed with TissueLyser LT in lysis buffer (Qiagen). After centrifuging at 13,000 rpm for 15 min at 4 °C, the protein concentration was determined by Bradford protein assay. Cell lysates were mixed with SDS sample buffer before boiling for 5 min. Then, cell lysates were separated by 7.5% or 10% SDS-PAGE and transferred onto nitrocellulose membranes. Proteins were detected by immunoblotting in TBST (150 mM NaCl, 10 mM Tris-Cl, pH 8.0, 0.5% Tween-20) containing 5% low-fat milk and antibodies against proteins of interest, followed by incubation with horseradish peroxidase (HRP)-conjugated secondary antibodies (Invitrogen) and enhanced chemiluminescence (Bio-rad). The following antibodies were used in this study. Anti-Ucp1 (Abcam, #ab10983), anti-Pgc-1 $\alpha$  (Novus, #NBP1-04676), anti- $\beta$ 3-AR (Santa Cruz, #sc-515763), anti-p-PKA substrate (CST, #9624), anti-p-Hsl (Ser563) (CST, #4139), anti-Hsl (CST, #4107), anti-p-Akt (Ser473) (CST, #9271), anti-p-Akt (Thr308) (CST, #9275), anti-Akt (CST, #9272), DDK (Flag) epitope (Origene, TA50011-100), anti-HDAC1 (GeneTex, #GTX100513), anti-HDAC3 (Abcam, #ab7030), anti- $\alpha$ -Tubulin (Sigma, #T5168), and anti- $\beta$ -actin (Sigma, #A5441).

## Luciferase Reporter Assay

Adipocytes or HEK293T cells were transfected with pREP4-Luc reporter constructs (Addgene, #124892) driven by the  $\beta 3$ -AR promoter, or pGL3-promoter vector (Promega) driven by *Ppargc1a* 2 kb promoter (Addgene, #8887) or *Ppargc1a* promoter  $\Delta$ CRE (Addgene, #8888) using Lipofectamine 2000 reagent (Invitrogen). The *Renilla* luciferase reporter construct (pRL-TK, Promega) was used to monitor transfection efficiency. To assess the effect of the catalytic activity of TET proteins, mammalian expression vectors for WT or catalytically inactive mutants of TET1, TET2, or TET3 were co-transfected with reporter constructs and a *Renilla* luciferase construct. Mutant TET constructs were generated by site-directed mutagenesis of the HxD catalytic motif by PCR using Pfu polymerase, Dpn I treatment, and transformation (10, 11). Lysates were collected 48 h after transfection, and firefly and *Renilla* luciferase activities were measured using a Dual-Luciferase Reporter System (Promega) according to the manufacturer's instructions. Luciferase activity was normalized to the activity of *Renilla* luciferase. The  $\beta 3$ -AR promoter 6 kb-driven luciferase plasmid was described elsewhere (12). The serially truncated versions of upstream fragments of the mouse  $\beta 3$ -AR gene shown in were cloned by PCR. The ENCODE cCRE in the  $\beta 3$ -AR locus was amplified by PCR. Primer sequences used for cloning are listed in Table S1. The truncated versions of the  $\beta 3$ -AR upstream fragments and  $\beta 3$ -AR promoter (1 kb) in both orientations were originally cloned into pGL3-promoter vector using primers shown in Table S1, followed by subcloning into the pREP4-Luc vector using Not I and Xho I enzymes.

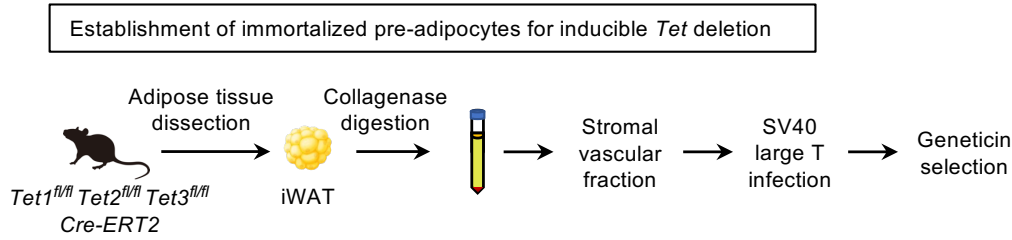
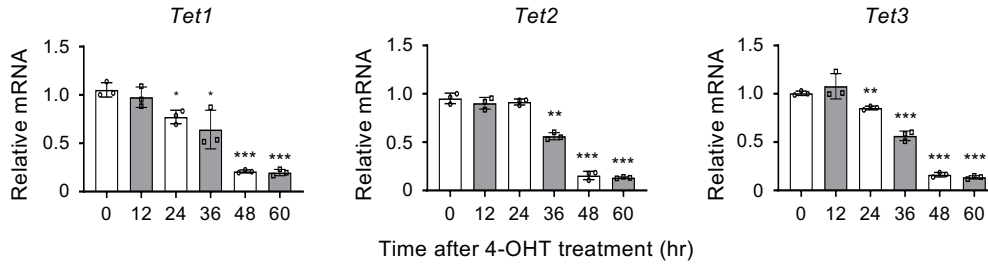
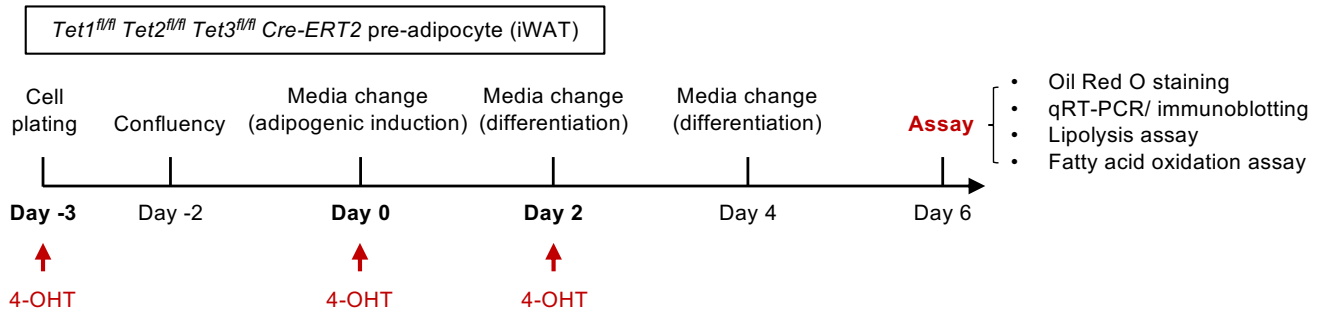
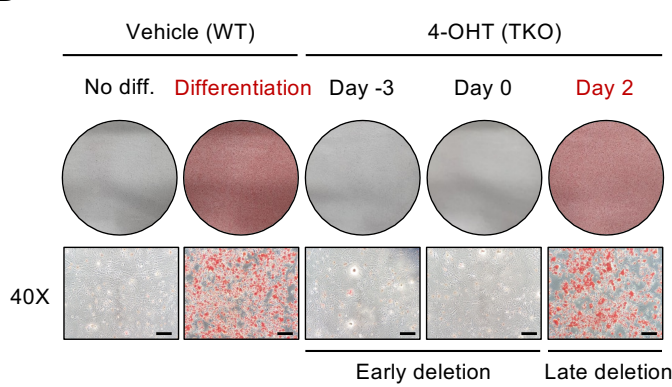
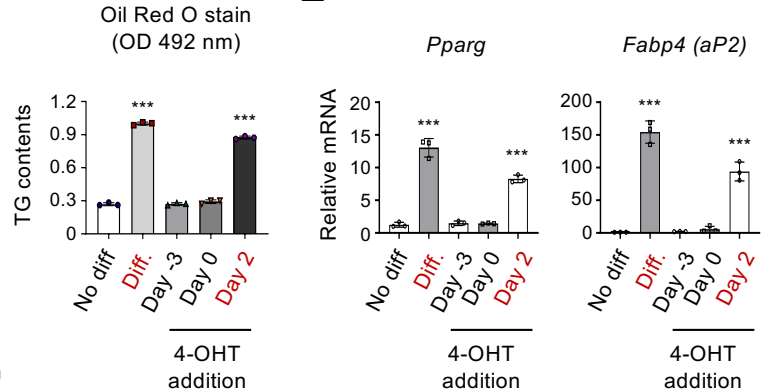
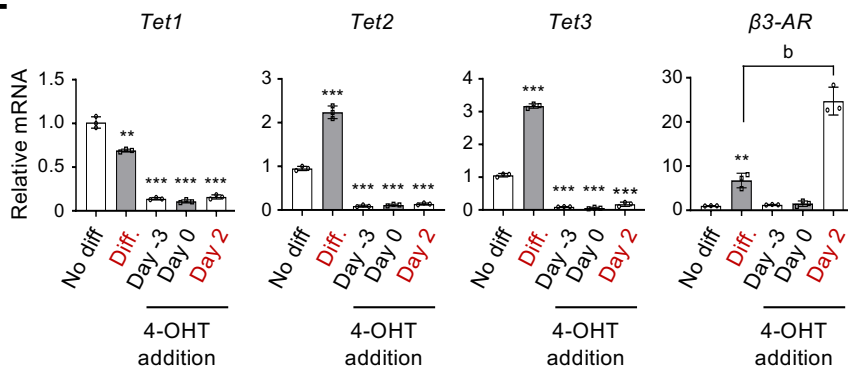
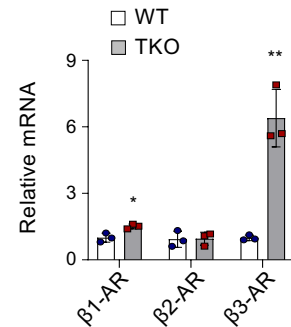
## Statistical Analysis

All statistics were performed with GraphPad Prism 8.0 software (GraphPad, CA, USA). All data are presented as the mean  $\pm$  s.d., except where noted. Statistical significance was analyzed by a two-tailed, unpaired Student's *t*-test unless stated otherwise. \* $P < 0.05$ , \*\*  $P < 0.005$ , and \*\*\* $P < 0.0005$  were considered significant. For RNA-seq data, significance was estimated by Kolmogorov-Smirnov test. The relationship between metabolic rate and body weight was statistically tested using ANCOVA (Penguin v0.3.12 Python package) with the significance threshold of  $p \leq 0.05$ .

## SI References

1. A. M. Johnson, J. M. Olefsky, The origins and drivers of insulin resistance. *Cell* **152**, 673-684 (2013).

2. L. I. Hudish, J. E. Reusch, L. Sussel, beta Cell dysfunction during progression of metabolic syndrome to type 2 diabetes. *J Clin Invest* **129**, 4001-4008 (2019).
3. E. Fabbrini, S. Sullivan, S. Klein, Obesity and nonalcoholic fatty liver disease: biochemical, metabolic, and clinical implications. *Hepatology* **51**, 679-689 (2010).
4. N. Ouchi, J. L. Parker, J. J. Lugus, K. Walsh, Adipokines in inflammation and metabolic disease. *Nat Rev Immunol* **11**, 85-97 (2011).
5. Y. S. Lee, J. Wollam, J. M. Olefsky, An Integrated View of Immunometabolism. *Cell* **172**, 22-40 (2018).
6. M. Ko *et al.*, Ten-Eleven-Translocation 2 (TET2) negatively regulates homeostasis and differentiation of hematopoietic stem cells in mice. *Proc Natl Acad Sci U S A* **108**, 14566-14571 (2011).
7. M. Ko *et al.*, TET proteins and 5-methylcytosine oxidation in hematological cancers. *Immunol Rev* **263**, 6-21 (2015).
8. J. Kang *et al.*, Simultaneous deletion of the methylcytosine oxidases Tet1 and Tet3 increases transcriptome variability in early embryogenesis. *Proc Natl Acad Sci U S A* **112**, E4236-4245 (2015).
9. E. Xu *et al.*, Temporal and tissue-specific requirements for T-lymphocyte IL-6 signalling in obesity-associated inflammation and insulin resistance. *Nat Commun* **8**, 14803 (2017).
10. M. Ko *et al.*, Modulation of TET2 expression and 5-methylcytosine oxidation by the CXXC domain protein IDAX. *Nature* **497**, 122-126 (2013).
11. M. Tahiliani *et al.*, Conversion of 5-methylcytosine to 5-hydroxymethylcytosine in mammalian DNA by MLL partner TET1. *Science* **324**, 930-935 (2009).
12. H. H. Lee *et al.*, TonEBP/NFAT5 promotes obesity and insulin resistance by epigenetic suppression of white adipose tissue beiging. *Nat Commun* **10**, 3536 (2019).

**A****B****C****D****E****F****G**

**Fig. S1. Inducible *Tet* deletion in immortalized preadipocytes *in vitro*.**

(A) Schematic representation of the establishment of immortalized preadipocytes for inducible *Tet* deletion.

(B) mRNA levels of *Tet1*, *Tet2*, and *Tet3* relative to *Gapdh* in immortalized preadipocytes after treatment with 4-OHT (1  $\mu$ M) for the indicated time periods. n = 3.

(C) Schematic representation of induction of *Tet* deletion during preadipocytes differentiation *in vitro*.

(D) Representative Oil Red O staining images of differentiated adipocytes after 4-OHT treatment at the indicated time points (*left*) and quantification of accumulated lipids by spectrometry (*right*). n = 3. Scale bar, 50  $\mu$ m.

(E and F) mRNA levels of the indicated genes relative to *Gapdh* in differentiated adipocytes after 4-OHT (1  $\mu$ M) treatment at the indicated time points. n = 3.

(G) mRNA levels of the indicated genes relative to *Gapdh* in WT and *Tet* TKO adipocytes. Preadipocytes were treated with or without 4-OHT on day 2 of differentiation. n = 3.

All data are presented as the mean  $\pm$  s.d. The *P*-values were determined by unpaired Student's *t*-test. \**P* < 0.05, \*\**P* < 0.005, \*\*\**P* < 0.0005 vs. 0 h (B), no diff (D-F), and WT (G); <sup>b</sup>*P* < 0.005.

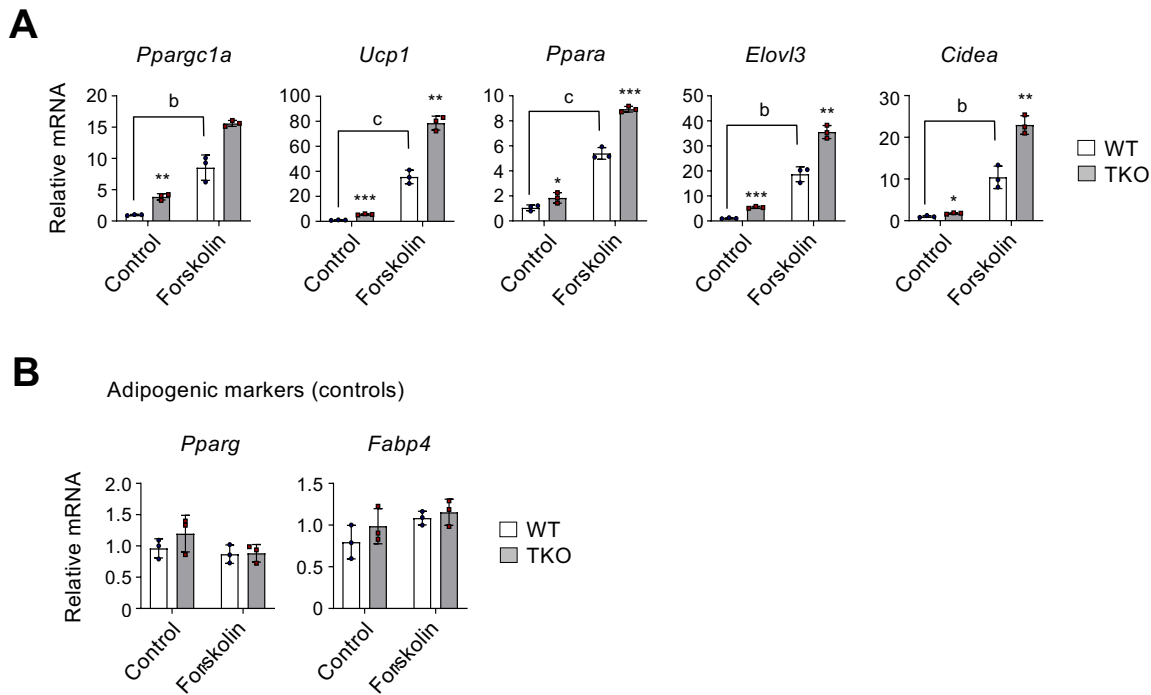


**Fig. S2. TET proteins suppress thermogenic gene expression.**

(A and B) mRNA levels of the indicated genes relative to *Gapdh* in WT and *Tet* TKO adipocytes stimulated with or without forskolin (20  $\mu$ M) for 6 h. Adipogenic marker gene expression (B) served as a negative control. n = 3.

All data are presented as the mean  $\pm$  s.d. The *P*-values were determined by unpaired Student's *t*-test. \*\**P* < 0.005, \*\*\**P* < 0.0005 vs. WT; <sup>b</sup>*P* < 0.005, <sup>c</sup>*P* < 0.0005.

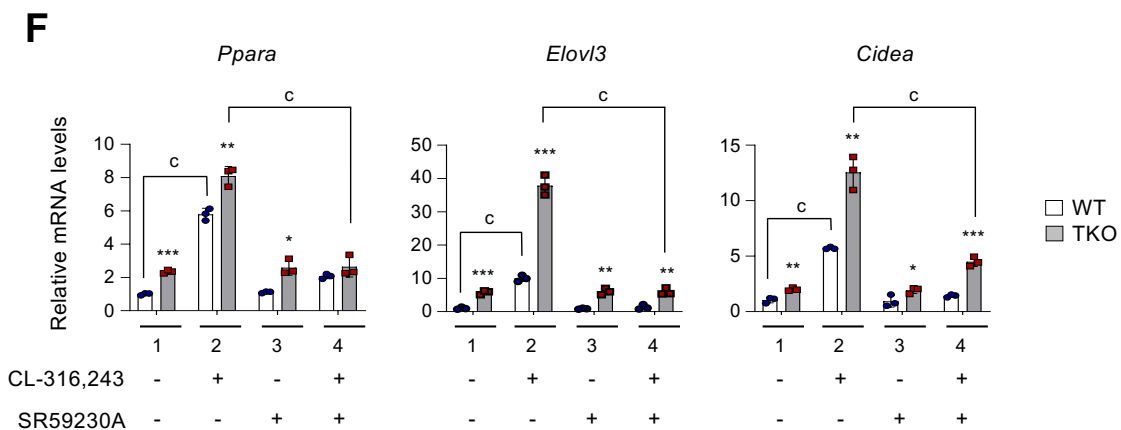
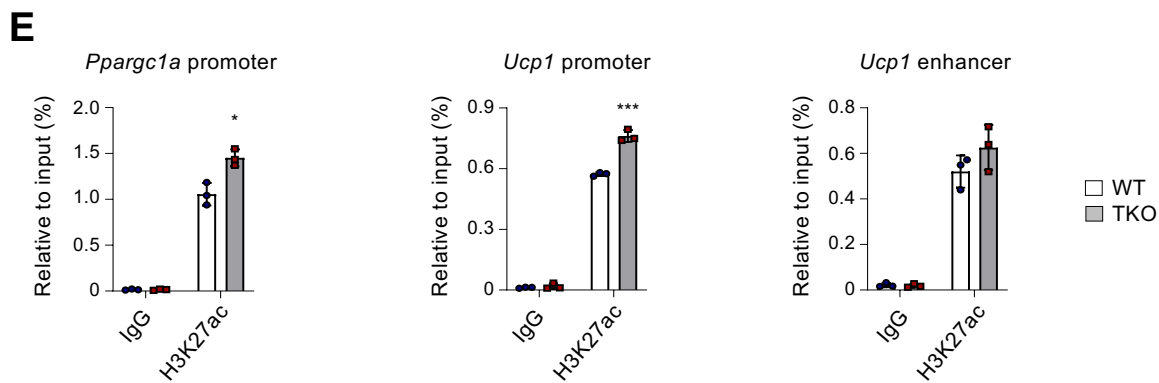
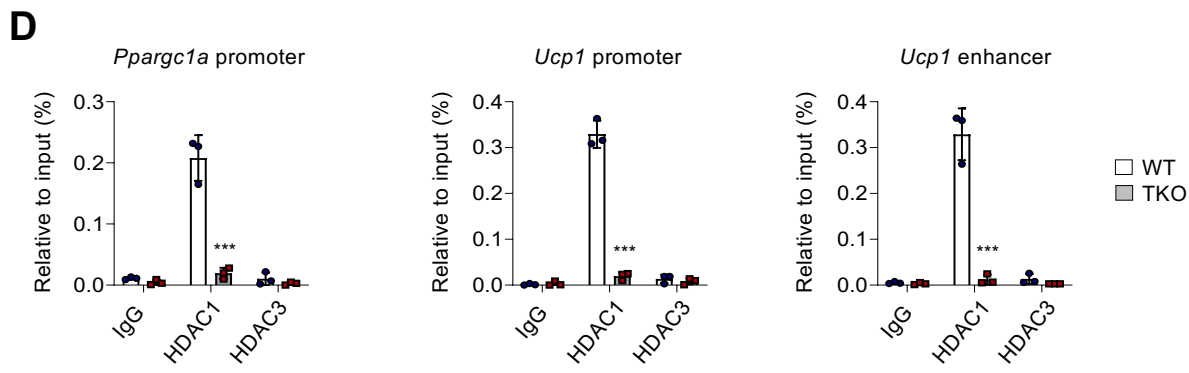
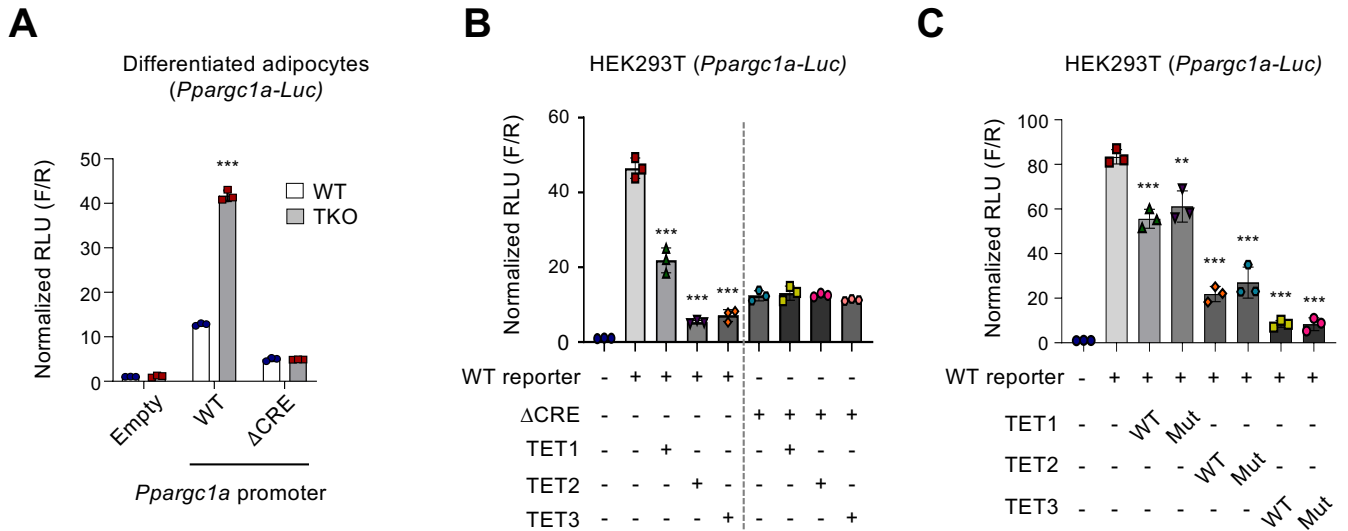


**Fig. S3. TET proteins cooperate with HDAC1 to suppress *Pparg1a* and *Ucp1* transcription.**

(A) Luciferase reporter activities driven by *Pparg1a* (2 kb) promoters (WT or  $\Delta$ CRE) in WT and *Tet* TKO adipocytes. Results were normalized to Renilla luciferase activity. RLU, relative light units. n = 3.

(B and C) Luciferase reporter activities driven by *Pparg1a* (2 kb) promoters (WT or  $\Delta$ CRE) in HEK293T cells transiently transfected with WT or mutant TET1, TET2, and TET3 plasmids. WT, wildtype; Mut, catalytically inactive mutant. n = 3.

(D and E) ChIP-qPCR for IgG, HDAC1, and HDAC3 (D) or H3K27ac (E) at the *Pparg1a* promoter and *Ucp1* promoter/enhancer regions in WT and *Tet* TKO adipocytes. n = 3.

(F) mRNA expression of the indicated genes relative to *Gapdh* in WT and *Tet* TKO adipocytes after stimulation with or without CL316,243 (1  $\mu$ M, 24 h). Cells were either untreated or pre-treated for 1 h with SR59230A (10  $\mu$ M), a  $\beta$ 3-AR antagonist, prior to CL216,243 treatments. n = 3.

All data are presented as the mean  $\pm$  s.d. The *P*-values were determined by unpaired Student's *t*-test. \**P* < 0.05, \*\**P* < 0.005, \*\*\**P* < 0.0005 vs. WT (A, D-F) and reporter only (B and C); <sup>c</sup>*P* < 0.0005.



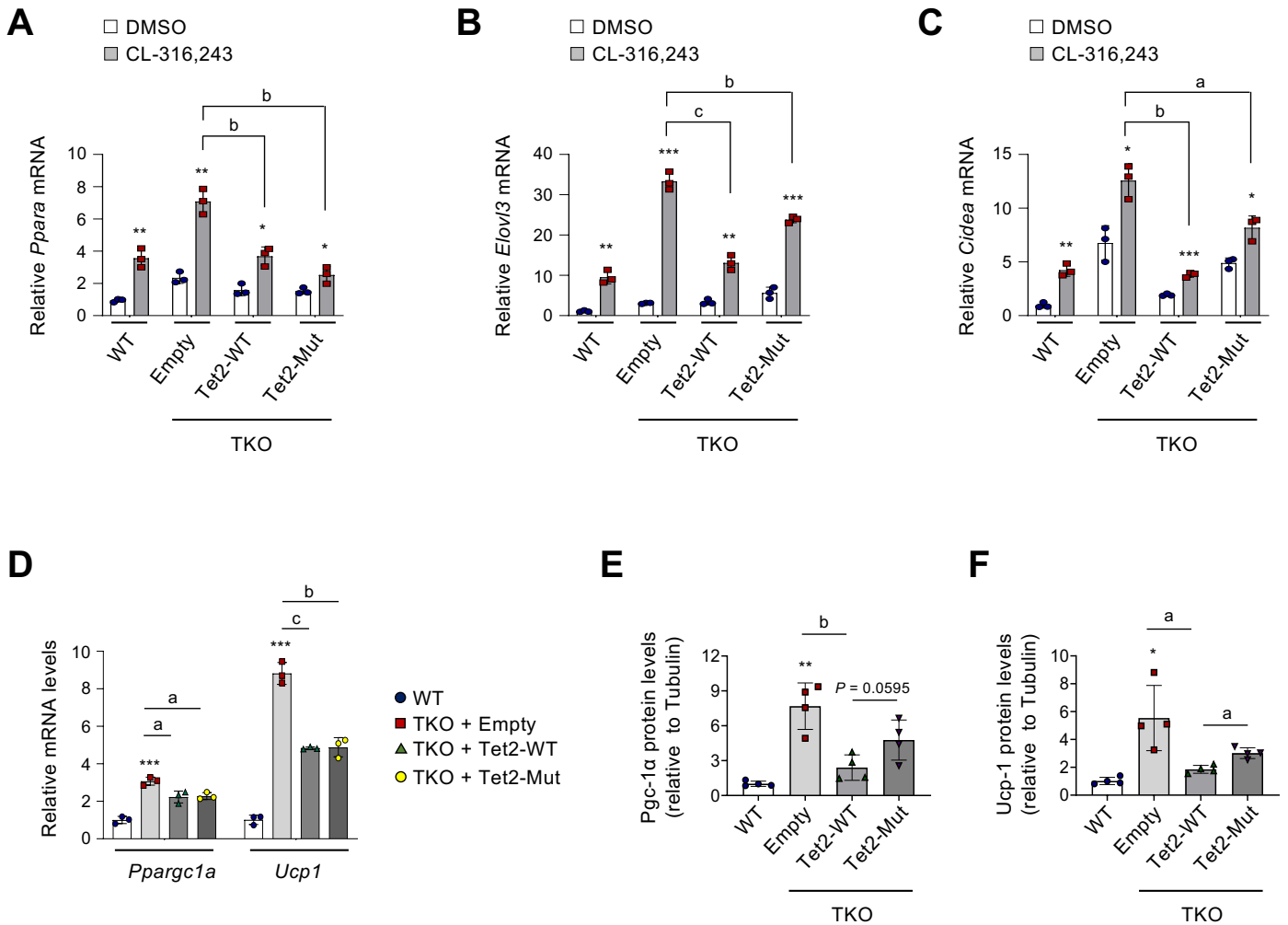


**Fig. S4. TET proteins suppress thermogenic gene expression in an enzymatic activity-independent manner.**

(A-C) mRNA expression of *Ppara* (A), *Elovl3* (B), and *Cidea* (C) relative to *Gapdh* in WT adipocytes or *Tet* TKO adipocytes expressing empty vector, WT, or mutant Tet2-CD with or without CL-316,243 stimulation.  $n = 3$ .

(D) mRNA expression of *Pparg1a* and *Ucp1* relative to *Gapdh* in adipocytes shown in Fig. 2C.  $n = 3$ .

(E and F) Quantification of Pgc-1α (E) and Ucp1 (F) protein levels shown in Fig. 2C.  $n = 4$ .

All data are presented as the mean  $\pm$  s.d. The  $P$ -values were determined by unpaired Student's t-test.

\* $P < 0.05$ , \*\* $P < 0.005$ , \*\*\* $P < 0.0005$  vs. WT; <sup>a</sup> $P < 0.05$ , <sup>b</sup> $P < 0.005$ , <sup>c</sup> $P < 0.0005$ .

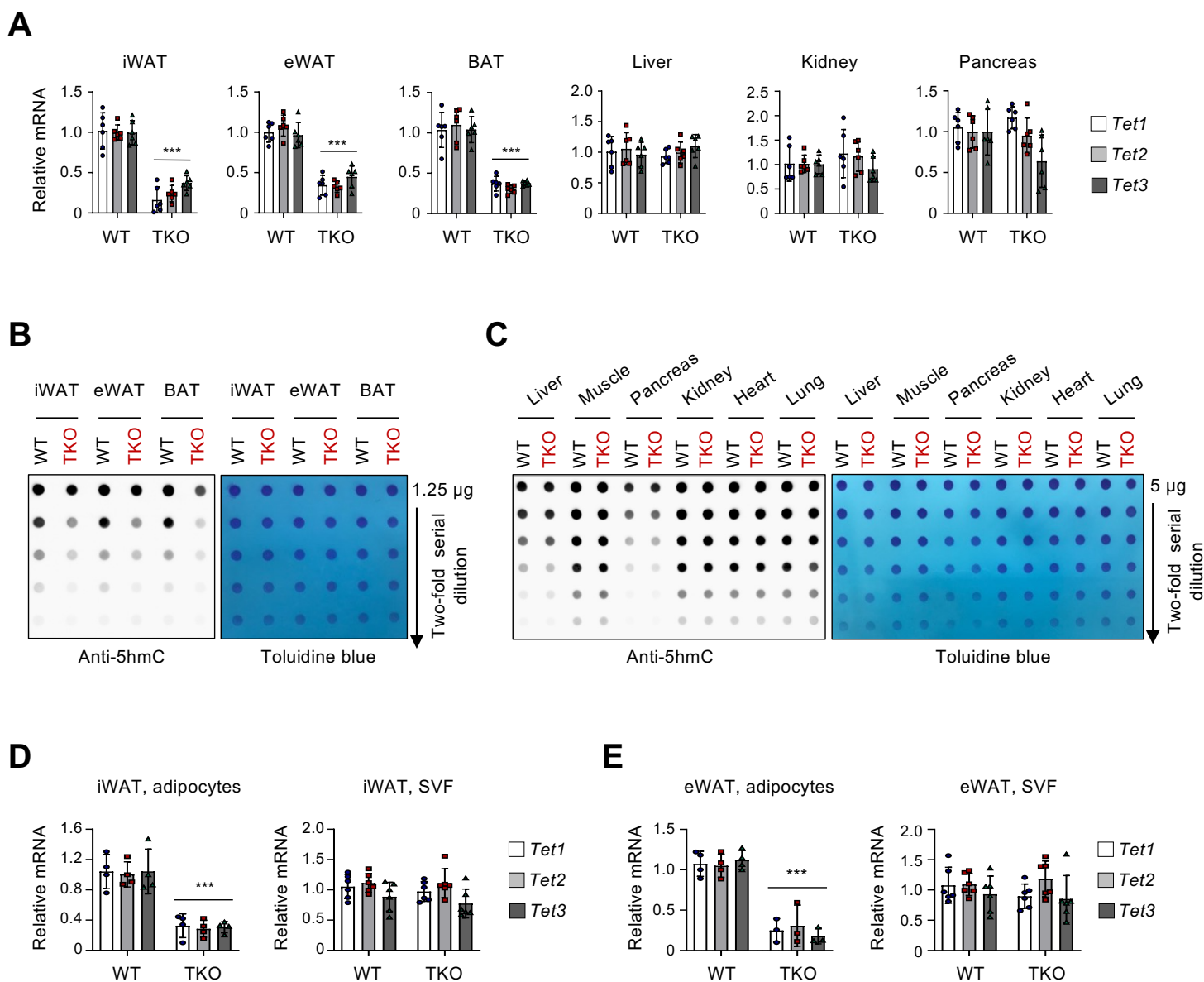


**Fig. S5. Generation of adipocyte-specific *Tet* triple knockout mice.**

(A) mRNA expression of *Tet1*, *Tet2*, and *Tet3* relative to *Gapdh* in the indicated organs from WT and *Tet* TKO mice at 8 weeks of age.  $n = 6$  mice per genotype.

(B and C) Dot blot analyses to quantify 5hmC levels in adipose tissues (B) and the indicated organs (C) isolated from WT and *Tet* TKO mice. Toluidine blue staining was performed to confirm blotting of equal amounts of DNAs.

(D and E) mRNA expression of *Tet1*, *Tet2*, and *Tet3* relative to *Gapdh* in mature adipocytes or stromal vascular fraction (SVF) cells separated from iWAT (D) and eWAT (E) of WT and *Tet* TKO mice.  $n = 3-4$  (for adipocytes) and  $n = 6$  (for SVF) mice per genotype.

All data are presented as the mean  $\pm$  s.d. The *P*-values were determined by unpaired Student's *t*-test. \* $P < 0.05$ , \*\* $P < 0.005$ , \*\*\* $P < 0.0005$  vs. WT.

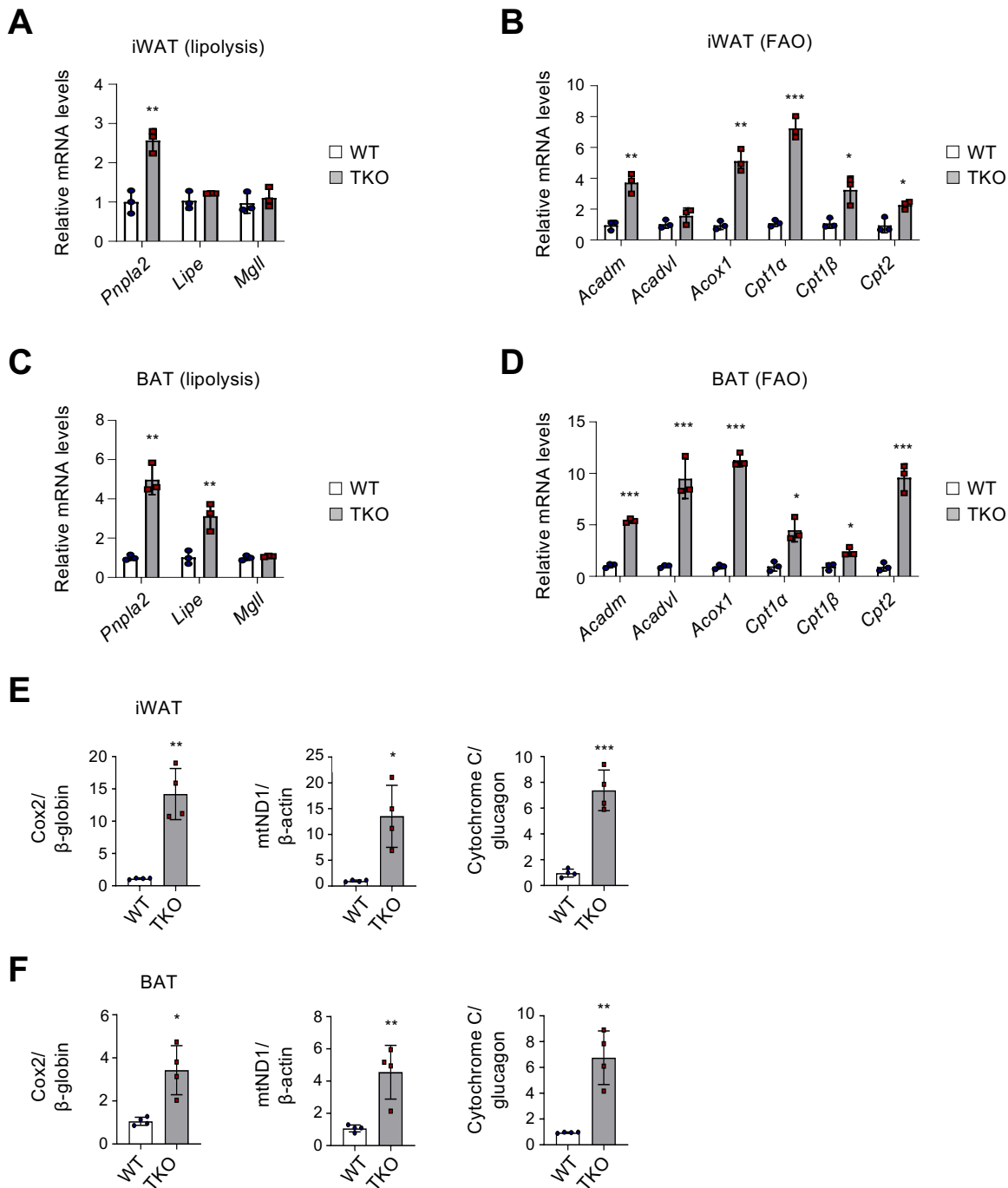


**Fig. S6. Expression of genes related to lipolysis and fatty acid oxidation in CL-316,243-stimulated wildtype and *Tet* TKO mice.**

WT and *Tet* TKO mice were administered intraperitoneally with CL-316,243 (1 mg/kg body weight/d) daily for 3 consecutive days.

(A and B) mRNA expression of genes related to lipolysis (A) or fatty acid oxidation (B) relative to *Gapdh* in iWAT of CL-316,243-stimulated mice. n = 3.

(C and D) mRNA expression of genes related to lipolysis (C) or fatty acid oxidation (D) relative to *Gapdh* in BAT of CL-316,243-stimulated mice. n = 3.

(E and F) Relative mitochondria DNA quantification of iWAT (E) and BAT (F) from CL-316,243-stimulated mice. n = 3

All data are presented as the mean ± s.d. The *P*-values were determined by unpaired Student's *t*-test. \**P* < 0.05, \*\**P* < 0.005, \*\*\**P* < 0.0005 vs. WT.

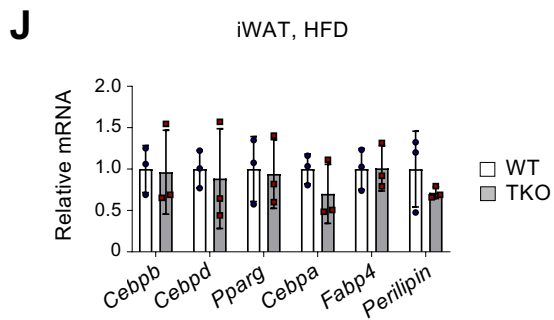
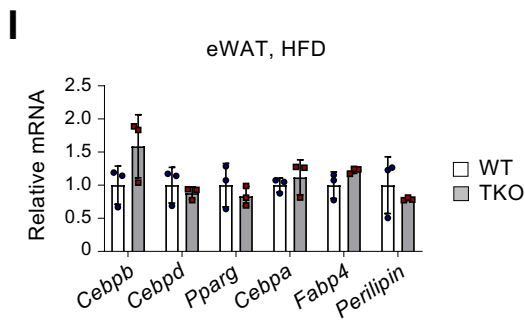
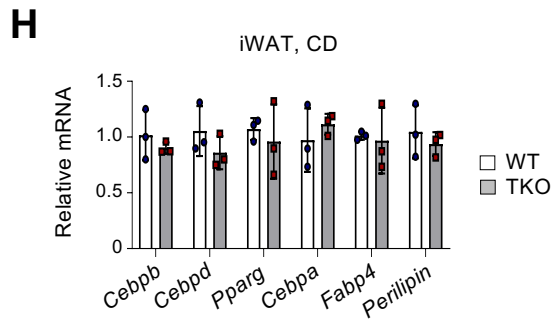
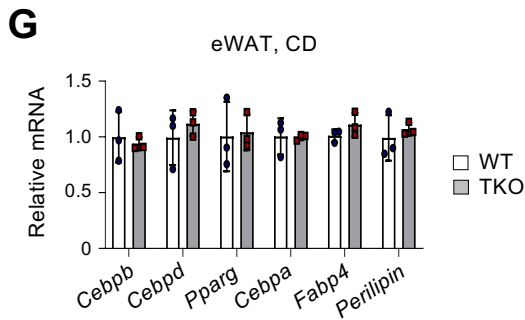
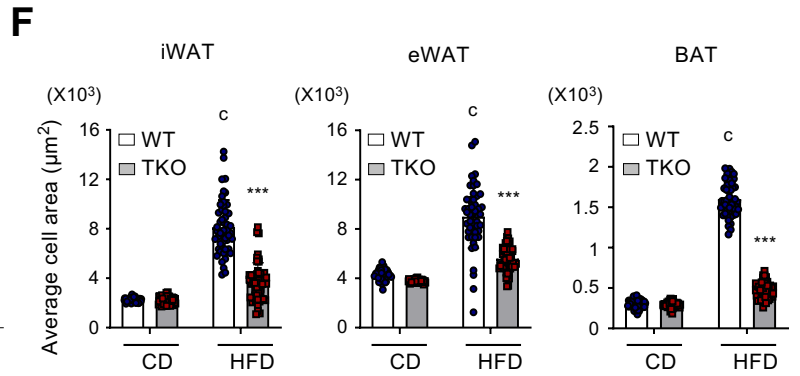
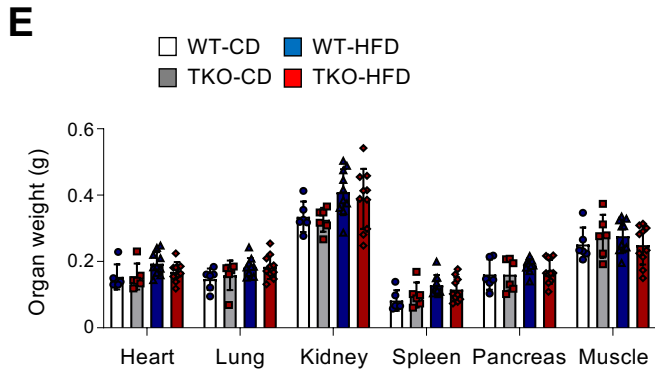
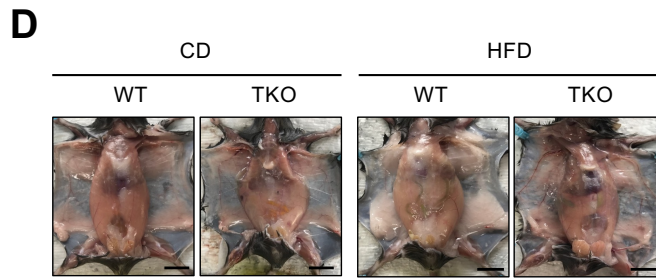
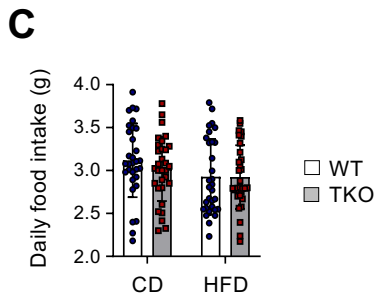
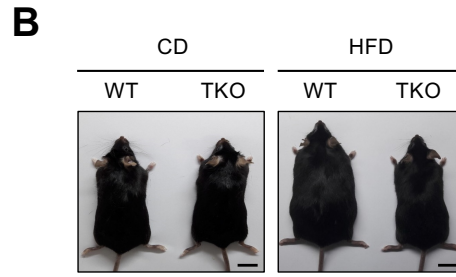
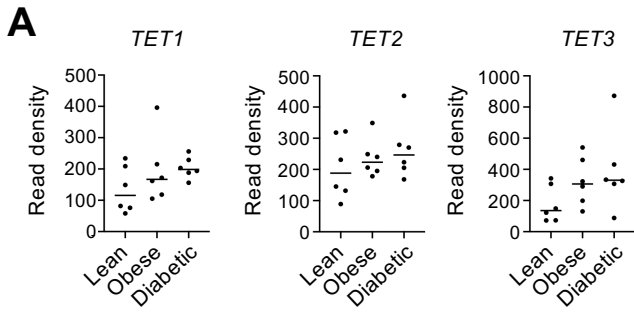


**Fig. S7. *Tet* TKO mice resist high-fat-diet-induced obesity.**

(A) *TET1*, *TET2*, and *TET3* mRNA levels in lean, obese, and type 2 diabetic human samples. RNA-sequencing data were from GSE133099.

(B) Representative photographs of WT and *Tet* TKO mice fed either CD or HFD for 12 weeks. n = 6. Scale bar, 1 cm.

(C) Daily food intake of WT and *Tet* TKO mice fed CD or HFD. n = 30.

(D) Representative photographs of dissected WT and *Tet* TKO mice fed either CD or HFD for 12 weeks. n = 10. Scale bar, 0.5 cm.

(E) Weights of internal organs of WT and *Tet* TKO mice fed either CD or HFD. n = 6 for CD and n = 10 for HFD.

(F) Average adipocyte volume of iWAT, eWAT, and BAT from WT and *Tet* TKO mice fed either CD or HFD.

(G-J) mRNA expression of representative adipogenic markers relative to *Gapdh* in eWAT and iWAT of WT and *Tet* TKO mice fed either CD (G and H) or HFD (I and J) for 12 weeks. n = 3.

All data are presented as the mean  $\pm$  s.d. The *P*-values were determined by unpaired Student's *t*-test. \**P* < 0.05, \*\**P* < 0.005, \*\*\**P* < 0.0005 vs. WT; <sup>c</sup>*P* < 0.0005 vs. CD.

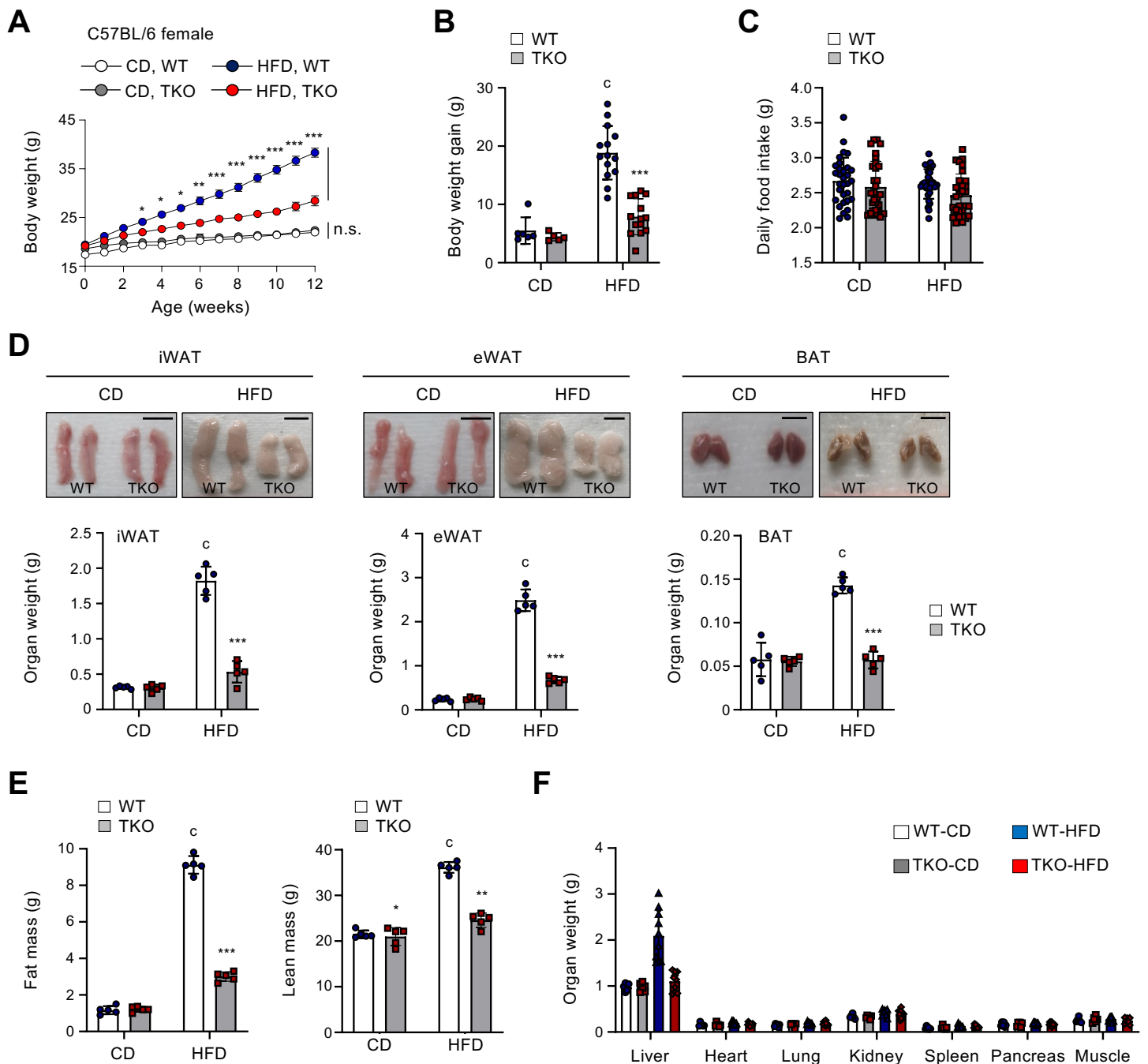


**Fig. S8. TET-deficient female mice are resistant to diet-induced obesity.**

(A) Changes in body weight of WT and *Tet* TKO female mice fed either CD or HFD.  $n = 5-6$ .

(B) Summary of body weight gain in WT and *Tet* TKO female mice fed either CD ( $n = 6$ ) or HFD ( $n = 14$ ) for 12 weeks.

(C) Daily food intake of WT and *Tet* TKO female mice fed either CD or HFD.  $n = 30$ .

(D) Representative photographs of iWAT, eWAT, and BAT from WT and *Tet* TKO female mice fed either CD or HFD (top). A summary of the weights of each fat pad is also shown (bottom).  $n = 5$ . Scale bar, 1cm.

(E) Absolute amount of fat mass (left) and lean mass (right) from WT and *Tet* TKO female mice fed either CD or HFD.  $n = 5$ .

(F) Weights of non-adipose organs of WT and *Tet* TKO female mice fed either CD or HFD.  $n = 5$ .

All data are presented as the mean  $\pm$  s.d. The  $P$ -values were determined by unpaired Student's  $t$ -test.  $*P < 0.05$ ,  $**P < 0.005$ ,  $***P < 0.0005$  vs. WT;  $^cP < 0.0005$  vs. CD. n.s. not significant.

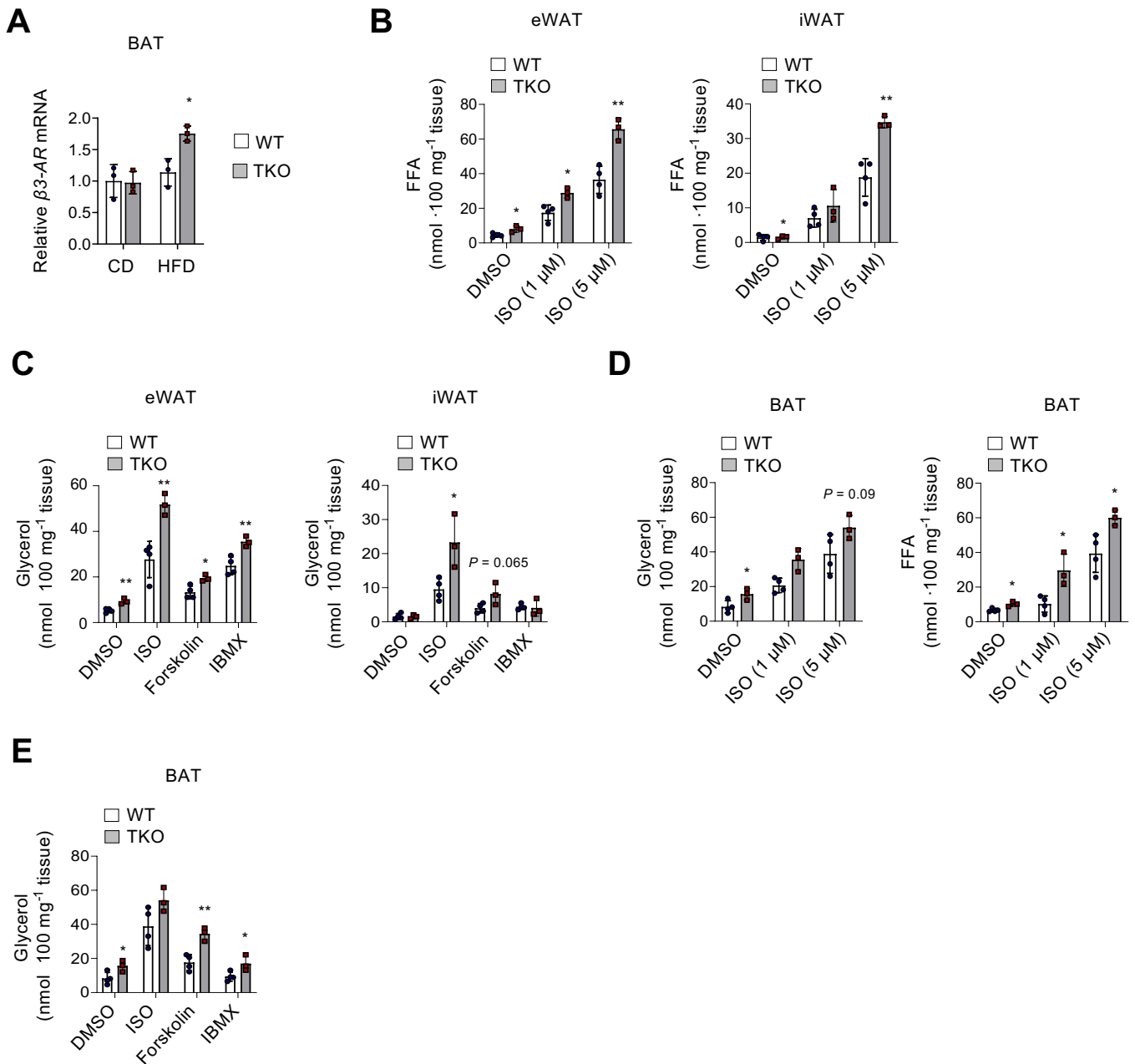


**Fig. S9. *Tet* TKO leads to the maintenance of higher levels of  $\beta 3$ -AR and lipolytic capacity in adipose tissues on a high-fat diet.**

(A)  $\beta 3$ -AR mRNA levels relative to *Gapdh* in BAT from WT and *Tet* TKO mice fed either CD or HFD.  $n = 3$ .

(B) *Ex vivo* lipolysis in eWAT (left) or iWAT (right) isolated from HFD-fed WT and *Tet* TKO mice stimulated with or without ISO at the indicated concentrations.  $n = 3-4$ .

(C) Glycerol concentrations in eWAT (left) and iWAT (right) isolated from HFD-fed WT and *Tet* TKO mice stimulated with or without ISO, forskolin, or IBMX as indicated.  $n = 3-4$ .

(D) *Ex vivo* lipolysis in BAT isolated from HFD-fed WT and *Tet* TKO mice stimulated with or without ISO at the indicated concentrations.  $n = 3-4$ .

(E) Glycerol concentrations in BAT explants isolated from HFD-fed WT and *Tet* TKO mice stimulated with or without ISO, forskolin, or IBMX as indicated.  $n = 3-4$ .

All data are presented as the mean  $\pm$  s.d. The  $P$ -values were determined by unpaired Student's  $t$ -test. \* $P < 0.05$ , \*\* $P < 0.005$  vs. WT.

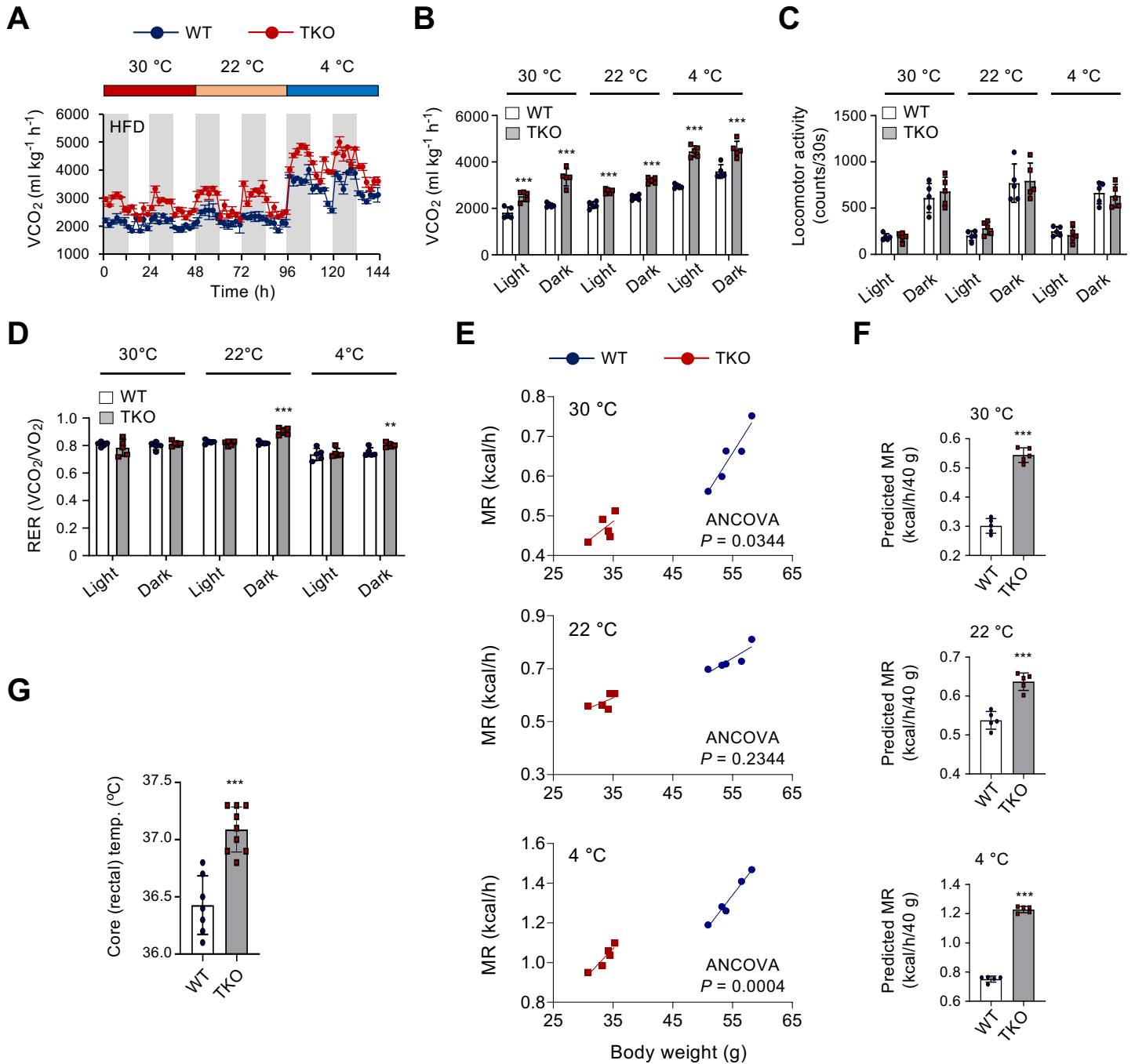


**Fig. S10. High-fat-diet-fed *Tet* TKO mice maintain a higher metabolic rate with no alterations in locomotor activity.**

(A and B) Indirect calorimetry of HFD-fed WT and *Tet* TKO mice maintained at 30 °C, 22 °C, and 4 °C to obtain VCO<sub>2</sub>. n = 5.

(C) Locomotor activity of HFD-fed WT and *Tet* TKO mice during the dark and light phases at the indicated temperatures. n = 5.

(D) Average respiratory exchange ratio (RER) of HFD-fed WT and *Tet* TKO mice at the indicated temperatures. n = 5.

(E) Regression-based analysis of absolute MR against body weight. n = 5. Data were analyzed using ANCOVA with body weight as covariate.

(F) Predicted MR at a given body mass of 40 g. n = 5.

(G) Rectal temperatures measured in HFD-fed WT and *Tet* TKO mice at RT for 12 weeks. n = 7 for WT and n = 9 for *Tet* TKO.

All data are presented as the mean ± s.d. The P-values were determined by unpaired Student's t-test.

\*\*P < 0.005, \*\*\*P < 0.0005 vs. WT.



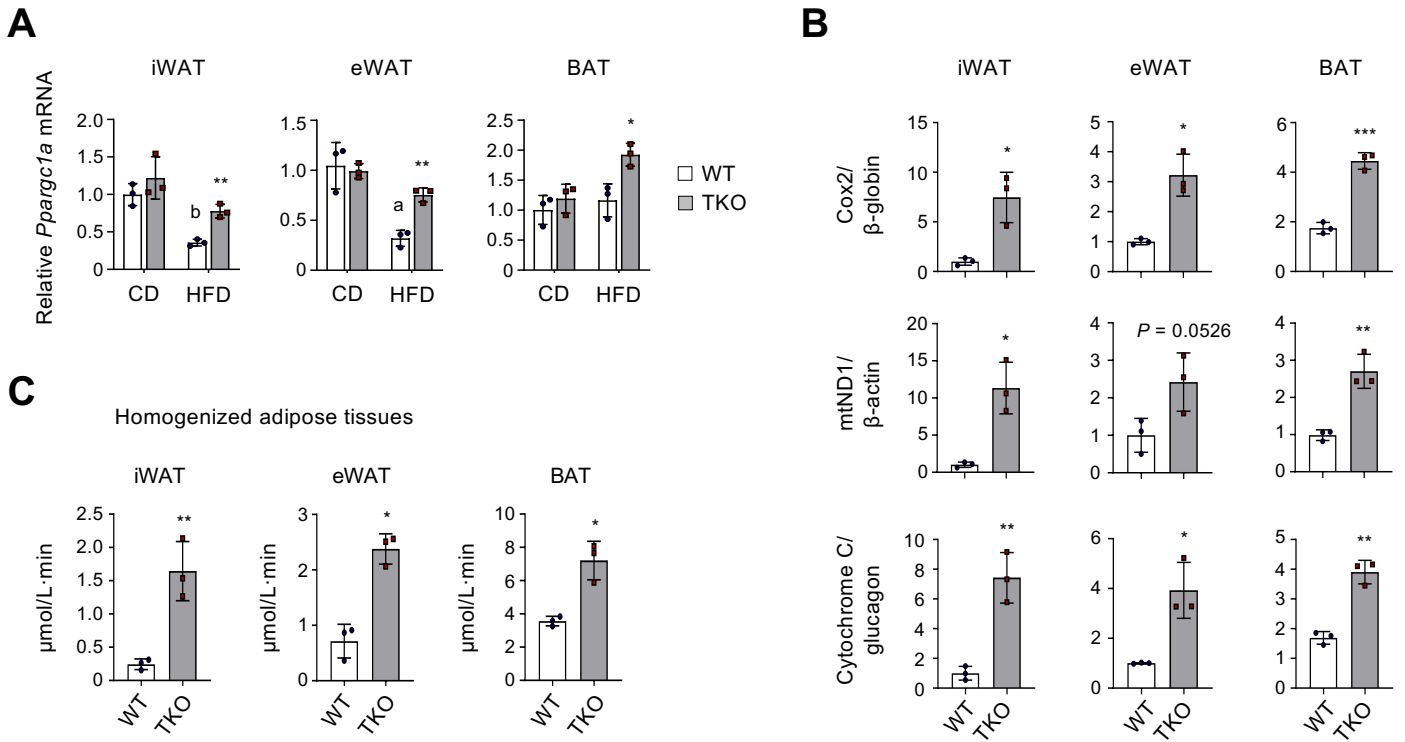


**Fig. S11. High-fat-diet-fed *Tet* TKO mice maintain higher levels of *Ppargc1a* expression, mitochondrial content, and fatty acid oxidation capacity.**

(A) *Ppargc1a* mRNA levels relative to *Gapdh* (A) in the indicated adipose depots (iWAT, eWAT, and BAT) from WT and *Tet* TKO mice fed either CD or HFD. n = 3.

(B and C) Relative mitochondria DNA content (B) and *ex vivo* fatty acid oxidation (C) in the indicated adipose depots from WT and *Tet* TKO mice fed a HFD. n = 3.

All data are presented as the mean  $\pm$  s.d. The *P*-values were determined by unpaired Student's *t*-test. \**P* < 0.05, \*\**P* < 0.005, \*\*\**P* < 0.0005 vs. WT; <sup>a</sup>*P* < 0.05, <sup>b</sup>*P* < 0.005 vs. CD.

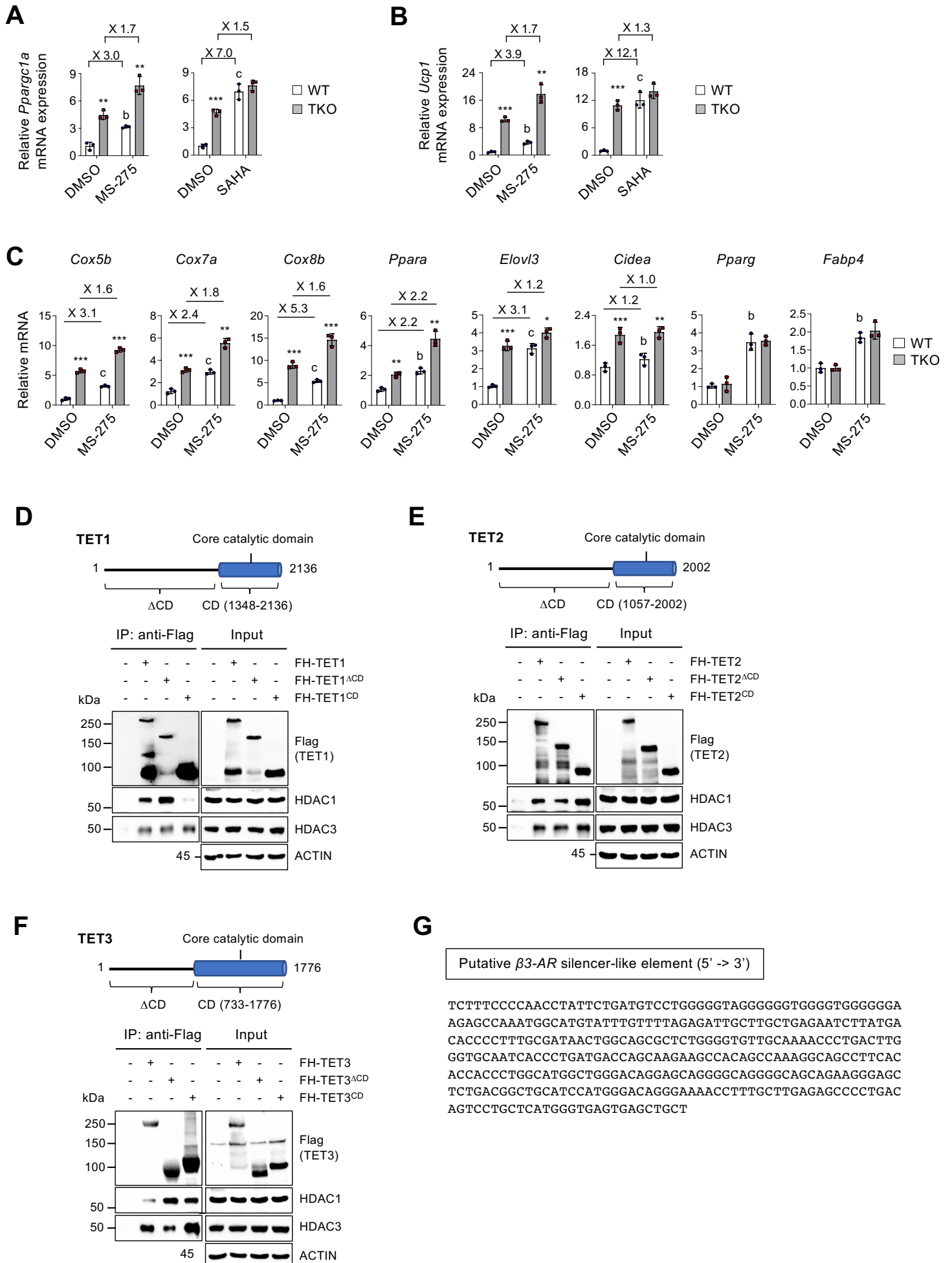


**Fig. S12. TET proteins cooperate with HDACs to repress thermogenic gene expression.**

(A and B) mRNA expression of *Ppargc1a* (A) and *Ucp1* (B) relative to *Gapdh* in WT and *Tet* TKO adipocytes stimulated with or without the indicated HDAC inhibitors (MS-275: 10  $\mu$ M, 24 h or SAHA: 20  $\mu$ M, 6 h). n = 3.

(C) mRNA expression of the indicated genes relative to *Gapdh* in WT and *Tet* TKO adipocytes stimulated with or without MS-275 (5  $\mu$ M) for 24 h. n = 3.

(D-F) Domain structures of TET1 (D), TET2 (E), and TET3 (F) proteins and co-immunoprecipitation with HDAC1 and HDAC3 in HEK293T cell lysates.

(G) Sequences of the putative silencer-like element at the  $\beta$ 3-AR locus.

All data are presented as the mean  $\pm$  s.d. The *P*-values were determined by unpaired Student's *t*-test. \**P* < 0.05, \*\**P* < 0.005, \*\*\**P* < 0.0005 vs. WT; <sup>b</sup>*P* < 0.005, <sup>c</sup>*P* < 0.0005 vs. DMSO.

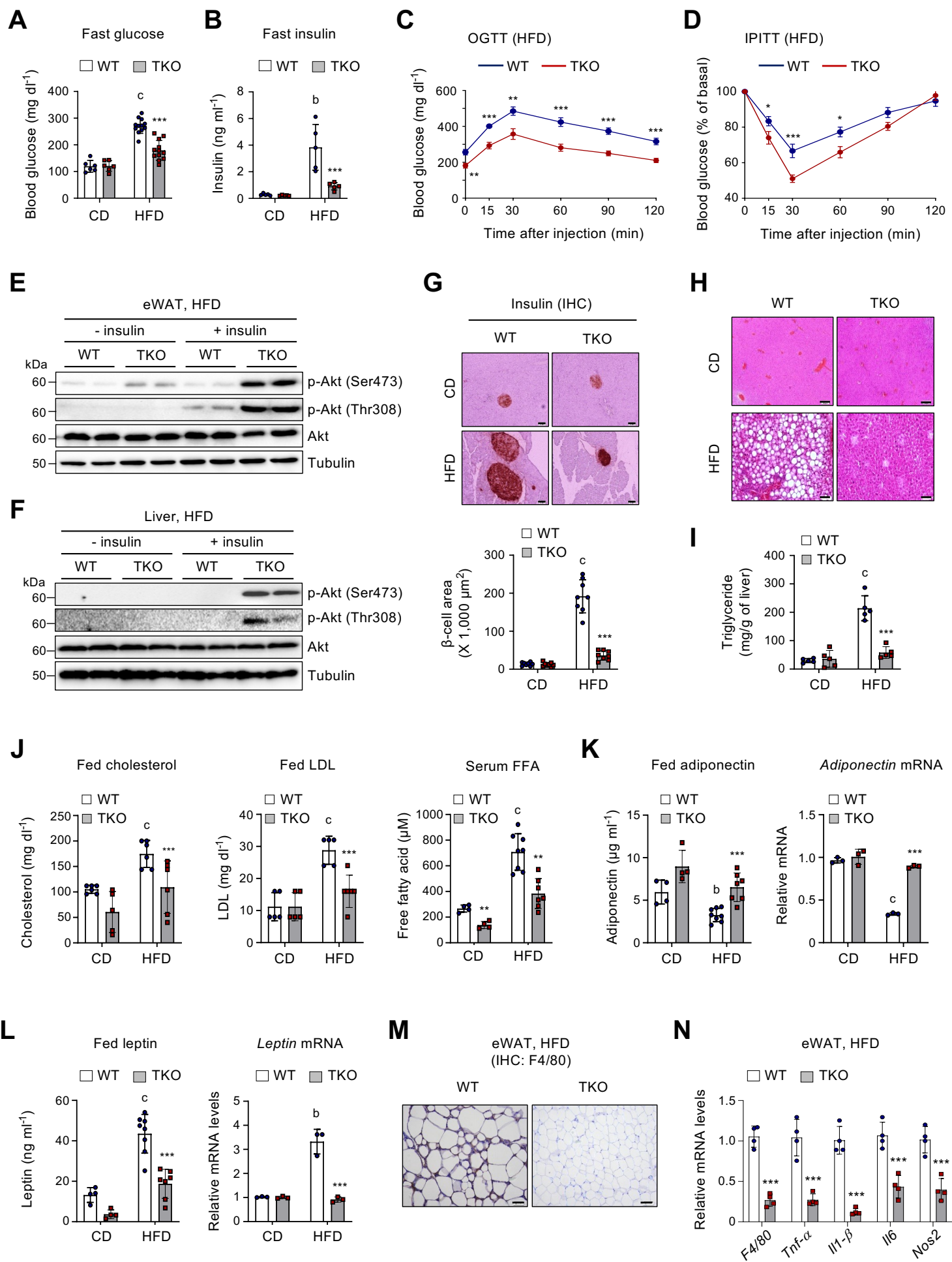


**Fig. S13. TET deficiency protects against the detrimental metabolic effects of obesity.**

(A) Fasting serum glucose concentrations in WT and *Tet* TKO mice fed either CD (n = 6) or HFD (n = 12) for 12 wk, starting at 8 wk of age.

(B) Fasting serum insulin concentrations in WT and *Tet* TKO mice fed either CD or HFD for 12 wk. n = 5.

(C and D) Oral glucose tolerance test (OGTT; n = 12) and intraperitoneal insulin tolerance test (IPITT; n = 10) in WT and *Tet* TKO mice fed a HFD for 12 wk.

(E and F) Immunoblot analysis of p-Akt (Ser-473), p-Akt (Thr-308), and total Akt proteins in eWAT (E) and the livers (F) from HFD-fed WT and *Tet* TKO mice stimulated with or without insulin (1.5 U/kg).  $\alpha$ -Tubulin served as a loading control. Quantification results are shown in *SI Appendix*, Fig. S14 D and E.

(G) Representative immunohistochemical staining for insulin in the pancreas of WT and *Tet* TKO mice fed either CD or HFD (*Top*) (n = 6). A summary of the average  $\beta$ -cell area is shown (*Bottom*). n = 8. (Scale bar, 50  $\mu$ m.)

(H) Representative hematoxylin and eosin staining of the livers from WT and *Tet* TKO mice fed either CD or HFD. n = 6. (Scale bar, 100  $\mu$ m.)

(I) Triglyceride levels in the livers from WT and *Tet* TKO mice fed either CD or HFD. n = 5.

(J) Plasma concentrations of cholesterol, low-density lipoprotein (LDL), and free fatty acid (FFA) in WT and *Tet* TKO mice fed either CD or HFD. n = 4–8.

(K) Plasma adiponectin concentrations in WT and *Tet* TKO mice fed either CD or HFD (*Left*; n = 4–8) and adiponectin mRNA levels relative to *Gapdh* in eWAT. n = 3.

(L) Plasma leptin concentrations in WT and *Tet* TKO mice fed either CD or HFD (*Left*; n = 4–8) and leptin mRNA levels relative to *Gapdh* in eWAT. n = 3.

(M) Representative immunohistochemical staining for F4/80 in eWAT of HFD-fed WT and *Tet* TKO mice. n = 4. (Scale bar, 100  $\mu$ m.)

(N) mRNA expression of proinflammatory molecules relative to *Gapdh* in eWAT of WT and *Tet* TKO mice fed an HFD. n = 4. All data are presented as the mean  $\pm$  SD. The *P* values were determined by unpaired Student's *t* test. \**P* < 0.05, \*\**P* < 0.005, \*\*\**P* < 0.0005 versus WT; <sup>b</sup>*P* < 0.005, <sup>c</sup>*P* < 0.0005 versus CD. IHC, immunohistochemistry.

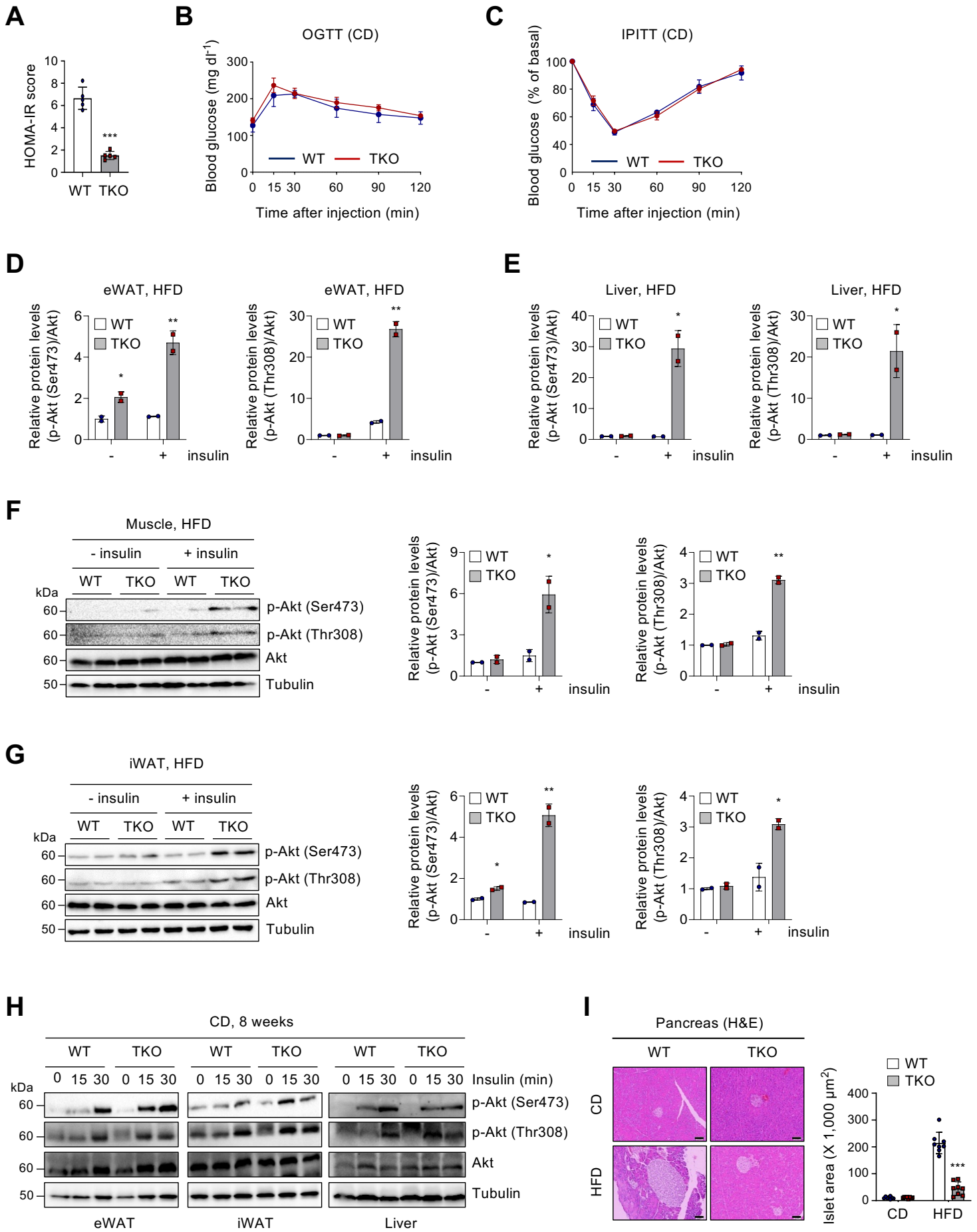


**Fig. S14. Effect of TET loss on glucose tolerance and insulin sensitivity *in vivo*.**

(A) HOMA-IR score in WT and *Tet* TKO mice fed a HFD. n = 5.

(B and C) Oral glucose tolerance (OGTT) (B) and insulin tolerance (IPITT) (C) tests in WT and *Tet* TKO mice fed a CD. n = 3–5.

(D and E) Quantification results of *SI Appendix*, Fig 13 E and F. Levels of p-Akt (Ser473) and p-Akt (Thr308) proteins relative to total Akt proteins in eWAT (D) and liver (E) of HFD-fed WT and *Tet* TKO mice stimulated with or without insulin (1.5 U/kg) are shown.

(F and G) Immunoblot analysis (*left*) and quantification (*right*) of p-Akt (Ser473), p-Akt (Thr308), and total Akt proteins in muscle (F) and iWAT (G) of HFD-fed WT and *Tet* TKO mice stimulated with or without insulin (1.5 U/kg).  $\alpha$ -Tubulin served as a loading control. n = 2.

(H) Immunoblot analysis of p-Akt (Ser 473), p-Akt (Thr 308), and total Akt proteins in eWAT, iWAT, and liver from CD-fed WT and *Tet* TKO mice stimulated with or without insulin (1.5 U/kg) for the indicated time periods.  $\alpha$ -Tubulin served as a loading control.

(I) Representative hematoxylin and eosin (H&E) staining (*left*) and quantification of the islet area (*right*) in the pancreas in WT and *Tet* TKO mice fed either CD or HFD. n = 8. Scale bar, 50  $\mu$ m.

All data are presented as the mean  $\pm$  s.d. The *P*-values were determined by unpaired Student's *t*-test. \**P* < 0.05 \*\**P* < 0.005, and \*\*\**P* < 0.0005 vs. WT.

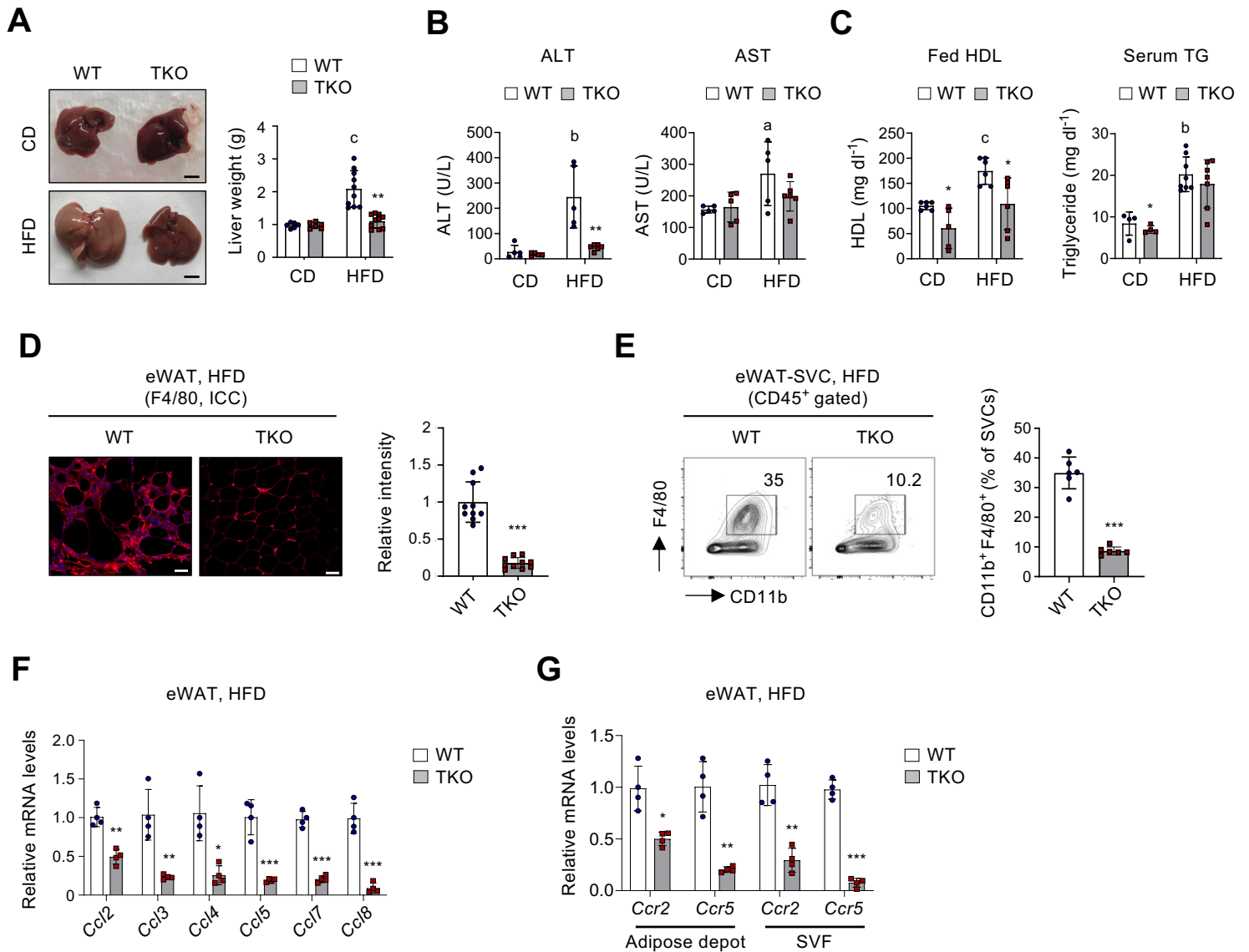


**Fig. S15. TET deficiency protects against the detrimental metabolic effects of obesity.**

(A) Representative photographs (*left*) and absolute weights (*right*) of the livers from WT and *Tet* TKO mice fed either CD or HFD.  $n = 6$  for CD and  $n = 10$  for HFD. Scale bar, 1 cm.

(B) Plasma alanine aminotransferase (ALT) and aspartate aminotransferase (AST) concentrations in WT and *Tet* TKO mice fed either CD or HFD.  $n = 5-6$ .

(C) Plasma concentrations of high-density lipoprotein (HDL) and triglycerides (TG) in WT and *Tet* TKO mice fed either CD or HFD.  $n = 4-8$ .

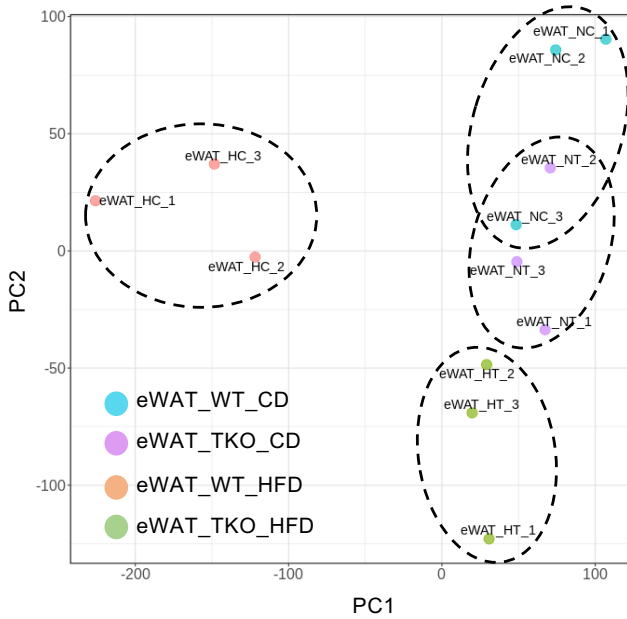
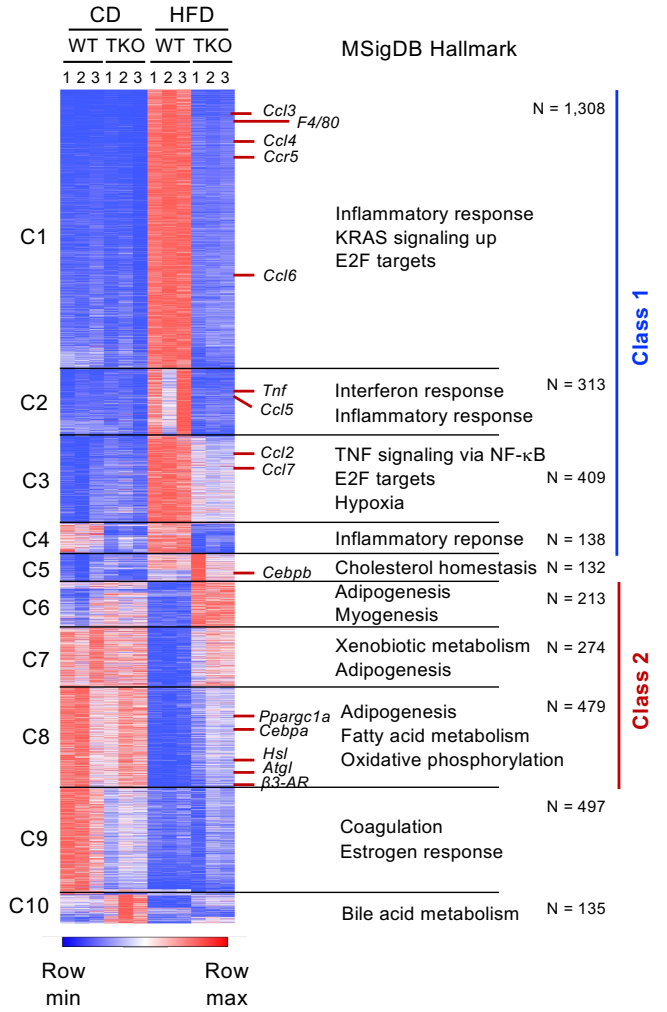
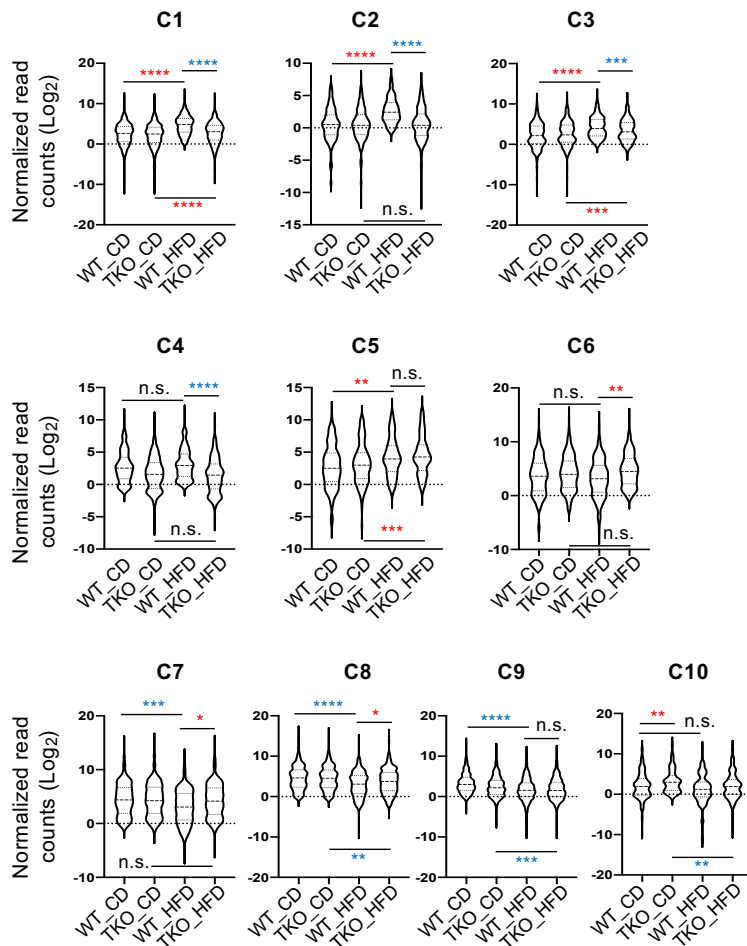
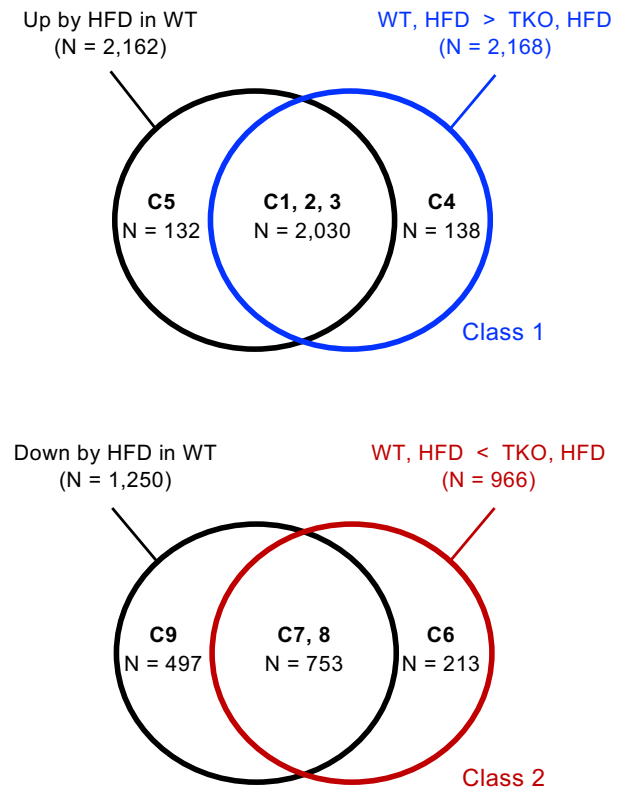
(D) Representative immunohistochemical staining for F4/80 in eWAT from HFD-fed WT and *Tet* TKO mice (*left*). Quantification results are also shown (*right*) ( $n = 10$ ). ICC, immunocytochemistry. Scale bar, 50  $\mu\text{m}$ .

(E) Flow cytometric analysis of macrophage infiltration in eWAT of HFD-fed WT and *Tet* TKO mice. CD45<sup>+</sup> CD11b<sup>+</sup> F4/80<sup>+</sup> cells were defined as macrophages. Representative contour plots (*left*) and quantification results (*right*) are shown.  $n = 6$ .

(F and G) mRNA expression of inflammatory chemokines (F) and macrophage markers (G) relative to *Gapdh* in eWAT from WT and *Tet* TKO mice fed a HFD.  $n = 4$ .

All data are presented as the mean  $\pm$  s.d. The  $P$ -values were determined by unpaired Student's  $t$ -test. \* $P < 0.05$ , \*\* $P < 0.005$ , \*\*\* $P < 0.0005$  vs. WT; <sup>a</sup> $P < 0.05$ , <sup>b</sup> $P < 0.005$ , <sup>c</sup> $P < 0.0005$  vs. CD.



**A****B****C****D**

**Fig. S16. TET proteins are critical for high fat diet-induced transcriptomic alterations in visceral adipose tissue.**

(A) Principal component analysis (PCA) plot of RNA-seq data of eWATs from WT and *Tet* TKO mice fed either CD or HFD.

(B) Clustering of differentially expressed genes ( $P$ -value  $\leq 0.01$ , fold change  $\geq 2$  or  $\leq 0.5$ ) in eWAT from WT or *Tet* TKO mice fed either CD or HFD for 12 weeks. GO categories of the MSigDB hallmark gene set of the genes within each cluster are shown on the right. N, number of genes.

(C) Violin plots presenting normalized read counts of genes within each cluster as shown in (B).  $*P < 0.05$ ,  $**P < 0.01$ ,  $***P < 0.001$  and  $****P < 0.0001$  (Kolmogorov-Smirnov test).

(D) Venn diagrams indicating the number of differentially expressed genes.

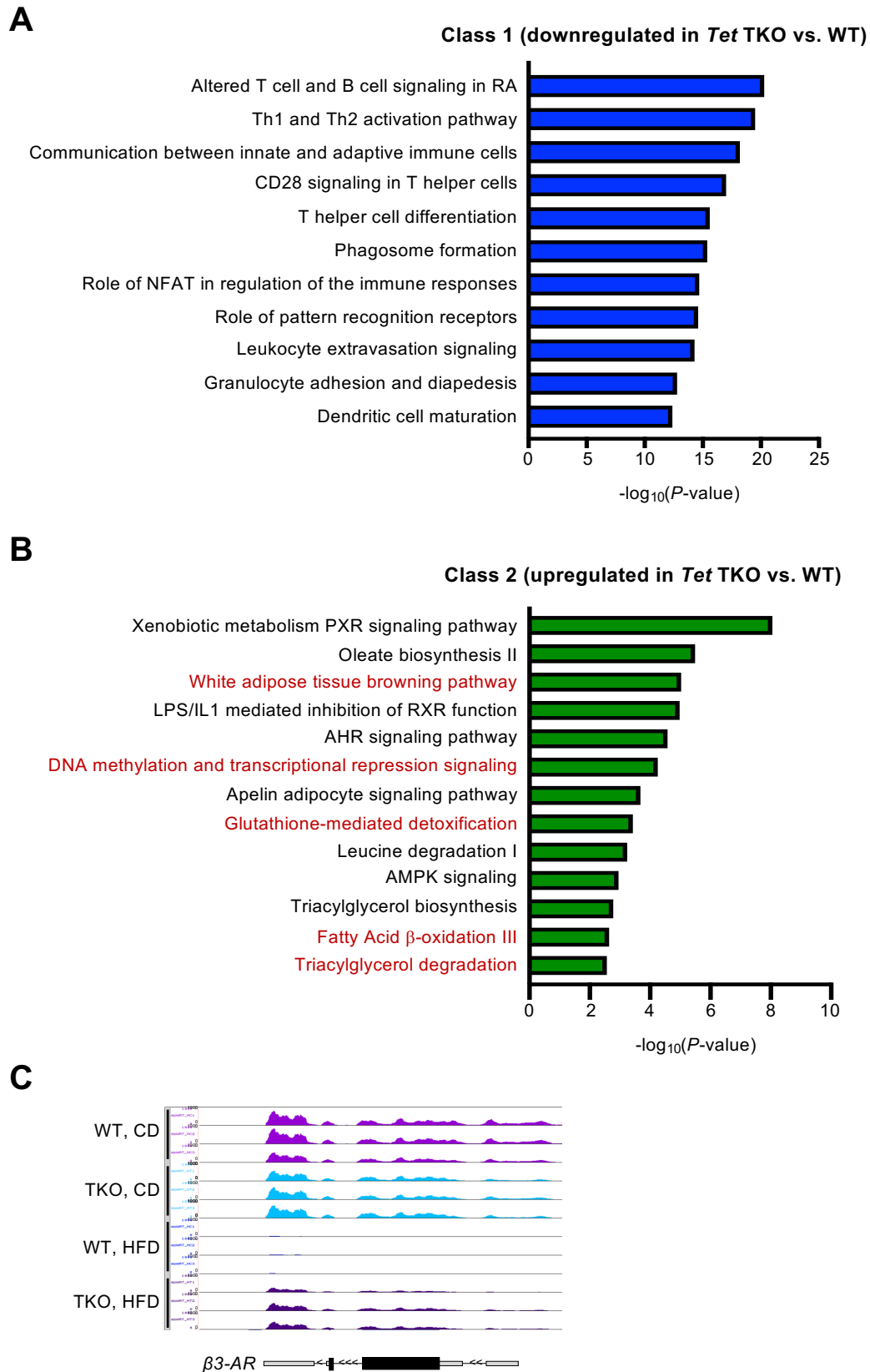


**Fig. S17. Ingenuity pathway analysis and  $\beta 3\text{-AR}$  expression in RNA-seq analysis.**

(A-B) Ingenuity pathway analysis (canonical pathways) of differentially expressed genes in eWAT of HFD-fed WT or *Tet* TKO mice (class 1, downregulated (A); class 2, upregulated genes (B) in HFD-fed *Tet* TKO vs. WT mice)

(C) UCSC genome browser tracks of  $\beta 3\text{-AR}$  mRNA expression in eWAT from WT and *Tet* TKO mice fed either CD or HFD.

**Table S1-List of oligonucleotides used in this study**

Target	Forward primer (5' → 3')	Reverse primer (5' → 3')	Assay
<i>Tet1</i>	GAGCCTGTTCTCGATGTGG	CAAACCCACTGAGGCTGTT	qRT-PCR
<i>Tet2</i>	AACCTGGCTACTGTCTTCTGCTCCA	ATGTTCTGCTGGTCTCTGTGGGAA	
<i>Tet3</i>	TCCGGATTGAGAAGTCATC	CCAGGCCAGGATCAAGATAA	
$\beta$ 1-AR	CTCATCGTGGTGGTAACGTG	ACACAGCAGCATCTACCGAA	
$\beta$ 2-AR	GGGAACGACAGCGACTTCTT	GCCAGGACGATAACCGACAT	
$\beta$ 3-AR	AGGCACAGGAATGCCACTCCAA	GCTTAGCCACAACGAACACTCG	
<i>Ucp1</i>	TCTCAGCCGGCTTAATGACTG	GGCTTGCATTCTGACCTTCAC	
<i>Ppdm16</i>	CCAAGGCAAGGGCGAAGAA	AGTCTGGTGGGATTGGAATGT	
<i>Ppargc1a</i>	TATGGAGTGACATAGAGTGTGCT	CCACTTCAATCCACCCAGAAAAG	
<i>Ppara</i>	AAGACTACCTGCTACCGAAATG	AACATTGGGCCGTTAAGA	
<i>Dio2</i>	CATTGATGAGGCTCACCTTC	GGTTCGGGTGCTTCTTAACCT	
<i>Cidea</i>	TCCTATGCTGCACAGATGACG	TGCTCTTCTGTATCGCCAGT	
<i>Elovl3</i>	GTGTGCTTGGCCATCTACAGC	CTCCCAGTTCAACAACCTTGC	
<i>Cox5b</i>	TTCAAGGTTACTTCGCGGAGT	CGGGACTAGATTAGGCTCTCC	
<i>Cox7a</i>	GCTCTGGTCCGGTCTTTAGC	GTAAGGGAGGTCATTGTCGG	
<i>Cox8b</i>	TGCTGGAACCATGAAGCCAAC	AGCCAGCCAAAACCTCCACTT	
<i>Cd137</i>	CCAAGTACCTTCTCCAGCATAGG	GCGTTGTGGTAGAGGAGCAA	
<i>Tmem26</i>	TGGTCTGGATACAGTGTCTCAC	GGTGCATTTCAAGAAGCCACAGG	
<i>Tbx1</i>	GGCAGGACAGCAATGTTTC	TTGTCTATCAGGGCACAAGG	
<i>Acadm</i>	TGACGGAGCAGCCAATGA	TCGTCAACCTTCTCTCTGCTT	
<i>Acadvl</i>	TTACATGCTGAGTGCCAACATG	CGCCTCCGAGCAAAAGATT	
<i>Acox1</i>	GCCATTGATACAGTGTGTGAG	CCGAGAAAGTGAAGGCATAGG	
<i>Cpt1a</i>	GGCATAAACGCAGAGCATTCTCG	CAGTGTCCATCTCTGAGTAGC	
<i>Cpt1<math>\beta</math></i>	GGTCCCATAAAGAAACAGACCTC	AGACGATGAAGGGCAGAAAGGG	
<i>Cpt2</i>	CCAAGCACAGTGTGGGCGAGC	AGGGTGACCCCTCTGGCTGCT	
<i>Cebpb</i>	AAGCTGAGCGACGAGTACAAGA	GTCAGCTCCAGCACCTTGTG	
<i>Cebpd</i>	CGACTTCAGCGCTACATTGA	CTAGCCGACAGACCCACAC	
<i>Pparg</i>	GATGGAAGCACTCGCATT	GGATCCGGCAGTTAAGATCA	
<i>Cebpa</i>	CAAGAACAGCAACGAGTACCG	GTCAGTGTCACTCCAGCAC	
<i>Fabp4</i>	TGGGAACCTGGAAGCTTGTCTC	GCTGATGATCATGTTGGGCTTG	
<i>Perilipin</i>	GGGACCTCTGAGTGTCTCC	GTATTGAAGAGCCGGGATCTTTT	
<i>Adiponectin</i>	TGTTCTCTTAATCCTGCCCA	CCAACTGCACAAGTTCCTTT	
<i>Leptin</i>	GGGCTTACCCCACTTCTGA	TGGCTATCTGCAGCACATTTTG	
<i>F4/80</i>	CCCCAGTGTCTTACAGAGTG	GTGCCAGAGTGGATGTCT	
<i>Tnfa</i>	GACGTGGAAGTGCAGAAAGAG	ACCGCCCTGGAGTTCTGGAA	
<i>Il-1b</i>	GCAACTGTTCTGAACTCAACT	ATCTTTTGGGTCGGTCAACT	
<i>Il6</i>	CCACGGCCTTCCCTACTTC	TTGGGAGTGGTATCCTGTGTA	
<i>iNOS</i>	ACATCGACCCGTCCACAGTAT	CAGAGGGGTAGGCTTGTCTC	
<i>Ccl2</i>	TTAAAACTGGATCGGAACCAA	GCATTAGCTTACAGATTACGGGT	
<i>Ccl5</i>	TGCCCTCACCATCATCCTCACT	GGCGGTTCTTCAGTGACA	
<i>Ccl3</i>	AGCCAGGTGTCTTTTCTG	CTCAAGCCCTGCTCTACAC	
<i>Ccl4</i>	CCTGACAAAAGAGGCAGAC	GAGGAGGCCCTCCTGAAGT	
<i>Ccl7</i>	GTGTCCCTGGAAAGCTGTTA	AGAAAGAACAGCGGTGAGGA	
<i>Ccr2</i>	ATTCTCCACCCCTGTTTCG	GATTCCTGGAAGTGGTCAA	
<i>Ccr5</i>	CGAAAACACATGGTCAAACG	GTTCTCTGTGGATCGGGTA	
<i>Ppargc1a-promoter</i>	GCGTTACTTCACTGAGGCAG	CCCCAGTCACATGACAAGC	ChIP-qPCR
<i>Ucp1-promoter</i>	CCCCTAGCAGCTCTTTGGA	CTGTGGAGCAGCTCAAAGGT	
<i>Ucp1-enhancer</i>	CTCCTCTACAGCGTACAGAGG	AGTCTGAGAAAGGGTTGA	
$\beta$ 3-AR-A	ATGACGACGCAAGAGCCACA	TCAGGGGCTCTCAAGCAAAAG	
$\beta$ 3-AR-B	TTCCCTAACTCCAGAGGCTTA	TATACAGTAAGATCAGCGCTCT	
$\beta$ 3-AR-C	GGGTTGAGAACCCTGTGCTA	GTTTTGAGAGGGAGGGGTG	
$\beta$ 3-AR-D	CCTCAGCATCCCAAGCTACA	CAGCTGATGAGTCCGTCCC	
$\beta$ 3-AR-E	TCTCTGGCTTTGTGGTCGG	GGGCATGGCTATGATTACC	
$\beta$ 3-AR-upstream	GCACAGGCTGAGATACAGTCA	GTGACTTCCATCCCGAGGTT	Reporter assay
$\beta$ 3-AR-5 kb-Forward	GAATTCACGCGTATTGTTGCCAACAGGAC	-	
$\beta$ 3-AR-4 kb-Forward	GAATTCACGCGTTTGGGGTCCACCATCAGCA	-	
$\beta$ 3-AR-3 kb-Forward	GAATTCACGCGTACACACCGGTCTGTTCTTA	-	
$\beta$ 3-AR-2 kb-Forward	GAATTCACGCGTGGGGCTCAGAGGCGTGATC	-	
$\beta$ 3-AR-1 kb-Forward	GAATTCACGCGTTGAAACAAGCGGTGTCTCC	-	
$\beta$ 3-AR-0.1 kb-Forward	GAATTCACGCGTCAGACCAATCTGGGCAACAT	-	
$\beta$ 3-AR-common reverse	-	GAATTCCTCAGAGTCACGAACAGTTGGTTAT	
<i><math>\beta</math>3-AR cCRE</i>	GAATTCACGCGTCTTTCCCAACCTATTCTGATG	GAATTCACGCGTAGCAGCTCACTACCCAT	Mitochondrial DNA quantification
<i>Cox2</i>	GCCGACTAAATCAAGCAACA	CAATGGGCATAAAGCTATGG	
<i>mtND1</i>	ACCATTTCAGACGCCATAA	TGAAATTTTGGGCTACGG	
<i>Cytochrome C</i>	CATTATATCGCGCCCTA	TGTTGGTTTGTGATCCTG	
$\beta$ -globin	GAAGCGATTCTAGGGAGCAG	GGAGCAGCGATTCTGAGTAGA	
$\beta$ -actin	TTGCTGACAGGATGCAGAAG	GAAAGGTTAAACGCAGC	
<i>glucagon</i>	CAGGGCCATCTCAGAACC	GCTATTGAAAGCCTTTC	